MONTHLY NOTICES

OF THE

ROYAL ASTRONOMICAL SOCIETY

Vol. 112 No. 1 1952

Published and Sold by the
ROYAL ASTRONOMICAL SOCIETY
BURLINGTON HOUSE
LONDON, W. 1

Price Thirteen Shillings and Sixpence

NOTICE TO AUTHORS

1. *Communications.*—Papers must be communicated to the Society by a Fellow. They should be accompanied by a summary at the *beginning* of the paper conveying briefly the content of the paper, and drawing attention to important new information and to the main conclusions. The summary should be intelligible in itself, without reference to the paper, to a reader with some knowledge of the subject; it should not normally exceed 200 words in length. **Authors are requested to submit MSS. in duplicate. These should be typed using double spacing and leaving a margin of not less than one inch on the left-hand side. Corrections to the MSS. should be made in the text and not in the margin.** Unless a paper reaches the Secretaries more than seven days before a Council meeting it will not normally be considered at that meeting. By Council decision, MSS. of accepted papers are retained by the Society for one year after publication; unless their return is then requested by the author, they are destroyed.

2. *Presentation.*—Authors are allowed considerable latitude, but they are requested to follow the general style and arrangement of *Monthly Notices*. References to literature should be given in the standard form, including a date, for printing either as footnotes or in a numbered list at the end of the paper. Each reference should give the **name and initials** of the author cited, irrespective of the occurrence of the name in the text (some latitude being permissible, however, in the case of an author referring to his own work). The following examples indicate the style of reference appropriate for a paper and a book, respectively :—

A. Corlin, *Zs. f. Astrophys.*, **15**, 239, 1938.
H. Jeffreys, *Theory of Probability*, 2nd edn., section 5.45, p. 258, Oxford, 1948.

3. *Notation.*—For technical astronomical terms, authors should conform closely to the recommendations of Commission 3 of the International Astronomical Union (*Trans. I.A.U.*, Vol. VI, p. 345, 1938). Council has decided to adopt the I.A.U. 4-letter abbreviations for constellations where contraction is desirable (Vol. IV, p. 221, 1932). In general matters, authors should follow the recommendations in *Symbols, Signs and Abbreviations* (London : Royal Society, 1951) except where these conflict with I.A.U. practice.

4. *Diagrams.*—**These should be designed to appear upright on the page, drawn about twice the size required in print and prepared for direct photographic reproduction except for the lettering, which should be inserted in pencil. Legends should be given in the manuscript indicating where in the text the figure should appear.** Blocks are retained by the Society for 10 years; unless the author requires them before the end of this period they are then destroyed.

5. *Tables.*—**These should be arranged so that they can be printed upright on the page.**

6. *Proofs.*—Costs of alterations exceeding 5 per cent of composition must be borne by the author. Fellows are warned that such costs have risen sharply in recent years, and it is in their own and the Society's interests to seek the maximum conciseness and simplification of symbols and equations consistent with clarity.

7. *Revised Manuscripts.*—When papers are submitted in revised form it is especially requested that they be accompanied by the original MS.

Reading of Papers at Meetings

8. When submitting papers authors are requested to indicate whether they will be willing and able to read the paper at the next or some subsequent meeting, and approximately how long they would like to be allotted for speaking.

9. Postcards giving the programme of each meeting are issued some days before the meeting concerned. Fellows wishing to receive such cards whether for Ordinary Meetings or for the Geophysical Discussions or both should notify the Assistant Secretary.

MONTHLY NOTICES

OF THE

ROYAL ASTRONOMICAL SOCIETY

Vol. 112 No. 1

MEETING OF 1952 JANUARY 11

Professor H. Dingle, President, in the Chair

The election by the Council of the following Fellows was duly confirmed:—

John Anthony Bancroft-Wilson, M.A., 18 Severn Road, Weston-super-Mare, Somerset (proposed by D. W. Dewhirst);

William George Barrett, Jun., 13 Heversham Road, Bexleyheath, Kent (proposed by A. C. Clarke);

John W. Boyle, 9 Pearson Grove, Caulfield, Victoria, Australia (proposed by N. R. L. Blackmore);

*Geoffrey Martin Brown, Department of Physics, University College of Swansea, Singleton Park, Swansea (proposed by F. J. M. Stratton);

Phyllis Betty Comrie, 131 Maze Hill, Blackheath, London, S.E.3 (proposed by W. M. H. Greaves);

*Phillip John David Gething, Ph.D., M.Sc., 6 Highmore Road, Blackheath, London, S.E.3 (proposed by G. J. Whitrow);

Murdoch MacDonald, K.C.M.G., C.B.(Mil.), M.I.C.E., 72 Victoria Street, London, S.W.1. (proposed by F. J. Hargreaves);

Edith Müller, D.Phil., University Observatory, St. Andrews, Scotland (proposed by R. O. Redman);

Colin Andrew Murray, M.A., Royal Observatory, Greenwich, London, S.E.10 (proposed by R. d'E. Atkinson);

C. Joy A. Penny, B.Sc., Norman House, St. George's Road, Bickley, Kent (proposed by R. d'E. Atkinson);

*Vincent Cartledge Reddish, B.Sc., 40 St. Helens Road, Leigh, Lancashire (proposed by A. Hunter);

*Dennis William Sciama, M.A., Cavendish Laboratory, Cambridge (proposed by T. Gold);

*Bryan Summers, 365 New King's Road, London, S.W.6 (proposed by J. McG. Bruckshaw);

Frank Cyril Drake Thomson, 13 Akenside Terrace, Jesmond, Newcastle-on-Tyne, 2 (proposed by H. Thomson); and

John Victor Thomson, Mirastelle, Woodland Way, Kingswood, Surrey (proposed by F. J. Hargreaves).

The election by the Council of the following Junior Members was duly confirmed :—

Kenneth Neilson Dodd, B.Sc., M.Sc., 36 Prospect Vale, Wallasey, Cheshire (proposed by W. H. McCrea);

Charles Beresford Rayner, 3 Warminster Road, South Norwood, London, S.E.15 (proposed by G. J. Whitrow); and

George Alan Wilkins, B.Sc., Ph.D., Royal Greenwich Observatory, Herstmonceux Castle, Sussex (proposed by D. H. Sadler).

Sixty-eight presents were announced as having been received since the last meeting, including :—

S. A. Mitchell, *Eclipses of the Sun*, 5th edition (presented by the author); and *Third Cape Catalogue for the equinox of 1925.0* (presented by the Royal Observatory, Cape of Good Hope).

The President announced that the Council had awarded the Gold Medal of the Society to Dr John Jackson, lately H.M. Astronomer at the Cape, for his work on stellar parallaxes and his contributions to the general problems of star positions and proper motions.

* Transferred from Junior Membership.

STAR-STREAMING FROM THE PROPER MOTIONS OF THE BOSS *GENERAL CATALOGUE*

T. R. Tannahill

(Communicated by the Director, University Observatory, Glasgow)

(Received 1951 September 14)

Summary

1. The proper motions of the Boss *General Catalogue* have been analysed, according to the two-streams hypothesis, by Eddington's method. A total of 22 374 stars of spectral types A5 to M have been used in the discussion.

2. The galactic coordinates of the vertex are ($343°{\cdot}1$, $-1°{\cdot}7$).

3. The equatorial coordinates of the solar apex are ($273°{\cdot}2$, $+35°{\cdot}4$).

4. There is a marked decrease in the solar speed and in the relative speed of the drifts with advancing spectral type, and a similar decrease with increasing galactic latitude.

---

1. The proper motions used in the present work are those of the *General Catalogue of 33 342 Stars* by Benjamin Boss (**1**). Preliminary work—the formation of a card-catalogue—was begun in 1939; various diversions, however, have combined to prevent the completion of the investigation until now. It is my pleasant duty to record my thanks to Dr R. A. Robb for help with the card-catalogue, and to Professor W. M. Smart for his encouragement throughout.

2. The object of the investigation is the determination of the constants of the star-streams and the direction of the solar motion, and the variations of these quantities with the spectral type and galactic latitude of the stars concerned. In previous investigations on the Cape photographic proper motions (**2, 3**), it was found that the stars of spectral type A form an anomalous group as regards the phenomenon of star-streaming, and 8751 of these have been omitted, with 1626 stars of types O and B, from the present discussion. Of the 33 342 stars in the catalogue as published, 476 have no spectral type assigned, and are also omitted, as are three stars designated as having peculiar spectra. Finally, 63 stars of the Taurus cluster (**4**) and 20 members and 28 doubtful members of the Ursa Major cluster (**5**)—not already omitted as being of early spectral type—were rejected. The Pleiades stars, being of early spectral type, are not concerned in the discussion; nor are the stars of the doubtful Scorpio–Centaurus group. There remain for discussion 22 374 stars * of spectral types from A5 onwards. These have been divided into three spectral groups designated A5–F5, F8–G5 and K0–M, the last group containing also the relatively few stars with spectral types later than M.

The Boss catalogue contains, besides the proper motions, estimates of the probable errors of the determinations in right ascension and declination. In the present work a rough system of weighting was adopted. A star is assigned half-weight if the probable errors of the centennial proper motions in both right

* One star has been mislaid during the investigation.

ascension and declination exceed 0″·075, or if either of these quantities exceeds 0″·085. This system is by no means perfect, but it is rapidly and easily applied. The process reduced the total weight of the stars used in the investigation to 17 953. It accounts for the presence of "half-stars" in Table II.

3. Systematic corrections to the Boss proper motions have been calculated by Smart (**6**). In applying these to the data, a preliminary division of the sky into small areas has been made. Each area is bounded by two parallels of declination 20° apart, and by two meridians 10° apart in right ascension, giving 324 areas in all. Equatorial areas (declination −10° to +10°) are indicated by the letter E, areas of north declination by A, B, C and D, and areas of south declination by α, β, γ and δ, as shown in Fig. 1. The right ascension of the centre of an area is indicated by one of the numbers 1–36. Thus area 15C is bounded by the parallels +50° and +70°, and by the meridians 145° and 155° of right ascension.

For the centre of each area the corrections in right ascension and declination have been obtained by interpolation from the tables given by Smart, and applied to the components of proper motion of each star within the area. Taking into account the probable errors of the proper motions, and the uncertainties of the corrections themselves, this procedure is considered to be sufficiently exact.

4. For the final analysis the sky was divided into 37 regions arranged, as far as possible, to lie in well-defined galactic zones. These regions are built up by combining the small areas described above. This division (of one hemisphere between 5° and 185° of right ascension) is shown in Fig. 1. Diametrically opposite regions of the sky are combined as explained in Section 5. During the analysis according to spectral type, it became apparent that certain of the regions near the pole of the celestial equator were too small in area and contained too few stars to permit of satisfactory analysis. Region 9 was accordingly combined with the region antipodal to 15, the composite region being designated 9–15; regions 27 and 36 were also combined. The original numbering of the regions has been retained throughout in order to prevent confusion.

Details of the limits and geometric centres of the regions, with the total number of stars in each, are given in Table I.* The arrangement described gives, in effect, five galactic zones and two polar calottes. Zone I consists of regions 1–6, the mean galactic latitude being −0°·2. Two zones consisting of regions 7–12 with the region antipodal to 15 (mean galactic latitude +19°·5) and regions 13, 14, 16–19 (mean galactic latitude −20°·7) form Zone II of the subsequent analysis. Regions 20–24 (mean galactic latitude +42°·5) and 25–30 and 36 (mean galactic latitude −43°·4) similarly form Zone III. Zone IV consists of the regions 31–33 (mean galactic latitude +64°·8) and 34, 35, 37 (mean galactic latitude −70°·1). Each region—and each zone as defined—is combined with the part of the sky diametrically opposite. For most practical purposes, therefore, the galactic latitudes of the zones adopted may be considered as 0°, 20°, 43° and 67°.

5. From the components of proper motion in right ascension and declination, corrected as described in Section 3, the total annual proper motion and position angle, to the nearest 0″·001 and 1°·0 respectively, were obtained by a graphical device. The position angles only are used in Eddington's method (**7**) of analysis into star-streams, the method adopted in this paper. The reference meridian for position angle, for an individual star, is that through the star itself. No appreciable error is committed if, in dealing with a small area of the sky, the

* Tables I to VI appear at the end of the paper.

reference meridian for all stars in the area is assumed to be that of the centre of the area. If, however, the regions are large (as in the present case), this error is only negligible where the meridians through the stars and that through the centre of the region are substantially parallel, i.e. near the celestial equator. For non-equatorial regions, therefore, the following procedure has been adopted to allow for the convergency of the meridians. Each small area—as described in Section 3—has been treated separately. Within each the position angles have been corrected by an angle

$$\phi = (\alpha - \alpha_s) \sin \delta,$$

(α, δ) being the coordinates of the centre of the region, and α_s the right ascension of the centre of the small area. For the most part these corrections are very small. In regions of high declination, however, they may be greater than 50°, but such circumstances apply to very few stars. Regions in which the corrections for convergency have been applied are marked with an asterisk in Table I.

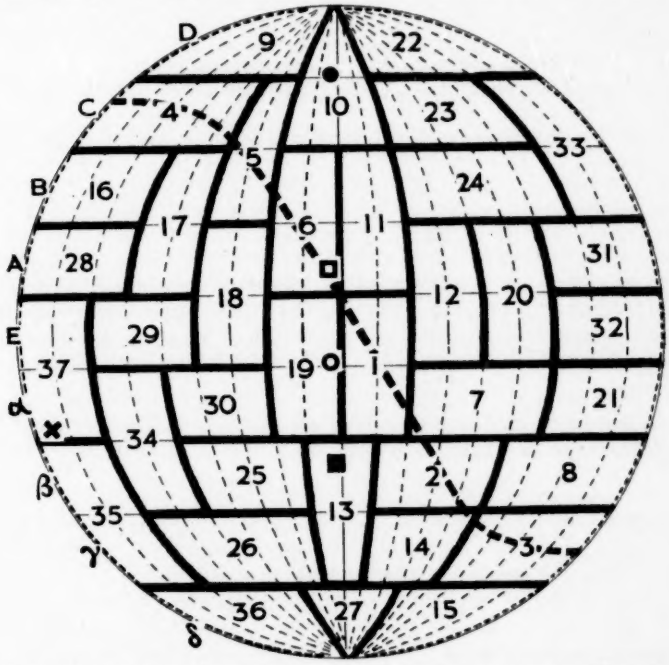

FIG. 1.—*Division of the celestial sphere. The faint broken lines show the division into small areas used in applying catalogue corrections and the corrections for convergency of the meridians. The heavy broken line is the galactic equator,* ✕ *the south galactic pole,* ○ *is the Drift I apex,* ● *the Drift II antapex,* □ *the vertex of star-streaming (opposite to centre of galaxy),* ■ *the antapex of the solar motion. The central meridian is at right ascension 95°.*

The regions shown in Fig. 1 have, as already stated, been combined with the diametrically opposite regions of the sky. If a star has position angle θ referred to a certain meridian, then referred to the anti-meridian, its position angle becomes, for our purpose, $360° - \theta$.

6. The position angles in each region, treated as described, have been grouped in 10° sectors, and the resulting distribution smoothed by taking running means of

three successive sectors. The frequency curves so obtained were then analysed by Eddington's "trial-and-error" method (**7**), fitting a curve of the form

$$\rho = 0{\cdot}0492\{N_1\phi(hV_1, \theta-\theta_1) + N_2\phi(hV_2, \theta-\theta_2)\},$$

where N_1, N_2 are the numbers of stars in the region belonging to Drift I and Drift II respectively, hV_1 and hV_2 are the projections of the space-velocities of the drifts on the tangent-plane at the centre of the region, θ_1 and θ_2 the position angles of the directions towards the respective apices, ρ the number of stars moving in direction θ. The function ϕ has been tabulated by Smart (**8**). In all cases N_1+N_2 is the total weight of stars in the region. Considerable difficulty was experienced in determining the constants in certain regions of the sky—particularly those of Drift II in the regions surrounding the Drift I apex, where the indeterminacy of θ_1 and the low value of hV_1 make the determination of hV_2 and θ_2 very uncertain. Generally, however, the separation of the drifts was not difficult, the regions being well populated; the best determinations required an estimate of θ_1 to within $2\frac{1}{2}°$, of θ_2 to within $5°$, and of hV_1 and hV_2 to within 0·05, in order to obtain a satisfactory fit.

The results of the analysis, for the three spectral groups and for the total data, are shown in Table II.

7. From the analysis two equations of condition for each drift are obtained for each region:

$$X\sin\alpha - Y\cos\alpha = -hV\sin\theta,$$
$$X\cos\alpha\sin\delta + Y\sin\alpha\sin\delta - Z\cos\delta = -hV\cos\theta.$$

X, Y and Z are the linear components of the space-velocity of a drift relative to the Sun, referred to the customary equatorial axes, and α, δ the coordinates of the centre of the region as given in Table I. In forming the normal equations equal weight was given to all regions. The solution of the normal equations gives X, Y and Z, from which the coordinates A, D of the drift apices may be found from the equations

$$\tan A = Y/X, \qquad \tan D = Z(X^2+Y^2)^{-1/2},$$

and the space-velocities hW of the drifts from

$$hW = (X^2+Y^2+Z^2)^{1/2}.$$

The results are shown in Table III, with the probable errors of the determinations. Separate solutions have been obtained for each galactic zone. The total weights of stars in each drift are given by n_1 and n_2.

The results largely confirm those of previous work, as may be seen from Table A, in which the present results for the total data are compared with the corresponding results obtained by Eddington (**7**) from a discussion of the proper motions of the PGC, and with those obtained from the Cape photographic proper motions (**3**) of stars within the same range of spectral type as is used in the present work, situated in the zone of south declination 40° to 52°.

TABLE A

	PGC	GC	Cape
A_1	90°·8	93°·4 ± 0°·9	90°·8 ± 1°·7
D_1	−14°·6	− 9°·9 ± 0°·9	− 5°·3 ± 2°·1
hW_1	1·516	1·500 ± 0·022	1·545 ± 0·041
A_2	287°·8	274°·4 ± 3°·6	304°·9 ± 8°·4
D_2	−64°·1	−70°·1 ± 1°·2	−76°·2 ± 2°·0
hW_2	0·855	0·797 ± 0·021	0·668 ± 0·029

A noteworthy feature of Table III is the decrease in the value of hW_1 with advancing spectral type. This variation with spectral type has already been noted in the previous work on the Cape data (**3**), but the probable errors of the determination were much higher in that case. The present results give a more definite indication that the effect is not accidental. No systematic trend is discernible in hW_2. There is a possibility of a slight increase in D_2 with advancing spectral type, but in view of the probable errors involved no definite conclusion may be drawn.

The value of hW_1 shows also a definite decrease with increasing galactic latitude. A similar effect has been found by Jones (**9**) in discussing the PGC stars: namely, a decrease from 1·727 at the galactic equator to 1·415 at latitude 43°. The present result—a decrease from 1·703 at the equator to 1·392 at latitude 43° and 1·364 at latitude 67°—amply confirms the conclusion reached by Jones.

No other significant variations with galactic latitude are apparent.

8. With the known values of the drift constants it is possible to calculate the theoretical values of hV and θ for each drift. This has been done for each grouping of the data, and the results are shown in the columns headed hV_c and θ_c in Tables IVA–IVE. The residuals $hV_c - hV$ and $\theta_c - \theta$ are also shown. These are small, generally, but high residuals occur—as expected—in regions near the drift apices, and—unexpectedly—in a few regions where there seems to be no excuse for their occurrence, e.g. in the value of $hV_c - hV_2$ of region 28, Table IVB.

A notable feature of Tables IVA–IVD is the preponderance of negative residuals in the upper half of the $hV_c - hV_1$ column, and of positive in the lower. This is a consequence of the decrease in hV_1 with increasing galactic latitude, and the fact that this effect shows itself even in the residuals of the spectral groups is further confirmation of its reality. The effect does not, for obvious reasons, show in Table IVE.

A somewhat better indication of the convergence of the great circles defined by the observed position angles of the drifts may be obtained by calculating the distance β of the apex from each great circle. The appropriate formula is

$$\sin\beta = \sin\lambda \sin(\theta_c - \theta),$$

where λ is the distance of the apex from the region concerned. The values of λ and β are given in Tables IVA–IVE. As regards β_1, only seven values exceed 10°, and all of these occur in the separate spectral groups, the highest value being 19°·0. Larger variations occur in β_2, a consequence of the lower hW value for Drift II and the greater difficulty of determining its direction in any particular region.

9. From the values of X, Y and Z given in Table III we calculate the linear components ξ, η, ζ of the motion of Drift I relative to Drift II, and hence the right ascension α_v and declination δ_v of the vertex of star-streaming and the relative space-velocity Ω of the drifts. The results are shown in Table V. There is a marked decrease in Ω with advancing spectral type—which might be expected as a consequence of the corresponding variation in hV_1. The Cape proper motions (**3**) also show this variation quite clearly. A decrease of Ω with increasing galactic latitude is also present, but is somewhat masked by the relatively poor determination of this quantity in Zone I. The effect is completely obscured in Jones's investigation of the PGC stars (**9**), owing doubtless to the higher probable errors involved.

Table B gives a comparison between the results obtained for the vertex of star-streaming in the present paper and those obtained in some previous investigations. Column (*a*) contains Eddington's results from the PGC stars (**7**), column (*b*) those from the Cape photographic proper motions (**3**), and column (*c*) those of the present paper. An analysis of the GC stars between magnitudes 6·0 and 7·5 has recently been made, on the ellipsoidal hypothesis, by Delhaye (**10**). The grouping used by Delhaye is rather different from that in the present paper, the material being divided into three spectral groups B8–A5, F0–F9, K0–K2, and into zones of high and low galactic latitude. The figures given in column (*d*) represent an average value, for the whole sky, of the F0–F9 and K0–K2 groups, comprising 7 187 stars of the magnitude range mentioned. The corrections applied to the proper motions in Delhaye's investigation were those calculated by Blaauw and Delhaye (**11**), and represent a compromise between the GC and the FK3 systems. It is evident that, in spite of the marked difference in the data and in its treatment in Delhaye's work and in the present paper, the two investigations agree with the earlier work in attributing to the vertex of star-streaming a direction significantly different from that towards the centre of the galaxy, namely 325° galactic longitude. For the brighter stars at least, therefore, the outstanding discrepancy in the theory of star-streaming remains.

TABLE B

	(*a*)	(*b*)	(*c*)	(*d*)
	PGC	Cape	GC	GC
l_v	347°	342°	343°	337°
b_v	−0°·5	−2°	−2°	−6°
Ω	1·87	1·75	1·82	...

It is to be remarked that the values of ξ, η and ζ in Table V refer to the vertex opposite to the centre of the galaxy.

10. From the analysis of Table II the ratio n_1/n_2 of the populations of the drifts may be obtained. If hU_0 is the solar motion relative to the stars concerned, and (A_0, D_0) is the apex of the motion on the celestial sphere, we may calculate hU_0 and (A_0, D_0) from the equations

$$(n_1+n_2)hU_0 \cos A_0 \cos D_0 + n_1 hW_1 \cos A_1 \cos D_1 + n_2 hW_2 \cos A_2 \cos D_2 = 0,$$
$$(n_1+n_2)hU_0 \sin A_0 \cos D_0 + n_1 hW_1 \sin A_1 \cos D_1 + n_2 hW_2 \sin A_2 \cos D_2 = 0,$$
$$(n_1+n_2)hU_0 \sin D_0 + n_1 hW_1 \sin D_1 + n_2 hW_2 \sin D_2 = 0,$$

the quantities A_1, D_1, hW_1, A_2, D_2, hW_2 and the ratio n_1/n_2 being known from the previous analysis.

The results of the solution are shown in Table VI, with the values of n_1/n_2 for each grouping of the data. Consequent on the corresponding variations in hW_1 (Table III), there is a well-marked decrease in hU_0 with advancing spectral type and with increasing galactic latitude. The decrease in hU_0 with advancing spectral type is noticeable also in the results from the Cape data (**3**).

Table C gives a comparison of the results for the solar motion as obtained (*a*) by Eddington (**7**) from the PGC stars, (*b*) by Smart and Tannahill (**3**) from the Cape photographic proper motions, (*c*) in the present investigation, and (*d*) by Delhaye (**10**) from the GC stars. In column (*d*), as in the corresponding column of Table B, the figures given represent a weighted mean of those given by Delhaye for the spectral groups F0–F9 and K0–K2.

TABLE C

	(*a*)	(*b*)	(*c*)	(*d*)
	PGC	Cape	GC	GC
l_0	29°	20°	30°	27°
b_0	+26°	+23°	+21°	+20°
hU_0	0·91	0·84	0·83	...
n_1/n_2	1·48	1·10	1·19	...

It is to be noted that Eddington's investigation of the PGC stars included the type A stars; the results in column (*a*) are therefore not quite comparable with the other results quoted. With regard to the value of n_1/n_2, numerous investigations since Eddington's work have agreed in bringing the value nearer unity, particularly for the fainter stars. The Cape stars (**2**), however, when the early types are included, give the value 1·41, in good agreement with Eddington.

University Observatory,
Glasgow, W.2:
1951 *September* 13.

References

(1) Benjamin Boss, *General Catalogue of 33 342 Stars*, Carnegie Institute of Washington, Publication 468, 1937.
(2) W. M. Smart and T. R. Tannahill, *M.N.*, **100**, 30, 1939.
(3) W. M. Smart and T. R. Tannahill, *M.N.*, **100**, 688, 1940.
(4) W. M. Smart, *M.N.*, **99**, 168, 1939.
(5) W. M. Smart, *M.N.*, **99**, 441 and 710, 1939.
(6) W. M. Smart, *M.N.*, **101**, 37, 1941.
(7) A. S. Eddington, *M.N.*, **71**, 4, 1910.
(8) W. M. Smart, *M.N.*, **87**, 128, 1926, and *Stellar Dynamics*, 104–105, 1938.
(9) R. D. H. Jones, *M.N.*, **91**, 563, 1931.
(10) J. Delhaye, *Contribution à l'étude de la distribution des vitesses stellaires*, Paris, 1951.
(11) A. Blaauw and J. Delhaye, *B.A.N.*, **10**, No. 400, 1949.

TABLE I

Region	Limits of R.A.		Limits of Dec.		α	δ	l	b	No. of stars
	°	°	°	°	°	° ′	°	°	
1	95 → 115		+10 → −30		105	− 9 24	190·6	0·0	699
*2	105	145	−30	−50	125	−39 16	225·4	− 0·5	720
*3	145	185	−50	−70	165	−58 31	257·2	+ 1·0	649
*4	5	55	+50	+70	30	+58 31	100·3	− 1·9	571
*5	55	75	+30	+70	65	+46 03	124·6	− 0·8	587
*6	75	95	+10	+50	85	+28 01	148·5	+ 1·1	733
*7	115	155	−10	−30	135	−19 41	215·5	+18·6	720
*8	145	185	−30	−50	165	−39 16	249·8	+18·8	675
*9–15	305	75	+70	+90	10	+75 54	90·0	+13·9	542
*10	75	115	+50	+90	95	+62 00	120·4	+22·2	645
*11	95	115	+10	+50	105	+28 01	156·7	+16·8	831
12	115	135	−10	+30	125	+ 9 24	183·3	+26·4	811
*13	85	105	−30	−70	95	−46 03	221·3	−23·0	722
*14	105	145	−50	−70	125	−58 31	241·1	−11·9	620
*16	5	35	+30	+50	20	+39 16	98·3	−22·1	561
*17	35	55	+10	+50	45	+28 01	123·9	−24·7	708
18	55	75	−10	+30	65	+ 9 24	153·1	−25·0	579
19	75	95	+10	−30	85	− 9 24	181·5	−17·6	690
20	135	155	−10	+30	145	+ 9 24	194·7	+43·8	748
*21	155	185	−10	−30	170	−19 41	245·7	+38·6	483
*22	115	185	+70	+90	150	+75 54	101·5	+38·3	378
*23	115	165	+50	+70	140	+58 31	123·9	+44·2	673
*24	115	165	+30	+50	140	+39 16	151·3	+47·4	792
*25	45	85	−30	−50	65	−39 16	208·9	−43·6	711
*26	25	85	−50	−70	55	−58 31	237·5	−46·6	870
*27–36	5	125	−70	−90	65	−75 54	255·8	−35·4	547
28	5	35	+10	+30	20	+19 41	102·6	−41·3	534
29	25	55	−10	+10	40	0 00	140·9	−49·9	491
*30	45	75	−10	−30	60	−19 41	181·0	−43·8	471
*31	155	185	+10	+30	170	+19 41	200·1	+69·9	480
32	155	185	−10	+10	170	0 00	232·2	+56·1	577
*33	165	185	+30	+70	175	+46 03	119·2	+68·4	626
*34	25	45	−10	−50	35	−28 01	186·0	−68·0	668
*35	5	25	−30	−70	15	−46 03	259·0	−71·5	582
37	5	25	+10	−30	15	− 9 24	105·2	−70·8	720

* Position angles corrected for convergency of meridians.

TABLE II

Analysis of the Drift Curves—Drift I

Region	A5–F5			F8–G5			Ko–M			A5–M		
	hV_1	θ_1	N_1	hV_1	θ_1	N_1	hV_1	θ_1	N_1	hV_1	θ_1	N_1
		°			°			°			°	
1	0·55	290	95½	0·55	290	84	0·5	270	130	0·5	285	299
2	1·4	300	50	1·05	315	54½	0·95	310	145½	0·9	305	306
3	1·6	275	54	2·0	285	30	1·7	282½	116	1·9	282½	183
4	1·6	125	59½	1·6	125	65	1·3	120	112	1·4	122½	260
5	1·7	145	75	1·3	145	67	1·4	140	87	1·5	145	242
6	1·05	160	59½	1·1	160	96	1·1	160	165	1·3	160	274
7	1·4	280	59	0·8	265	105½	0·85	275	159	0·9	275	360
8	1·7	265	71	1·7	270	58	1·7	270	128	1·6	267½	254
9–15	2·0	97½	67	1·9	95	69½	1·3	95	144½	1·7	95	268½
10	1·8	180	57	2·0	185	62½	1·4	180	132½	1·5	180	296
11	1·2	195	59	1·05	180	108	0·8	215	126½	0·8	195	376½
12	1·2	250	71	0·8	235	162½	0·7	270	121	0·8	250	390
13	1·6	357½	60½	0·7	350	75	0·6	355	171	0·9	355	285
14	1·7	322½	67½	1·2	325	50½	1·2	315	126	1·4	317½	242½
16	2·0	105	65½	1·9	110	51	1·2	115	110	1·75	110	201
17	1·75	125	78	2·0	120	59½	1·7	122½	116	1·5	122½	294½
18	1·2	120	57	0·9	145	98	1·2	140	98	1·0	130	238
19	0·4	10	75	0·25	200	96	0·1	50	159	0·1	20	343
20	1·1	250	117	1·05	260	104	1·05	250	146	1·2	255	304
21	2·0	267½	45	1·4	265	52	1·00	267½	125½	1·3	265	234
22	1·9	245	39	1·8	240	45	1·25	240	75½	1·3	240	191
23	1·9	225	86	1·0	230	81	1·2	215	161	1·4	222½	299½
24	1·6	235	73½	1·1	230	90	1·0	230	144	1·0	230	428½
25	0·7	40	89½	0·7	40	102	0·75	55	133½	0·6	50	370½
26	1·3	50	89½	1·3	50	85½	0·85	65	189	1·15	55	331
27–36	1·2	30	77½	1·9	35	62	1·5	40	79	1·8	35	198
28	1·6	100	80	1·05	110	112	1·7	105	87	1·4	107½	291
29	1·5	110	49	1·3	97½	88	1·2	97½	69	1·1	102½	244
30	0·7	85	43	0·7	55	63	1·5	65	46	0·85	65	166
31	1·7	262½	63½	1·6	260	73½	1·4	257½	91	1·5	260	237
32	1·6	255	78	1·4	255	87½	0·9	255	162	1·3	255	296½
33	1·6	260	67	1·2	255	75	1·2	245	106	1·2	255	282
34	1·3	90	65	1·2	80	81	1·0	80	117	1·3	80	223
35	1·5	85	53	1·4	85	86	1·3	100	104	1·35	90	228
37	1·55	92½	73½	1·4	100	91	1·35	100	126	1·25	100	325

Analysis of the Drift Curves—Drift II

Region	A5–F5			F8–G5			Ko–M			A5–M		
	hV_2	θ_2	N_2	hV_2	θ_2	N_2	hV_2	θ_2	N_2	hV_2	θ_2	N_2
		°			°			°			°	
1	1·5	175	43	1·05	175	81	0·7	175	148	0·9	175	282½
2	0·5	210	65	0·45	190	69	0·6	185	170	0·6	180	248
3	0·5	170	49	0·45	180	63	0·4	185	165	0·4	190	294
4	0·45	225	41	0·6	240	38½	0·4	195	102	0·5	220	158
5	0·45	220	48½	0·4	210	59½	0·5	210	83	0·5	220	178
6	0·5	200	79½	0·7	205	59	0·4	200	112	0·4	205	297

TABLE II (*cont.*)

Analysis of the Drift Curves—Drift II

Region	A5–F5			F8–G5			Ko–M			A5–M		
	hV_2	θ_2	N_2	hV_2	θ_2	N_2	hV_2	θ_2	N_2	hV_2	θ_2	N_2
		°			°			°			°	
7	0·55	190	61	1·2	155	47	0·65	160	142½	0·95	155	214
8	1·0	140	38	0·6	160	55	0·6	175	160	0·6	165	256
9–15	0·65	240	32½	0·3	270	38	0·2	280	92	0·3	265	175
10	0·3	205	64	0·3	160	67	0·3	130	106	0·25	110	193
11	0·3	180	90	0·5	210	85	0·6	175	195	0·5	180	287
12	0·5	190	90	1·6	152½	59	0·8	190	205	0·8	175	318½
13	0·55	220	68½	0·9	180	64	0·75	170	122	0·65	185	276
14	0·6	210	55	0·55	195	49	0·6	155	137	0·55	170	242½
16	0·7	195	43	0·4	190	77	0·9	210	75½	0·65	200	221
17	0·4	200	55	0·6	195	104	0·6	200	142	0·6	205	260
18	0·45	195	75	0·55	190	67	0·5	200	109	0·6	190	266
19	1·2	180	73	1·1	165	67½	1·5	170	114½	1·4	170	242
20	0·5	150	55	0·7	185	99	0·75	170	162	0·6	180	379
21	0·7	170	45	0·6	155	63	0·9	155	67	0·8	155	163½
22	0·15	90	40½	0·5	60	32½	0·3	120	61	0·4	80	102½
23	0·3	40	55½	0·5	120	55	0·45	110	65	0·3	150	204
24	0·3	160	79	0·6	150	75	0·6	185	148	0·6	140	181
25	0·8	190	42½	1·05	200	52	0·7	180	120	1·0	190	169
26	0·45	220	81	0·6	190	83	0·6	185	114	0·55	190	311
27–36	0·8	220	38	0·4	205	59	0·1	210	106	0·3	220	223½
28	0·7	215	30½	1·7	215	45	0·55	185	106½	0·9	210	170
29	0·6	195	47	1·2	190	80	0·6	195	110	0·9	195	199
30	1·3	210	31	0·9	170	57	0·6	170	138	0·75	180	212
31	0·7	140	35	0·8	170	61	0·7	150	95	0·75	155	182
32	0·55	155	43	0·8	155	67	0·9	160	97	0·75	155	238
33	0·3	130	63	0·3	190	71½	0·5	130	102½	0·5	130	203
34	0·4	180	63	0·65	195	89½	0·9	195	118	0·55	185	310½
35	0·7	225	45	0·7	220	65½	0·6	195	89½	0·55	205	215
37	0·5	200	74	0·6	190	136	0·55	190	143½	0·6	200	319

TABLE III

The Drift Constants

Drift I

	A5–F5	F8–G5	Ko–M	A5–M
X_1	−0·032 ± 0·026	−0·079 ± 0·032	−0·142 ± 0·030	−0·087 ± 0·023
Y_1	+1·748 0·026	+1·537 0·031	+1·353 0·030	+1·475 0·022
Z_1	−0·275 0·027	−0·279 0·033	−0·259 0·031	−0·258 0·023
A_1	91°·1 0°·9	92°·9 1°·2	96°·0 1°·3	93°·4 0°·9
D_1	−8°·9 0°·9	−10°·3 1°·2	−10°·8 1°·3	−9°·9 0°·9
hW_1	1·770 0·026	1·564 0·031	1·385 0·030	1·500 0·022
n_1	2371	2771	4308	9761

	Zone I	Zone II	Zone III	Zone IV
X_1	−0·119 ± 0·062	−0·088 ± 0·028	−0·113 ± 0·043	−0·103 ± 0·073
Y_1	+1·670 0·072	+1·597 0·032	+1·371 0·039	+1·344 0·033
Z_1	−0·312 0·077	−0·268 0·031	−0·210 0·045	−0·227 0·046
A_1	94°·1 2°·1	93°·1 1°·0	94°·7 1°·8	94°·4 6°·4
D_1	−10°·6 2°·6	−9°·5 1°·1	−8°·7 1°·8	−9°·6 1°·9
hW_1	1·703 0·071	1·622 0·031	1·392 0·039	1·364 0·033
n_1	1564	3548	3058	1591

TABLE III (*cont.*)

Drift II

	A5–F5	F8–G5	K0–M	A5–M
X_2	+0·169 ± 0·029	+0·018 ± 0·033	−0·015 ± 0·023	+0·021 ± 0·020
Y_2	−0·282 0·029	−0·288 0·033	−0·206 0·023	−0·270 0·020
Z_2	−0·657 0·030	−0·840 0·035	−0·741 0·024	−0·750 0·021
A_2	301°·0 5°·1	273°·5 6°·6	265°·8 6°·3	274°·4 3°·6
D_2	−63°·4 2°·3	−71°·0 2°·1	−74°·4 1°·7	−70°·1 1°·2
hW_2	0·735 0·030	0·889 0·034	0·770 0·024	0·797 0·021
n_2	1939	2341	4223	8192

	Zone I	Zone II	Zone III	Zone IV
X_2	+0·132 ± 0·043	−0·059 ± 0·036	+0·029 ± 0·034	−0·089 ± 0·059
Y_2	−0·187 0·050	−0·279 0·041	−0·300 0·031	−0·273 0·026
Z_2	−0·661 0·054	−0·833 0·040	−0·780 0·035	−0·583 0·037
A_2	305°·2 11°·4	258°·0 7°·4	275°·5 6°·4	251°·9 11°·0
D_2	−70°·9 4°·1	−71°·1 2°·6	−68°·9 2°·2	−63°·8 3°·6
hW_2	0·700 0·052	0·880 0·041	0·836 0·034	0·650 0·029
n_2	1458	2952	2314	1468

TABLE IVA

A5–F5 *stars*

Region	Drift I						Drift II					
	θ_c °	$\theta_c-\theta_1$ °	β_1 °	λ_1 °	hV_c	hV_c-hV_1	θ_c °	$\theta_c-\theta_2$ °	β_2 °	λ_2 °	hV_c	hV_c-hV_2
1	271·0	−19·0	4·5	13·7	0·42	−0·13	187·4	+12·4	11·9	106·1	0·71	−0·79
2	305·9	+ 5·9	4·0	42·9	1·20	−0·20	178·2	−31·8	30·9	77·3	0·72	+0·22
3	279·2	+ 4·2	4·0	74·0	1·70	+0·10	157·2	−12·8	10·3	53·5	0·59	+0·09
4	119·4	− 5·6	5·6	83·3	1·76	+0·16	223·4	− 1·6	1·0	139·3	0·48	+0·03
5	149·8	+ 4·8	4·1	59·7	1·53	−0·17	220·1	+ 0·1	0·1	144·8	0·42	−0·03
6	170·0	+10·0	6·1	37·4	1·07	+0·02	203·0	+ 3·0	2·0	137·7	0·49	−0·01
7	277·8	− 2·2	1·5	43·7	1·22	−0·18	173·8	−16·2	16·1	96·2	0·73	+0·18
8	273·2	+ 8·2	7·8	71·9	1·68	−0·02	160·9	+20·9	19·8	71·6	0·70	−0·30
9–15	100·8	+ 3·3	3·3	96·5	1·76	−0·24	228·2	−11·8	6·6	145·9	0·41	−0·24
10	184·1	+ 4·1	3·9	71·0	1·67	−0·13	251·9	+46·9	8·7	168·1	0·15	−0·15
11	202·0	+ 7·0	4·4	39·3	1·12	−0·08	191·9	+11·9	7·1	143·2	0·44	+0·14
12	242·5	− 7·5	4·7	38·4	1·10	−0·10	177·8	−12·2	9·9	125·9	0·60	+0·10
13	353·6	− 3·9	2·4	37·3	1·07	−0·53	192·2	−27·8	25·7	68·6	0·68	+0·13
14	318·3	− 4·2	3·5	55·9	1·47	−0·23	177·9	−32·1	26·7	58·0	0·62	+0·02
16	109·0	+ 4·0	4·0	81·4	1·75	−0·25	210·5	+15·5	13·4	120·0	0·64	−0·06
17	122·8	− 2·2	1·9	57·9	1·50	−0·25	210·5	+10·5	9·0	121·1	0·63	+0·23
18	124·4	+ 4·4	2·3	31·8	0·93	−0·27	203·8	+ 8·8	8·1	113·2	0·68	+0·23
19	85·6	+75·6	5·9	6·0	0·19	−0·21	195·6	+15·6	15·3	102·2	0·72	−0·48
20	252·7	+ 2·7	2·3	56·7	1·48	+0·38	167·4	+17·4	14·5	123·4	0·61	+0·11
21	265·2	− 2·3	2·2	76·6	1·72	−0·28	160·3	− 9·7	9·7	88·6	0·73	+0·03
22	237·8	− 7·2	7·2	91·5	1·77	−0·13	53·2	−36·8	9·3	164·3	0·20	+0·05
23	229·5	+ 4·5	4·4	78·0	1·73	−0·17	126·0	+86·0	10·4	169·6	0·23	−0·17
24	234·5	− 0·5	0·5	66·1	1·62	+0·02	161·1	+ 1·1	0·3	152·3	0·21	−0·09
25	44·5	+ 4·5	2·8	38·3	1·10	+0·40	203·6	+13·6	12·6	68·2	0·68	−0·12
26	44·1	− 5·9	4·9	56·7	1·48	+0·18	213·3	− 6·7	5·0	48·1	0·55	+0·10
27–36	27·9	− 2·1	2·0	68·5	1·65	+0·45	218·9	− 1·1	0·7	36·3	0·43	−0·37
28	105·2	+ 5·2	5·0	75·6	1·71	+0·11	206·8	− 8·2	8·0	102·8	0·72	+0·02
29	101·4	− 8·6	6·7	51·6	1·39	−0·11	206·3	+11·3	11·3	94·0	0·73	+0·13
30	74·8	−10·2	5·4	31·9	0·94	+0·24	203·2	− 6·8	6·8	84·5	0·73	−0·57
31	257·8	− 4·7	4·7	82·7	1·76	+0·06	155·5	+15·5	12·6	125·3	0·60	−0·10
32	260·9	+ 5·9	5·8	79·0	1·74	+0·14	159·3	+ 4·3	4·1	107·1	0·70	+0·15
33	259·5	− 0·5	0·5	92·2	1·77	+0·17	139·9	+ 9·9	5·6	145·7	0·41	+0·11
34	81·5	− 8·5	7·0	56·0	1·47	+0·17	209·0	+29·0	26·5	66·9	0·68	+0·28
35	86·2	+ 1·2	1·2	74·0	1·70	+0·20	219·0	− 6·0	4·1	43·2	0·50	−0·20
37	96·8	+ 4·3	4·2	75·0	1·71	+0·16	206·5	+6·5	6·3	74·5	0·71	+0·21

Table IVb
F8–G5 *stars*

Region	Drift I						Drift II					
	θ_c °	$\theta_c-\theta_1$ °	β_1 °	λ_1 °	hV_c	hV_c-hV_1	θ_c °	$\theta_c-\theta_2$ °	β_2 °	λ_2 °	hV_c	hV_c-hV_2
1	264·7	− 25·3	5·1	11·9	0·32	−0·23	176·2	+ 1·2	1·2	99·2	0·88	−0·17
2	306·6	− 8·4	5·5	40·7	1·02	−0·03	169·4	−20·6	19·0	67·5	0·82	+0·37
3	280·0	− 5·0	4·8	71·9	1·49	−0·51	152·0	−28·0	18·1	41·2	0·59	+0·14
4	118·5	− 6·5	6·5	85·3	1·56	−0·04	218·2	−21·8	10·1	151·9	0·42	−0·18
5	148·5	+ 3·5	3·1	61·6	1·38	+0·08	199·1	−10·9	5·2	151·6	0·42	+0·02
6	167·6	+ 7·6	4·8	39·1	0·99	−0·11	184·0	−21·0	14·2	136·8	0·61	−0·09
7	276·7	+ 11·7	7·8	41·6	1·04	+0·24	167·5	+12·5	12·5	84·9	0·89	−0·31
8	273·3	+ 3·3	3·1	69·7	1·47	−0·23	158·8	− 1·2	1·0	58·8	0·76	+0·16
9–15	99·4	+ 4·4	4·4	98·3	1·55	−0·35	239·0	−31·0	11·2	157·8	0·34	+0·04
10	182·2	− 2·8	2·7	72·3	1·49	−0·51	176·9	+16·9	2·6	171·0	0·14	−0·16
11	198·7	+ 18·7	11·9	40·1	1·01	−0·04	174·6	−35·4	23·5	136·5	0·61	+0·11
12	239·1	+ 4·1	2·5	37·6	0·95	+0·15	169·1	+16·6	15·0	115·4	0·80	−0·80
13	356·5	+ 6·5	3·8	35·8	0·91	+0·21	179·5	− 0·5	0·4	63·0	0·79	−0·11
14	319·7	− 5·3	4·3	54·0	1·27	+0·07	166·9	−28·1	20·7	48·6	0·67	+0·12
16	108·9	− 1·1	1·1	83·6	1·55	−0·35	204·9	+14·9	11·1	132·1	0·66	+0·26
17	122·7	+ 2·7	2·3	60·1	1·36	−0·64	198·4	+ 3·4	2·6	129·4	0·69	+0·09
18	124·7	− 20·3	11·2	34·0	0·88	−0·02	190·0	0·0	0·0	115·9	0·80	+0·25
19	97·2	−102·8	7·6	7·8	0·21	−0·04	182·8	+17·8	17·6	99·4	0·88	−0·22
20	250·5	− 9·5	7·8	55·5	1·29	+0·24	164·2	−20·8	19·4	110·8	0·83	+0·13
21	264·4	− 0·6	0·6	74·5	1·51	+0·11	160·9	+ 5·9	5·7	75·7	0·86	+0·26
22	235·8	− 4·2	4·2	92·5	1·56	−0·24	101·6	+41·6	10·6	163·9	0·25	−0·25
23	227·3	− 2·7	2·6	78·6	1·53	+0·53	142·0	+22·0	8·1	157·9	0·33	−0·17
24	232·0	+ 2·0	1·8	66·1	1·43	+0·33	158·2	+ 8·2	5·2	140·5	0·57	−0·03
25	48·2	+ 8·2	5·1	38·2	0·97	+0·27	189·6	−10·4	9·6	67·9	0·82	−0·23
26	46·7	− 3·3	2·7	56·1	1·30	0·00	195·9	+ 5·9	4·4	47·7	0·66	+0·06
27–36	29·9	− 5·1	4·7	67·4	1·44	−0·46	197·0	− 8·0	4·2	32·1	0·47	+0·07
28	105·8	− 4·2	4·1	77·8	1·53	+0·48	200·0	−15·0	13·7	113·9	0·81	−0·89
29	102·8	+ 5·3	4·3	53·6	1·26	−0·04	195·5	+ 5·5	5·4	101·2	0·87	−0·33
30	78·4	+ 23·4	12·5	33·1	0·85	+0·15	190·4	+20·4	20·4	86·4	0·89	−0·01
31	255·8	− 4·2	4·2	81·6	1·55	−0·05	159·9	−10·1	9·3	112·9	0·82	+0·02
32	259·4	+ 4·4	4·3	77·3	1·53	+0·13	161·5	+ 6·5	6·5	94·4	0·89	+0·09
33	257·2	+ 2·2	2·2	92·0	1·56	+0·36	152·6	−37·4	25·2	135·6	0·62	+0·32
34	84·0	+ 4·0	3·4	56·9	1·31	+0·11	196·9	+ 1·9	1·8	72·9	0·85	+0·20
35	88·5	+ 3·5	3·4	74·2	1·51	+0·11	204·4	−15·6	12·0	50·5	0·69	−0·01
37	98·4	− 1·6	1·6	76·5	1·52	+0·12	198·7	+ 8·7	8·7	84·8	0·89	+0·29

Table IVc
Ko–M *stars*

Region	Drift I						Drift II					
	θ_c °	$\theta_c-\theta_1$ °	β_1 °	λ_1 °	hV_c	hV_c-hV_1	θ_c °	$\theta_c-\theta_2$ °	β_2 °	λ_2 °	hV_c	hV_c-hV_2
1	260·3	− 9·7	1·5	9·0	0·21	−0·29	174·9	− 0·1	0·1	95·3	0·77	+0·07
2	309·9	− 0·1	0·1	38·4	0·86	−0·09	169·1	−15·9	14·2	63·4	0·69	+0·09
3	282·4	− 0·1	0·1	69·9	1·30	−0·40	154·2	−30·8	18·1	37·3	0·47	+0·07
4	116·0	− 4·0	4·0	87·2	1·38	+0·08	210·7	+15·7	6·8	154·3	0·33	−0·07
5	145·5	+ 5·5	4·9	63·3	1·24	−0·16	191·1	−18·9	9·4	150·2	0·38	−0·12
6	163·1	+ 3·1	2·0	40·2	0·89	−0·21	180·3	−19·7	14·1	133·6	0·56	+0·16
7	277·4	+ 2·4	1·5	38·6	0·86	+0·01	168·1	+ 8·1	8·0	80·9	0·76	+0·11
8	274·8	+ 4·8	4·4	67·0	1·27	−0·43	161·2	−13·8	11·3	55·2	0·63	+0·03
9–15	96·5	+ 1·5	1·5	99·5	1·37	+0·07	236·8	−43·2	12·3	161·9	0·24	+0·04
10	179·0	− 1·0	1·0	72·8	1·32	−0·08	168·8	+38·8	8·0	167·2	0·17	−0·13
11	193·9	−21·1	13·3	39·8	0·89	+0·09	173·1	− 1·9	1·4	132·6	0·57	−0·03
12	235·6	−34·4	19·0	35·2	0·80	+0·10	169·5	−20·5	19·0	111·3	0·72	−0·08
13	1·7	+ 6·7	3·9	35·3	0·80	+0·20	177·1	+ 7·1	6·1	59·4	0·66	−0·09
14	323·1	+ 8·1	6·4	52·5	1·10	−0·10	166·0	+11·0	7·7	44·6	0·54	−0·06
16	107·2	− 7·8	7·8	86·3	1·38	+0·18	200·0	−10·0	7·2	134·0	0·55	−0·35
17	120·8	− 1·7	1·5	62·8	1·23	−0·47	193·1	− 6·9	5·3	129·2	0·60	0·00
18	122·5	−17·5	10·5	36·9	0·83	−0·37	186·0	−14·0	12·8	113·9	0·70	+0·20
19	98·2	+48·2	8·2	10·9	0·26	+0·16	180·1	+10·1	10·0	96·2	0·77	−0·73

TABLE IVc (*cont.*)

Ko–M *stars*

Region	Drift I						Drift II					
	θ_c	$\theta_c-\theta_1$	β_1	λ_1	hV_c	hV_c-hV_1	θ_c	$\theta_c-\theta_2$	β_2	λ_2	hV_c	hV_c-hV_c
	°	°	°	°			°	°	°	°		
20	248·6	− 1·4	1·1	52·8	1·10	+0·05	166·0	− 4·0	3·8	107·1	0·74	−0·01
21	264·8	− 2·7	2·6	71·5	1·31	+0·31	163·7	+ 8·7	8·3	72·6	0·73	−0·17
22	232·7	− 7·3	7·3	92·4	1·38	+0·13	116·6	− 3·4	0·9	164·3	0·21	−0·09
23	224·3	+ 9·3	9·1	77·9	1·35	+0·15	149·4	+39·4	15·8	154·6	0·33	−0·12
24	229·0	− 1·0	0·9	64·6	1·25	+0·25	161·4	−23·6	15·8	137·0	0·53	−0·07
25	52·5	− 2·5	1·6	39·6	0·88	+0·13	186·0	+ 6·0	5·5	65·5	0·70	0·00
26	50·3	−14·7	12·3	56·8	1·16	+0·31	191·1	+ 6·1	4·3	45·5	0·55	−0·05
27–36	33·3	− 6·7	6·2	67·2	1·28	−0·22	191·3	−18·7	9·0	29·2	0·38	+0·28
28	105·1	+ 0·1	0·1	80·8	1·37	−0·33	195·7	+10·7	9·7	115·4	0·70	+0·15
29	103·0	+ 5·5	4·6	56·7	1·16	−0·04	191·3	− 3·7	3·6	100·8	0·76	+0·16
30	81·0	+16·0	9·3	35·8	0·81	−0·69	186·8	+16·8	16·7	84·5	0·77	+0·17
31	254·2	− 3·3	3·2	78·9	1·36	−0·04	163·4	+13·4	12·6	110·5	0·72	+0·02
32	258·8	+ 3·8	3·7	74·3	1·33	+0·43	164·5	+ 4·5	4·5	91·6	0·77	−0·13
33	254·6	+ 9·6	9·6	90·3	1·38	+0·18	158·0	+28·0	19·7	134·1	0·55	+0·05
34	86·1	+ 6·1	5·3	59·4	1·19	+0·19	192·6	− 2·4	2·3	72·4	0·73	−0·17
35	91·2	− 8·8	8·5	76·0	1·34	+0·04	199·1	+ 4·1	3·2	50·8	0·60	0·00
37	99·3	− 0·7	0·7	79·5	1·36	+0·01	194·7	+ 4·7	4·7	86·0	0·77	+0·22

TABLE IVd

A5–M *stars*

Region	Drift I						Drift II					
	θ_c	$\theta_c-\theta_1$	β_1	λ_1	hV_c	hV_c-hV_1	θ_c	$\theta_c-\theta_2$	β_2	λ_2	hV_c	hV_c-hV_c
	°	°	°	°			°	°	°	°		
1	266·6	−18·4	3·6	11·4	0·30	−0·20	176·5	+ 1·5	1·5	100·1	0·79	−0·11
2	307·6	+ 2·6	1·7	40·7	0·98	+0·08	169·3	−10·7	9·9	68·3	0·74	+0·14
3	280·6	− 1·9	1·8	72·0	1·43	−0·47	151·5	−38·5	24·5	41·9	0·53	+0·13
4	117·9	− 4·6	4·6	85·2	1·49	+0·09	219·8	− 0·2	0·1	151·5	0·38	−0·12
5	147·8	+ 2·8	2·5	61·5	1·32	−0·18	200·7	−19·3	8·9	151·9	0·38	−0·12
6	166·7	+ 6·7	4·2	38·8	0·94	−0·36	184·7	−20·3	13·5	137·5	0·54	+0·14
7	277·5	+ 2·5	1·7	41·3	0·99	+0·09	167·2	+12·2	12·2	85·7	0·80	−0·15
8	273·9	+ 6·4	6·0	69·6	1·41	−0·19	158·2	− 6·8	5·9	59·5	0·69	+0·09
9–15	98·8	+ 3·8	3·8	98·0	1·49	−0·21	239·7	−25·3	9·6	157·0	0·31	+0·01
10	181·6	+ 1·6	1·5	71·9	1·43	−0·07	178·6	+68·6	7·7	171·8	0·11	−0·14
11	198·1	+ 3·1	2·0	39·6	0·96	+0·16	174·7	− 5·3	3·6	137·4	0·54	+0·04
12	239·3	−10·7	6·4	36·9	0·90	+0·10	168·9	− 6·1	5·5	116·2	0·72	−0·08
13	357·3	+ 2·3	1·4	36·2	0·89	−0·01	179·8	− 5·2	4·7	63·8	0·72	+0·07
14	320·5	+ 3·0	2·4	54·2	1·22	−0·18	166·9	− 3·1	2·4	49·4	0·61	+0·06
16	108·3	− 1·7	1·7	83·7	1·49	−0·26	205·9	+ 5·9	4·4	131·8	0·60	−0·05
17	121·9	− 0·6	0·5	60·2	1·30	−0·20	199·5	− 5·5	4·2	129·6	0·62	+0·02
18	123·6	− 6·4	3·6	34·2	0·84	−0·16	190·7	+ 0·7	0·6	116·4	0·71	+0·11
19	94·1	+74·1	8·0	8·3	0·22	+0·12	183·2	+13·2	13·0	100·1	0·79	−0·61
20	250·7	− 4·3	3·5	54·9	1·23	+0·03	163·7	−16·3	15·2	111·5	0·74	+0·14
21	264·9	− 0·1	0·1	74·2	1·44	+0·14	160·3	+ 5·3	5·1	76·3	0·78	−0·02
22	235·4	− 4·6	4·6	92·0	1·50	+0·20	98·9	+18·9	5·3	163·6	0·23	−0·17
23	227·0	+ 4·5	4·4	78·1	1·47	+0·07	140·1	− 9·9	3·7	157·9	0·30	0·00
24	231·9	+ 1·9	1·7	65·5	1·36	+0·36	157·3	+17·3	10·8	141·2	0·50	−0·10
25	48·5	− 1·5	0·9	38·8	0·94	+0·34	190·3	+ 0·3	0·3	68·5	0·74	−0·26
26	47·1	− 7·9	6·6	56·7	1·25	+0·10	196·7	+ 6·7	5·0	48·3	0·60	+0·05
27–36	30·4	− 4·6	4·3	67·8	1·39	−0·41	197·9	−22·1	11·8	32·8	0·43	+0·13
28	105·2	− 2·3	2·2	78·0	1·47	+0·07	200·9	− 9·1	8·3	113·8	0·73	−0·17
29	102·3	− 0·2	0·2	54·0	1·21	+0·11	196·3	+ 1·3	1·3	101·4	0·78	−0·12
30	78·0	+13·0	7·2	33·7	0·83	−0·02	191·0	+11·0	11·0	86·9	0·80	+0·05
31	256·0	− 4·0	4·0	81·0	1·48	−0·02	159·1	+ 4·1	3·8	113·4	0·73	−0·02
32	259·8	+ 4·8	4·7	76·8	1·46	+0·16	160·8	+ 5·8	5·8	94·8	0·80	+0·05
33	257·1	+ 2·1	2·1	91·4	1·50	+0·30	151·4	+21·4	14·8	135·7	0·56	+0·06
34	83·8	+ 3·8	3·2	57·6	1·27	−0·03	197·7	+12·7	12·2	73·2	0·76	+0·21
35	88·6	− 1·4	1·4	74·9	1·45	+0·10	205·5	+ 0·5	0·4	50·7	0·62	+0·07
37	98·1	− 1·9	1·9	77·1	1·46	+0·21	199·5	− 0·5	0·5	84·7	0·79	+0·19

TABLE IVe

Galactic Zones

Region	Drift I						Drift II					
	θ_c	$\theta_c-\theta_1$	β_1	λ_1	hV_c	hV_c-hV_1	θ_c	$\theta_c-\theta_2$	β_2	λ_2	hV_c	hV_c-hV_2
	°	°	°	°			°	°	°	°		
1	262·8	−22·2	4·0	10·8	0·32	−0·18	186·6	+11·6	11·5	98·6	0·69	−0·21
2	307·8	+ 2·8	1·8	39·7	1·09	+0·19	180·1	+ 0·1	0·1	69·8	0·66	+0·06
3	280·9	− 1·6	1·5	71·1	1·61	−0·29	163·5	−26·5	19·2	47·6	0·52	+0·12
4	117·6	− 4·9	4·9	86·2	1·70	+0·30	212·2	− 7·8	4·8	142·2	0·43	−0·07
5	147·4	+ 2·4	2·1	62·4	1·51	+0·01	207·8	−12·2	7·4	142·5	0·43	−0·07
6	165·9	+ 5·9	3·8	39·6	1·09	−0·21	196·4	− 8·6	6·4	131·6	0·52	+0·12
7	277·9	+ 2·9	1·9	41·7	1·08	+0·18	164·0	+ 9·0	8·9	81·2	0·87	−0·08
8	274·0	+ 6·5	6·1	70·0	1·52	−0·08	156·5	− 8·5	6·9	54·2	0·71	+0·11
9–15	99·0	+ 4·0	4·0	97·5	1·61	−0·09	249·4	−15·6	5·0	161·3	0·28	−0·02
10	182·0	+ 2·0	1·9	71·5	1·54	+0·04	150·9	+40·9	7·3	168·8	0·17	−0·08
11	198·7	+ 3·7	2·3	39·2	1·03	+0·23	168·1	−11·9	8·5	134·4	0·63	+0·13
12	240·1	− 9·9	5·9	37·0	0·98	+0·18	165·2	− 9·8	9·1	111·9	0·82	+0·02
13	356·8	+ 1·8	1·1	36·6	0·97	+0·07	173·9	−11·1	9·8	62·2	0·78	+0·13
14	320·3	+ 2·8	2·3	54·7	1·32	−0·08	160·9	− 9·1	6·6	46·2	0·64	+0·09
16	108·2	− 1·8	1·8	83·3	1·61	−0·14	203·8	+ 3·8	2·6	137·0	0·60	−0·05
17	121·8	− 0·7	0·6	59·7	1·40	−0·10	194·0	−11·0	8·0	133·2	0·64	+0·04
18	123·3	− 6·7	3·7	33·8	0·90	−0·10	184·7	− 5·3	4·7	117·8	0·78	+0·18
19	91·2	+71·2	7·6	8·0	0·23	+0·13	177·7	+ 7·7	7·6	99·4	0·87	−0·53
20	251·6	− 3·4	2·7	53·3	1·12	−0·08	162·8	−17·2	15·9	112·5	0·77	+0·17
21	266·5	+ 1·5	1·4	73·3	1·33	+0·03	159·2	+ 4·2	4·1	77·1	0·81	+0·01
22	234·4	− 5·6	5·6	90·6	1·39	+0·09	94·8	+14·8	4·4	162·9	0·25	−0·15
23	226·3	+ 3·8	3·7	76·5	1·35	−0·05	136·7	−13·3	4·9	158·4	0·31	+0·01
24	231·6	+ 1·6	1·4	63·7	1·25	+0·25	155·7	+15·7	9·6	142·1	0·51	−0·09
25	49·0	− 1·0	0·6	40·5	0·90	+0·30	191·3	+ 1·3	1·2	69·5	0·78	−0·22
26	47·9	− 7·1	6·0	58·3	1·18	+0·03	198·0	+ 8·0	6·1	49·2	0·63	+0·08
27–36	31·6	− 3·4	3·2	69·2	1·30	−0·50	199·1	−20·9	11·5	34·0	0·47	+0·17
28	103·6	− 3·9	3·8	78·8	1·37	−0·03	202·3	− 7·7	7·1	113·5	0·77	−0·13
29	100·6	− 1·9	1·6	55·2	1·14	+0·04	197·6	+ 2·6	2·5	101·8	0·82	−0·08
30	76·9	+11·9	6·9	35·3	0·80	−0·05	192·1	+12·1	12·1	87·8	0·84	+0·09
31	255·9	− 4·1	4·0	79·9	1·34	−0·16	153·2	− 1·8	1·7	104·1	0·63	−0·12
32	260·1	+ 5·1	4·9	75·8	1·32	+0·02	154·0	− 1·0	1·0	86·4	0·65	−0·10
33	256·6	+ 1·6	1·6	90·5	1·36	+0·16	148·3	+18·3	14·9	125·2	0·53	+0·03
34	84·1	+ 4·1	3·5	58·6	1·16	−0·14	195·5	+10·5	10·4	83·7	0·65	+0·10
35	89·1	− 0·9	0·9	75·8	1·32	−0·03	204·9	− 0·1	0·1	61·4	0·57	+0·02
37	97·9	− 2·1	2·1	78·1	1·33	+0·08	201·8	+ 1·8	1·8	95·2	0·65	+0·05

TABLE V

The Vertex of Star-Streaming

	A5–F5		F8–G5		Ko–M		A5–M	
ξ	−0·202	±0·039	−0·097	±0·046	−0·127	±0·038	−0·108	±0·030
η	+2·030	0·039	+1·825	0·045	+1·560	0·038	+1·745	0·029
ζ	+0·382	0·040	+0·561	0·048	+0·482	0·039	+0·492	0·031
α_v	275°·7	1°·2	273°·0	1°·5	274°·6	1°·5	273°·5	1°·0
δ_v	−10°·6	1°·2	−17°·1	1°·6	−17°·1	1°·5	−15°·7	1°·1
Ω	2·075	0·039	1·912	0·046	1·638	0·038	1·816	0·030
l_v	348°·6	1°·1	341°·7	1°·4	342°·4	1°·4	343°·1	1°·0
b_v	−1°·2	1°·1	−2°·0	1°·5	−3°·4	1°·4	−1°·7	1°·0

TABLE V (*cont.*)

The Vertex of Star-Streaming

	Zone I	Zone II	Zone III	Zone IV
ξ	-0.251 ± 0.075	-0.028 ± 0.046	-0.141 ± 0.055	-0.013 ± 0.094
η	$+1.857$ 0.088	$+1.876$ 0.052	$+1.671$ 0.050	$+1.618$ 0.042
ζ	$+0.350$ 0.094	$+0.564$ 0.051	$+0.569$ 0.057	$+0.356$ 0.059
α_v	$277^\circ.7$ $2^\circ.6$	$270^\circ.9$ $1^\circ.4$	$274^\circ.8$ $2^\circ.0$	$270^\circ.5$ $3^\circ.3$
δ_v	$-10^\circ.6$ $2^\circ.9$	$-16^\circ.8$ $1^\circ.6$	$-18^\circ.8$ $2^\circ.0$	$-12^\circ.4$ $2^\circ.1$
Ω	1.906 0.088	1.960 0.052	1.771 0.051	1.657 0.043
l_v	$349^\circ.6$ $2^\circ.7$	$341^\circ.0$ $1^\circ.5$	$341^\circ.0$ $1^\circ.8$	$344^\circ.6$ $2^\circ.3$
b_v	$-2^\circ.9$ $2^\circ.8$	$-0^\circ.1$ $1^\circ.5$	$-4^\circ.3$ $1^\circ.8$	$+2^\circ.4$ $2^\circ.1$

TABLE VI

The Solar Motion

	A5–F5	F8–G5	K0–M	A5–M	Zone I	Zone II	Zone III	Zone IV
$A_\odot$	$266^\circ.0$	$272^\circ.8$	$277^\circ.8$	$273^\circ.2$	$269^\circ.9$	$275^\circ.7$	$274^\circ.5$	$279^\circ.6$
$D_\odot$	$+28^\circ.1$	$+37^\circ.4$	$+40^\circ.3$	$+35^\circ.4$	$+31^\circ.9$	$+35^\circ.0$	$+34^\circ.9$	$+34^\circ.6$
$hU_\odot$	0.948	0.883	0.770	0.834	0.911	0.914	0.797	0.701
n_1/n_2	1.22	1.18	1.02	1.19	1.07	1.20	1.32	1.08

A TWO-PLATE CATADIOPTRIC SYSTEM FOR ASTRONOMICAL PHOTOGRAPHY

P. A. Wayman

(Received 1951 September 28)

Summary

It is shown that a two-plate aplanatic optical system with a single spherical mirror can be designed to give good images over a considerable field and with a smaller tube-length than is used in the classical Schmidt camera. Alternatively, an anastigmatic design with a non-spherical mirror is possible.

Wright (**1**) and Väisälä (**2**) suggested a method for overcoming the disadvantage, in the classical Schmidt camera, of great overall tube-length. The condition of zero Seidel astigmatism is abandoned and the corrector-plate at the centre of curvature of the mirror is replaced by a corrector-plate nearer to the focal surface. The curvature of the focal surface remains unchanged but the mirror has to be figured with a non-spherical profile. Primary astigmatism is then the dominant aberration and is large enough to prohibit application of this principle to systems of appreciable power. With a total tube-length of about six feet, the circle of least confusion $1\frac{1}{2}^\circ$ off-axis in a 12-in. $f/6$ system would be 50 microns in diameter. If the total tube-length is increased to eight feet the maximum image-diameter is reduced to the tolerable value of 33 microns. For systems with a focal length much less than six feet, the disadvantage of long tube-length in the classical Schmidt camera is not serious. Thus it would appear that the useful applications of the Wright–Väisälä system are definitely limited. Furthermore, there is an additional disadvantage in that the main mirror has the figure of an oblate spheroid, presenting difficulties with regard to optical testing.

With the use of two corrector-plates there will be more freedom in the optical design. The "plate-diagram" of such a system is shown in Fig. 1. (See Burch (**3**) for the original discussion of plate-diagram analysis.)

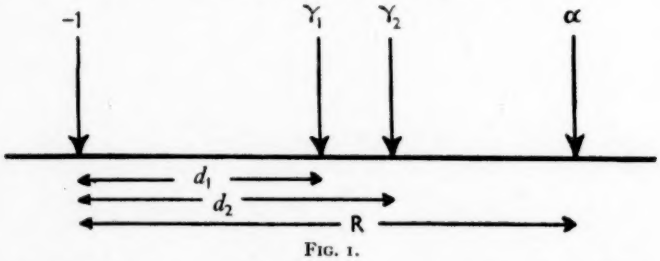

FIG. 1.

We take as unit of "strength" for the corrector-plate that of the anastigmatising plate for a spherical mirror of radius R, which we suppose to be the paraxial radius of curvature of the main mirror. γ_1 and γ_2 are the strengths of two corrector-plates, at distances d_1 and d_2 from the point which represents the

paraxial centre of curvature of the mirror. α is the strength of the figuring on the mirror in the same units. (A value $\alpha = 1$ would apply to a paraboloidal mirror and $\alpha = 0$ to a spherical mirror.)

For zero spherical aberration, in Seidel approximation, we must have

$$\alpha + \gamma_1 + \gamma_2 - 1 = 0. \tag{1}$$

For zero primary coma

$$\gamma_1 d_1 + \gamma_2 d_2 + \alpha R = 0. \tag{2}$$

The astigmatism will then be proportional to the quantity

$$A = \gamma_1 d_1^2 + \gamma_2 d_2^2 + \alpha R^2. \tag{3}$$

The Wright–Väisälä system with a total tube length $\frac{4}{3}$ times the focal length is given by

$$\gamma_2 = 0 \qquad \text{and} \qquad d_1 = \tfrac{1}{3}R.$$

The eqns. (1) and (2) require that

$$\alpha = -\tfrac{1}{2} \qquad \text{and} \qquad \gamma_1 = \tfrac{3}{2}.$$

Substituting these values in (3), we have $A = -\frac{1}{9}R^2$.

Suppose now that we consider a two-plate system with a spherical mirror also having an overall length $\frac{4}{3}$ times the focal length. The position of the first plate is given by $d_1 = \frac{1}{3}R$, and we will choose to put the second plate immediately in front of the focal surface and so will write $d_2 = \frac{1}{2}R$. Also, $\alpha = 0$ for a spherical mirror.

From (1) and (2) we have, inserting these values,

$$\gamma_1 + \gamma_2 = 1,$$

and

$$\tfrac{1}{3}\gamma_1 + \tfrac{1}{2}\gamma_2 = 0,$$

giving $\gamma_1 = 3$ and $\gamma_2 = -2$.

From (3), $A = -R^2/6$.

Thus with a spherical mirror and two corrector-plates we have less astigmatism (by a factor of two) and no greater overall length than in the one-plate Wright–Väisälä system. With a total field of 3°·75 and an aperture of 15 in. a system with a focal length of six feet could be built in which the diameter of the largest astigmatic images would be 33 microns. With an overall length of eight feet and with a spherical mirror such a system would constitute a convenient and useful instrument for objective-prism photography.

Alternatively, we can investigate the solutions of the eqns. (1), (2) and (3) with the astigmatism $A = 0$. If, as before, we take $d_1 = \frac{1}{3}R$, $d_2 = \frac{1}{2}R$ we easily obtain

$$\gamma_1 = 4{\cdot}5, \qquad \gamma_2 = -4, \qquad \alpha = 0{\cdot}5.$$

Thus an anastigmatic design is possible in which the mirror has a figuring-layer half that of a normal paraboloid, i.e. that of a prolate spheroid. This does not have the same disadvantage with regard to testing as an oblate spheroid.

Full consideration of the image-quality of these systems will be treated in a further paper, but a brief examination of the chromatic aberrations to be expected seems appropriate here.

In the case already discussed of the 15-in. $f/4{\cdot}8$ system with a spherical mirror, the on-axis chromatism need be little more than that of the corresponding classical Schmidt camera, since the "strengths" of the two plates partly compensate one another. Off the axis there would be a slight "shearing" of the plates which

would lead to a small asymmetrical colour-error. Now the maximum plate-slope of a corrector-plate determines the greatest amount of lateral chromatic aberration which that plate introduces. It can easily be shown that the maximum plate-slope occurring on the first and stronger plate of the system here considered is less than that on the plate of an $f/3$ classical Schmidt camera with the same focal length, in which the colour-error is known to be satisfactorily small. Thus, even ignoring the fact that in the case of the off-axis pencils the chromatic aberrations of the two plates still compensate one another to a certain extent, it can be seen that the total chromatic aberrations need not be excessive.

In the case of the anastigmatic design with a non-spherical mirror, it is, in fact, the chromatic aberrations which will set a lower limit to the focal ratio which can be used. A detailed investigation is necessary in order to show exactly what this limit is likely to be, but the considerations of the preceding paragraph, together with the fact that in this case the strengths of the plates, though larger, are more nearly equal, indicate that it will not be unduly large. Furthermore, the system is intended to be relatively inexpensive and if larger optical elements are contemplated other designs would probably be preferable.

Yerkes Observatory,
Williams Bay, Wisconsin:
1951 *September* 15.

References

(1) F. B. Wright, *P.A.S.P.*, **47**, 300, 1935.
(2) Y. Väisälä, *Astr. Nach.*, **259**, 157, 1936.
(3) C. R. Burch, *M.N.*, **102**, 159, 1942.

THE VELOCITY DISTRIBUTION OF SPORADIC METEORS. II

Mary Almond, J. G. Davies and A. C. B. Lovell

(Communicated by A. C. B. Lovell)

(Received 1951 September 28)

Summary

The work on the velocity distribution of sporadic meteors described in Part I has been extended to fainter meteors. The results are similar and give no evidence for a significant hyperbolic velocity component. A fuller discussion of the magnitude range is given and it is concluded that the majority of meteors in these new experiments were probably in the magnitude range 6·0 to 7·5.

---

1. *Introduction.*—Part I of these papers* gave an account of the application of the radio echo technique to the study of the velocity distribution of sporadic meteors. In this paper the extension of the work to fainter meteors is described. An alternative method of estimating the magnitude range leads to more definite information regarding the meteor magnitudes covered by the series of experiments.

2. *Apparatus.*—The apparatus was basically similar to the 8·13 metre apparatus described in Part I. The aerial system was fixed to produce a beam at an elevation of 10° with its main axis in an easterly direction (azimuth 90°) as before, but its gain was increased by the addition of more elements.

The parameters of the apparatus were as follows:—

Wave-length		$\lambda = 8{\cdot}13$ metres
Peak transmitter power		$P = 240$ kW
Aerial beam width to half power	Azimuth	$= \pm 12°$
	Elevation	$= \pm 5°$
Aerial power gain over isotropic source		$G = 36{\cdot}6$
Receiver noise level		$\epsilon_0 = 1{\cdot}3 \times 10^{-13}$ watts

The additional sensitivity over the apparatus described in Part I was achieved by increases in transmitter power P and aerial gain G. The apparatus and technique for velocity measurement remained the same.

With this equipment two series of experiments were carried out: (i) during the autumn mornings of 1950 (apex experiment), (ii) during the spring evenings of 1951 (antapex experiment).

3. *The 1950 apex experiment.*—Due to the specular reflection properties of meteor trails† an infinitely narrow beam directed at azimuth 90° at 06^h would record only those meteors lying in a great circle plane through the apex of the Earth's way, cutting the horizon in the north and south. The meteors recorded

* Almond, Mary, Davies, J. G. and Lovell, A. C. B., *M.N.*, **111**, 585, 1951.

† Hey, J. S. and Stewart, G. S., *Proc. Phys. Soc.*, **59**, 858, 1947. Lovell, A. C. B., Banwell, C. J. and Clegg, J. A., *M.N.*, **107**, 164, 1947.

by a beam of finite width, such as that used in the present experiments, will be those whose radiants lie between two small circle planes enclosing the apex. It is desirable to carry out such an experiment when the apex is in the neighbourhood of its greatest altitude so that the sporadic meteor rates are a maximum. The first experiment was therefore made between the hours of approximately 05^h and 07^h in the autumn mornings. The details of the experiment which was carried out between 1950 November 8 and 1950 December 14 are given in Table I. In 10·7 hours of observation 335 velocity measurements were made. The times and details of these measurements are given in Table II and the number distribution of velocities in Fig. 1.

TABLE I

Details of apex experiment; autumn 1950
(*Wave-length* 8·13 *m*)

Date 1950	Limits of watch U.T.	Total time	No. of echoes	Hourly rate	No. of velocities
	h m h m	h m			
Nov. 8	05 00–06 48	1 48	600	333	80
11	05 00–07 00	2 00	344	172	39
17	05 00–05 20	0 20	29	87	6
18	05 00–07 00	2 00	564	282	63
23	05 03–07 08	2 05	570	274	60
25	05 07–07 10	2 03	653	319	80
Dec. 14	05 47–06 14	0 27	64	142	7
	Totals	10 43	2824	264	335

The velocity distribution to be expected under such conditions, on the assumption that the meteors are moving at the parabolic velocity limit and in random directions, has been calculated by Clegg.* This calculation takes into account the shape of the aerial beam and the altitude of the apex, and the result for the specific conditions of this experiment is shown in Fig. 1 with the measured distribution. The experimental errors of measurement have been combined with the theoretical distribution as described in Part I.

There is no sign of a hyperbolic velocity component, but in view of criticisms† that limitations of technique were responsible for the high-velocity cut-off, a further experiment on the antapex was carried out as in Part I.

4. *The* 1951 *antapex experiment.*—The experiment described above was repeated between the hours of approximately 17^h and 19^h from 1951 March 29 to May 18. At these times the antapex occupies the position in the sky previously taken by the apex. In 56·5 hours of observation 57 velocity measurements were made. The details of the experiment are given in Table III and of the measured velocities in Table IV. The velocity distribution is shown in Fig. 2, together with the theoretical distribution calculated as before by the method described by Clegg.* There is again no sign of any hyperbolic velocity component, and it is evident from a comparison of Figs. 1 and 2 that instrumental cut-off, even if it existed, could not be responsible for the low velocity distribution observed in the antapex experiment.

* Clegg, J. A., *M.N.*, **112**, No. 4, 1952.
† Öpik, E. J., *Irish Astr. J.*, **1**, 80, 1950.

TABLE II

Data for velocity measurements during apex experiment; autumn 1950

Date 1950	Time U.T.	Velocity $V \pm dV$ km/sec	Range R km	Amplitude A (Signal to noise ratio)	$\gamma = \frac{AR^{3/2}}{G}$ (R in units of 95 km)	Electron line density (α) $\times 10^{10}$ electrons/cm path
1	2 h m	3	4	5	6	7
Nov. 8	05 03	49·8 ± 2·1	670	11	11·2	40·1
	05 07	50·5 ± 2·4	320	11	6·1	21·8
	05 13	69·6 ± 1·7	830	13	54·0	193·0
	05 08	43·0 ± 2·0	435	10	3·4	12·2
	05 12	53·4 ± 4·6	420	6	2·1	7·5
	05 14	60·3 ± 2·3	540	15	7·1	25·4
	05 14	49·8 ± 2·5	595	10	6·2	22·2
	05 15	41·6 ± 1·9	335	13	6·2	22·2
	05 16	25·7 ± 1·4	335	12	5·7	20·4
	05 16	41·2 ± 2·9	540	12	5·7	20·4
	05 17	53·9 ± 4·3	690	14	1·6	5·7
	05 22	51·2 ± 3·9	550	12	6·0	21·5
	05 25	57·8 ± 2·1	580	14	7·9	28·3
	05 28	53·2 ± 3·4	350	14	6·1	21·8
	05 28	58·8 ± 2·0	380	15	5·6	20·0
	05 29	55·0 ± 1·9	440	14	4·9	17·5
	05 30	54·0 ± 1·3	490	14	5·5	19·7
	05 30	54·5 ± 3·2	310	10	6·2	22·2
	05 31	55·2 ± 1·4	410	15	5·2	18·6
	05 32	60·3 ± 3·6	500	14	5·7	20·4
	05 33	62·5 ± 3·0	355	11	4·6	16·5
	05 34	53·8 ± 2·6	270	12	...	...
	05 34	37·8 ± 1·9	530	9	4·1	14·7
	05 35	63·0 ± 3·7	425	13	4·5	16·1
	05 35	61·2 ± 3·7	365	12	4·8	17·2
	05 36	48·3 ± 4·1	490	13	5·1	18·3
	05 40	57·8 ± 4·8	520	12	5·3	19·0
	05 41	63·2 ± 2·6	370	14	5·4	19·3
	05 42	64·6 ± 6·6	390	9	3·2	11·5
	05 42	66·1 ± 3·7	520	12	5·2	18·6
	05 45	53·2 ± 2·0	410	Sat.	>5·2	>18·6
	05 46	51·3 ± 1·8	770	8	17·0	61·0
	05 46	72·6 ± 2·8	620	12	8·9	31·8
	05 46	61·2 ± 2·3	395	11	3·9	14·0
	05 48	54·7 ± 2·1	405	14	4·8	17·2
	05 49	39·7 ± 1·3	275	13	23·0	82·0
	05 50	63·5 ± 2·7	500	11	4·4	15·8
	05 51	72·8 ± 2·6	430	13	4·5	16·1
	05 51	70·3 ± 2·6	495	15	6·0	21·5
	05 52	62·1 ± 3·6	425	9	3·1	11·1
	05 52	27·5 ± 1·6	290	6	5·0	17·9
	05 53	68·0 ± 3·0	495	13	4·5	16·1
	05 54	54·2 ± 2·7	585	12	7·2	25·8
	05 54	58·4 ± 3·1	340	14	6·4	22·9
	05 55	72·6 ± 2·8	495	14	5·6	20·0
	05 55	56·1 ± 3·9	320	13	7·2	25·8
	05 55	63·5 ± 2·9	555	14	7·2	25·8
	05 57	60·1 ± 2·5	600	12	7·7	27·6
	06 02	57·5 ± 2·7	430	14	4·8	17·2
	06 03	25·4 ± 1·2	135	13	...	...

TABLE II (*cont.*)

Date 1950	Time U.T.	Velocity $V \pm dV$ km/sec	Range R km	Amplitude A (Signal to noise ratio)	$\gamma = \frac{AR^{3/2}}{G}$ (R in units of 95 km)	Electron line density (α) $\times 10^{10}$ electrons/cm path
1	2 h m	3	4	5	6	7
Nov. 8	06 04	63·1 ± 3·7	580	11	6·3	22·6
	06 05	70·8 ± 3·8	635	14	11·2	40·0
	06 05	69·0 ± 4·7	390	13	4·6	16·5
	06 09	60·1 ± 4·0	410	14	4·8	17·2
	06 10	60·1 ± 2·7	620	13	9·6	34·4
	06 10	43·2 ± 1·9	500	12	4·8	17·2
	06 10	59·4 ± 3·4	390	13	4·6	16·5
	06 13	63·3 ± 2·2	430	15	5·2	18·6
	06 15	51·2 ± 3·5	310	13	8·1	29·0
	06 17	43·5 ± 1·8	405	11	3·8	13·6
	06 20	58·7 ± 5·8	660	13	12·4	44·4
	06 21	59·2 ± 2·8	315	13	7·4	26·5
	06 22	66·8 ± 2·5	585	14	8·2	29·4
	06 23	29·7 ± 1·0	410	13	4·5	16·1
	06 26	63·1 ± 3·9	625	13	10·0	35·8
	06 27	28·5 ± 1·2	95	8	...	...
	06 27	59·2 ± 2·4	375	14	5·3	19·0
	06 29	70·2 ± 3·5	730	12	18·5	66·4
	06 29	56·9 ± 3·7	385	15	5·4	19·3
	06 32	62·1 ± 3·5	590	14	8·7	31·2
	06 32	60·5 ± 2·3	360	13	5·3	19·0
	06 34	53·4 ± 2·4	395	15	5·3	19·0
	06 34	64·0 ± 4·3	340	14	6·4	22·9
	06 35	53·7 ± 2·7	430	14	4·8	17·2
	06 36	68·6 ± 4·7	370	10	3·8	13·6
	06 39	55·2 ± 3·1	330	13	6·5	23·3
	06 40	68·8 ± 7·9	390	15	5·4	19·3
	06 44	59·2 ± 3·9	400	6	2·1	7·5
	06 45	64·6 ± 2·7	350	13	5·7	20·4
	06 46	58·6 ± 2·3	330	14	7·0	25·0
Nov 11	05 18	55·4 ± 2·0	405	14	4·8	17·2
	05 20	47·6 ± 2·8	600	14	9·0	32·2
	05 21	25·6 ± 2·0	120	8	...	...
	05 25	68·9 ± 4·6	390	12	4·3	15·4
	05 26	71·6 ± 3·2	370	14	5·4	19·3
	05 29	47·0 ± 2·2	645	11	9·6	34·4
	05 34	54·7 ± 2·2	340	14	6·4	22·9
	05 36	55·4 ± 3·4	395	15	5·3	19·0
	05 37	59·1 ± 4·7	840	11	69·0	247·0
	05 38	58·2 ± 2·0	380	14	5·2	18·6
	05 39	49·0 ± 2·4	340	13	5·9	21·1
	05 43	62·5 ± 2·6	330	13	6·5	23·2
	05 55	64·5 ± 2·5	650	14	12·7	45·5
	05 58	57·2 ± 3·4	450	14	5·0	17·9
	06 00	40·9 ± 2·9	125	12	...	...
	06 03	57·7 ± 6·3	420	9	3·1	11·1
	06 04	51·5 ± 2·7	410	14	4·8	17·2
	06 09	53·4 ± 4·4	630	10	8·0	28·6
	06 09	47·5 ± 4·9	650	8	7·3	26·2
	06 10	49·5 ± 2·3	330	14	7·0	25·1
	06 12	60·7 ± 3·1	680	12	13·3	47·6

TABLE II (*cont.*)

Date 1950	Time U.T.	Velocity $V \pm dV$ km/sec	Range R km	Amplitude A (Signal to noise ratio)	$\gamma = \frac{AR^{3/2}}{G}$ (R in units of 95 km)	Electron line density (α) $\times 10^{10}$ electrons/cm path
1	2 h m	3	4	5	6	7
Nov. 11	06 12	61·8 ± 3·4	450	9	3·2	11·5
	06 12	57·2 ± 4·7	540	8	3·8	13·6
	06 14	52·4 ± 2·5	445	11	3·9	14·0
	06 14	63·0 ± 3·7	410	11	3·8	13·6
	06 16	49·3 ± 3·1	340	14	6·4	22·9
	06 18	52·8 ± 2·0	360	13	5·3	19·0
	06 19	62·1 ± 3·5	600	12	7·8	28·0
	06 22	61·1 ± 2·6	370	13	5·0	17·9
	06 23	48·1 ± 4·2	620	11	8·1	29·0
	06 24	54·9 ± 2·7	365	12	4·8	17·2
	06 25	61·4 ± 4·0	430	12	4·1	14·7
	06 28	62·9 ± 2·1	435	14	4·8	17·2
	06 29	55·8 ± 2·8	620	11	8·1	29·0
	06 33	62·5 ± 1·8	850	12	80·0	286·0
	06 34	59·8 ± 3·3	440	10	3·5	12·5
	06 34	55·1 ± 3·1	350	10	4·3	15·4
	06 36	56·8 ± 3·2	500	12	4·8	17·2
	06 37	47·0 ± 2·6	345	12	5·3	19·0
Nov. 17	05 05	62·0 ± 3·7	390	10	3·6	12·9
	05 07	56·1 ± 3·9	570	13	7·2	25·8
	05 07	54·7 ± 2·8	630	15	11·5	41·2
	05 11	57·5 ± 2·2	360	17	6·9	24·7
	05 12	57·8 ± 1·8	560	18	9·5	34·0
	05 14	30·0 ± 1·8	125	13	...	...
Nov. 18	05 02	78·8 ± 5·1	430	9	3·1	11·1
	05 05	67·3 ± 2·2	530	13	5·9	21·1
	05 07	39·4 ± 1·7	125	11	...	...
	05 07	52·5 ± 1·9	440	12	4·2	15·0
	05 09	58·1 ± 2·3	430	11	3·8	13·6
	05 10	40·7 ± 1·4	410	10	3·4	12·2
	05 14	56·1 ± 2·9	420	9	3·1	11·1
	05 14	51·3 ± 2·3	660	10	9·5	34·0
	05 15	30·5 ± 1·7	340	8	3·6	12·9
	05 16	69·8 ± 4·1	420	12	4·1	14·7
	05 18	54·8 ± 1·4	420	12	4·1	14·7
	05 18	62·5 ± 3·6	430	6	2·1	7·5
	05 18	54·7 ± 3·1	450	10	3·6	12·9
	05 21	80·4 ± 8·1	700	6	7·5	26·8
	05 22	62·8 ± 6·0	650	10	9·1	32·6
	05 23	33·1 ± 3·2	370	8	3·1	11·1
	05 24	31·4 ± 1·5	680	11	12·2	43·7
	05 25	68·2 ± 4·2	620	11	8·1	29·0
	05 25	63·8 ± 2·7	680	12	13·3	47·6
	05 27	68·4 ± 3·2	620	10	7·4	26·5
	05 29	57·8 ± 2·1	450	10	3·6	12·9
	05 36	57·6 ± 3·2	530	11	5·0	17·9
	05 36	58·2 ± 3·4	365	10	4·0	14·3
	05 36	60·3 ± 3·0	330	9	4·5	16·1
	05 40	47·3 ± 3·7	670	8	8·4	30·0
	05 42	51·4 ± 5·1	400	12	4·2	15·0
	05 44	62·5 ± 2·7	580	12	6·8	24·4

TABLE II (*cont.*)

Date 1950	Time U.T.	Velocity $V \pm dV$ km/sec	Range R km	Amplitude A (Signal to noise ratio)	$\gamma = \frac{AR^{3/2}}{G}$ (R in units of 95 km)	Electron line density (α) $\times 10^{10}$ electrons/cm path
1	2 h m	3	4	5	6	7
Nov. 18	05 45	63·8 ± 4·0	520	9	4·0	14·3
	05 48	61·5 ± 3·0	350	9	3·9	14·0
	05 49	52·8 ± 2·4	375	9	3·5	12·5
	05 51	70·1 ± 2·8	640	12	10·0	35·8
	05 53	26·6 ± 1·9	440	7	2·5	8·9
	05 54	35·2 ± 1·7	350	10	4·3	15·4
	05 55	28·0 ± 0·9	120	8	...	...
	05 56	59·8 ± 4·1	370	8	3·1	11·1
	05 57	41·0 ± 2·0	430	11	3·8	13·6
	06 00	59·9 ± 6·1	380	8	3·0	10·7
	06 02	50·9 ± 2·5	530	9	4·1	14·7
	06 03	48·2 ± 2·1	360	10	4·1	14·7
	06 04	58·8 ± 6·1	495	10	4·0	14·3
	06 06	55·9 ± 5·4	370	9	3·5	12·5
	06 06	53·1 ± 3·0	320	7	3·9	14·0
	06 08	55·5 ± 5·9	410	7	2·4	8·6
	06 10	47·9 ± 2·5	430	10	3·4	12·2
	06 10	75·3 ± 4·2	680	9	10·0	35·8
	06 15	48·4 ± 2·5	330	13	6·5	13·3
	06 20	57·4 ± 6·2	410	8	2·8	10·0
	06 28	64·6 ± 6·0	520	9	3·9	14·0
	06 34	57·3 ± 2·7	430	10	3·4	12·2
	06 36	50·2 ± 2·9	380	11	4·1	14·7
	06 38	61·7 ± 6·7	360	10	4·1	14·7
	06 39	35·9 ± 1·5	370	11	4·2	15·0
	06 40	64·1 ± 3·7	600	12	8·0	28·6
	06 40	61·7 ± 4·5	350	8	3·5	12·5
	06 42	69·6 ± 9·4	495	12	4·8	17·2
	06 43	68·4 ± 5·5	335	12	5·7	20·4
	06 44	60·1 ± 5·6	450	12	4·3	15·4
	06 44	56·5 ± 3·5	420	12	8·9	31·9
	06 46	43·6 ± 8·7	380	6	2·2	7·9
	06 47	59·9 ± 5·9	380	11	4·1	14·7
	06 49	73·8 ± 4·2	850	7	46·0	165·0
	06 51	63·3 ± 7·0	610	11	7·6	27·2
	06 52	46·3 ± 2·4	490	11	4·3	15·4
Nov. 23	05 03	41·3 ± 1·8	320	12	6·7	24·0
	05 09	32·7 ± 2·0	140	12	...	...
	05 10	56·8 ± 2·3	350	13	5·6	20·0
	05 10	69·3 ± 2·9	600	12	7·8	28·0
	05 12	63·5 ± 3·3	435	10	3·4	12·2
	05 14	51·6 ± 2·4	500	6	2·4	8·6
	05 23	49·0 ± 3·8	440	11	3·9	14·0
	05 25	39·7 ± 2·2	350	6	2·6	9·3
	05 29	49·2 ± 1·2	500	10	4·0	14·3
	05 30	60·4 ± 2·5	625	10	7·7	27·6
	05 33	58·9 ± 4·1	440	8	2·8	10·0
	05 38	36·6 ± 2·4	490	11	4·3	15·4
	05 41	69·0 ± 7·3	640	9	7·5	26·8
	05 43	43·6 ± 2·1	350	12	4·8	17·2
	05 45	66·6 ± 3·4	615	10	7·1	25·4

TABLE II (*cont.*)

Date 1950	Time U.T.	Velocity $V \pm dV$ km/sec	Range R km	Amplitude A (Signal to noise ratio)	$\gamma = \frac{AR^{3/2}}{G}$ (R in units of 95 km)	Electron line density (α) $\times 10^{10}$ electrons/cm path
1	2 h m	3	4	5	6	7
Nov. 23	05 45	61·7 ± 6·6	500	11	4·4	15·8
	05 50	66·2 ± 3·2	680	12	13·3	44·7
	05 55	57·8 ± 3·3	350	13	5·6	20·0
	05 58	49·0 ± 2·3	460	12	4·4	15·8
	06 00	60·9 ± 3·2	680	6	6·7	24·0
	06 01	63·2 ± 6·6	405	8	2·8	10·0
	06 01	55·0 ± 1·6	440	13	4·6	16·5
	06 09	63·3 ± 2·6	420	11	3·8	13·6
	06 10	41·7 ± 4·2	550	11	5·5	19·7
	06 18	59·5 ± 3·0	290	11	9·1	32·6
	06 20	58·5 ± 5·5	840	7	35·0	125·0
	06 21	42·5 ± 1·5	500	12	4·9	17·5
	06 22	49·8 ± 2·8	360	12	4·9	17·5
	06 25	71·5 ± 4·6	495	12	4·8	17·2
	06 26	50·8 ± 1·9	495	13	5·2	18·6
	06 26	64·5 ± 3·3	360	12	4·9	17·5
	06 32	62·1 ± 3·1	445	14	4·9	17·5
	06 33	39·8 ± 3·8	660	12	11·4	40·8
	06 33	64·0 ± 3·0	410	12	4·1	14·7
	06 38	52·3 ± 2·2	330	14	7·0	25·0
	06 41	63·0 ± 3·6	360	14	5·7	20·4
	06 47	43·9 ± 2·4	330	10	5·0	17·9
	06 48	62·5 ± 1·5	400	14	4·9	17·5
	06 48	60·8 ± 1·0	420	14	4·8	17·2
	06 50	46·2 ± 1·5	350	13	5·7	20·4
	06 52	24·9 ± 1·3	350	6	2·6	9·3
	06 52	60·6 ± 2·7	720	7	10·0	35·8
	06 52	56·8 ± 1·9	530	13	5·5	19·7
	06 52	56·8 ± 3·4	610	8	5·5	19·7
	06 53	57·6 ± 3·5	550	13	6·5	23·3
	06 53	55·7 ± 2·9	340	14	6·4	22·9
	06 53	58·1 ± 2·6	380	9	3·3	11·8
	06 55	49·3 ± 3·5	520	8	3·5	12·5
	06 56	34·8 ± 1·9	120	14	...	...
	06 57	56·4 ± 5·6	560	8	4·2	15·0
	06 57	56·9 ± 2·0	525	13	5·9	21·1
	06 58	52·3 ± 2·6	390	9	3·2	11·5
	06 59	83·6 ± 3·9	485	13	5·0	17·9
	07 02	58·9 ± 2·7	495	13	5·2	18·6
	07 02	50·0 ± 5·6	655	9	8·2	29·4
	07 05	58·5 ± 6·0	350	13	5·6	20·0
	07 05	60·5 ± 2·6	350	13	5·6	20·0
	07 07	52·4 ± 5·5	800	10	28·5	104·0
	07 07	64·5 ± 2·0	430	14	4·8	17·2
	07 08	63·6 ± 3·2	340	13	6·4	22·9
Nov. 25	05 07	60·1 ± 4·0	410	10	3·4	12·2
	05 08	37·9 ± 2·2	495	9	3·6	12·9
	05 09	53·3 ± 5·1	580	10	5·7	20·4
	05 10	58·0 ± 2·2	770	10	20·0	71·6
	05 10	54·6 ± 2·4	280	8	10·0	35·8
	05 16	41·1 ± 2·3	430	10	3·4	12·2

TABLE II (*cont.*)

Date 1950	Time U.T.	Velocity $V \pm dV$ km/sec	Range R km	Amplitude A (Signal to noise ratio)	$\gamma = \frac{AR^{3/2}}{G}$ (R in units of 95 km)	Electron line density (α) $\times 10^{10}$ electrons/cm path
1	2 h m	3	4	5	6	7
Nov. 25	05 18	29·9 ± 2·0	520	10	4·3	15·4
	05 19	35·7 ± 3·6	410	6	2·1	7·5
	05 20	60·5 ± 2·1	850	10	66·5	238·0
	05 21	55·1 ± 2·1	450	10	3·6	12·9
	05 21	64·6 ± 2·2	440	11	3·8	13·6
	05 22	58·1 ± 3·2	410	9	3·1	11·1
	05 22	71·9 ± 3·4	830	7	30·5	109·0
	05 25	59·8 ± 2·5	360	10	4·1	14·7
	05 26	58·2 ± 2·9	400	13	4·5	16·1
	05 26	63·0 ± 3·4	620	10	7·4	26·5
	05 26	69·3 ± 7·4	640	10	8·3	29·7
	05 29	47·1 ± 3·7	710	6	8·0	28·6
	05 31	51·6 ± 2·1	395	11	3·5	12·5
	05 32	30·5 ± 2·2	490	9	3·5	12·5
	05 33	56·2 ± 4·7	490	9	3·5	12·5
	05 34	57·2 ± 2·3	370	11	4·2	15·0
	05 34	54·6 ± 1·9	370	10	3·8	13·6
	05 34	59·3 ± 3·5	620	10	7·4	26·5
	05 35	49·4 ± 1·7	445	9	3·2	11·5
	05 36	28·4 ± 1·6	120	11	...	...
	05 36	53·8 ± 3·0	350	8	3·4	12·2
	05 37	56·7 ± 1·8	650	10	9·1	32·6
	05 38	59·5 ± 3·2	620	10	7·4	26·5
	05 41	28·3 ± 2·4	420	10	3·4	12·2
	05 42	32·9 ± 1·8	490	8	3·1	11·1
	05 42	58·8 ± 3·0	445	10	3·5	12·5
	05 43	50·8 ± 4·5	600	10	6·4	22·9
	05 55	55·8 ± 2·6	420	10	3·4	12·2
	05 55	51·7 ± 2·1	580	7	4·0	14·3
	05 57	63·7 ± 5·0	405	11	3·8	13·6
	05 58	49·9 ± 2·7	410	10	3·4	12·2
	06 00	45·8 ± 2·3	445	10	3·5	12·5
	06 00	61·9 ± 3·5	780	10	22·2	79·5
	06 03	65·7 ± 2·1	450	10	3·6	12·9
	06 03	65·6 ± 2·4	450	10	3·6	12·9
	06 04	39·7 ± 1·8	380	10	3·7	13·2
	06 04	64·5 ± 5·6	600	8	5·2	18·6
	06 05	31·3 ± 1·9	350	9	3·8	13·6
	06 05	54·3 ± 1·8	440	10	3·5	12·5
	06 06	52·7 ± 4·6	540	9	4·3	15·4
	06 09	63·3 ± 6·7	530	8	3·6	12·9
	06 09	54·8 ± 1·9	530	10	4·5	16·1
	06 09	67·3 ± 4·8	530	11	5·0	17·9
	06 10	52·1 ± 3·1	490	11	4·3	15·4
	06 10	62·9 ± 4·8	340	11	5·0	17·9
	06 11	50·0 ± 2·4	360	10	4·1	14·7
	06 11	69·6 ± 4·3	620	10	7·4	26·4
	06 12	59·5 ± 3·6	400	10	3·4	12·2
	06 13	59·8 ± 3·7	560	10	5·1	18·3
	06 15	59·0 ± 5·7	410	9	3·1	11·1
	06 17	47·2 ± 2·0	450	8	2·9	10·4

TABLE II (*cont.*)

Date 1950	Time U.T.	Velocity $V \pm dV$ km/sec	Range R km	Amplitude A (Signal to noise ratio)	$\gamma = \frac{AR^{3/2}}{G}$ (R in units of 95 km)	Electron line density (α) $\times 10^{10}$ electrons/cm path
1	2 h m	3	4	5	6	7
Nov. 25	06 19	49·9 ± 5·0	370	9	3·5	12·5
	06 19	55·5 ± 4·8	445	10	3·5	12·5
	06 20	50·7 ± 2·4	390	10	3·6	12·9
	06 22	55·9 ± 4·9	620	10	7·4	26·4
	06 23	62·3 ± 2·5	500	11	4·4	15·7
	06 25	53·5 ± 2·3	330	10	5·0	17·9
	06 25	46·8 ± 2·9	490	10	3·9	14·0
	06 29	49·4 ± 1·9	360	10	4·1	14·7
	06 33	61·5 ± 5·7	660	10	9·5	34·0
	06 38	41·4 ± 3·1	120	10	...	...
	06 39	53·4 ± 2·0	390	11	3·9	14·0
	06 39	67·6 ± 2·7	410	11	3·8	13·6
	06 43	45·6 ± 2·4	330	10	4·9	17·5
	06 45	34·2 ± 3·3	410	10	3·4	12·2
	06 53	50·9 ± 1·4	440	10	3·5	12·5
	06 55	57·1 ± 4·9	600	10	6·7	24·0
	06 58	48·2 ± 4·3	430	8	3·0	10·7
	06 59	59·8 ± 2·0	400	10	3·4	12·2
	07 00	60·7 ± 4·9	370	9	3·5	12·5
	07 01	56·5 ± 5·1	330	11	5·5	19·7
	07 05	45·0 ± 2·4	390	10	3·6	12·9
	07 08	63·1 ± 3·6	450	10	3·6	12·9
	07 10	32·3 ± 2·2	330	10	5·0	17·9
Dec. 14	05 55	69·2 ± 2·1	610	15	10·3	36·9
	05 58	54·3 ± 3·0	330	16	8·0	28·6
	06 00	40·4 ± 5·7	310	15	9·4	33·6
	06 00	34·8 ± 1·4	140	14	...	...
	06 07	58·9 ± 2·8	560	10	5·3	19·0
	06 07	36·8 ± 3·9	130	14	...	...
	06 09	30·0 ± 0·7	120	16	...	...

5. *The discrepancy between the theoretical and experimental distributions.*— Although Figs. 1 and 2 show satisfactorily that there can be no appreciable number of meteors with velocities in excess of the parabolic limit, there is, nevertheless, a marked discrepancy between the theoretical and experimental curves; the experimental distributions lying at much lower velocities than those predicted by the theory. A similar discrepancy was remarked upon in Part I in connection with the antapex distribution. Since the publication of Part I an error has been found in the method of summation used to obtain the theoretical distributions. The correct theoretical distributions are similar to those used in the present paper. Although the theoretical distribution for the antapex is not changed appreciably, that for the apex shows a much greater concentration near the parabolic limit. Hence, in the case of the apex results of Part I the experimental distributions also lie at much lower velocities than those predicted by theory.

Thus in all the experiments described in Parts I and II the results not only show the absence of hyperbolic velocities, but also indicate that a large proportion of sporadic meteors must have relatively short-period orbits.

6. *The influence of meteors from the helion and antihelion points on the measured distribution.*—A number of meteors included in Tables II and IV were observed at ranges less than about 250 km. These represent meteors which are not observed in the main beam of the aerial system and are not therefore included in

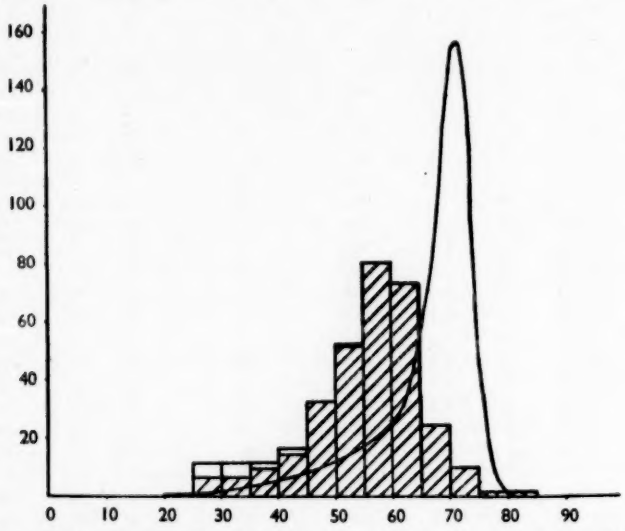

FIG. 1.—*The measured velocity distribution (histogram) for the 1950 apex experiment. The non-hatched areas show the influence of the antihelion component. The theoretical distribution, calculated on the assumption of uniformly distributed parabolic meteors, is shown in the smooth curve. The theoretical curve is normalized to the equivalent number of observations.*
Ordinates : number of meteors.
Abscissae : velocity in km/sec.

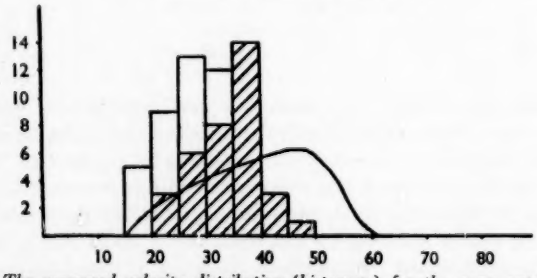

FIG. 2.—*The measured velocity distribution (histogram) for the 1951 antapex experiment. The non-hatched areas show the influence of the helion component. The theoretical distribution, calculated on the assumption of uniformly distributed parabolic meteors, is shown in the smooth curve. The theoretical curve is normalized to the equivalent number of (hatched) observations.*
Ordinates : number of meteors.
Abscissae : velocity in km/sec.

the theoretical distribution. Since these meteors are observed in a lobe of the aerial beam at high elevation in an easterly direction their most probable radiant is low in the west; that is, from the antihelion point in the apex experiment, and from the helion point in the antapex experiment. Marked concentrations of activity from these regions have been observed in the radio echo survey of the

sporadic activity.* For a true comparison with the theoretical velocity distribution this short-range component must be subtracted from the main distribution. Table II (apex) contains 15 of these short-range meteors out of 335 total. The influence of this antihelion component in the apex distribution, illustrated in Fig. 1, is therefore very small. In the case of the antapex experiment Table IV contains 22 short-range meteors out of 57 total, and the influence of this helion component on the antapex distribution is marked, as shown in Fig. 2. Similar adjustments apply to the distributions measured in Part I. It is evident that the removal of these components from the velocity distribution in no way affects the conclusions reached about the non-existence of hyperbolic velocities. As regards the helion and antihelion components shown in Figs. 1 and 2, calculations show that the most probable heliocentric velocity is also non-hyperbolic.

7. *The magnitude range.*—In Part I the magnitude range of the meteors was estimated by computation of the electron densities in the trails, followed by a conversion of these densities to visual meteor magnitudes. This process is repeated for the present data obtained with more sensitive equipment. In addition, alternative estimates from a comparison of the visual and radio echo rates are made both for the previous results in Part I and for the measurements described in this paper.

(a) *Magnitude estimates from electron densities in the trails.*—For a received signal of strength ϵ, and for an apparatus with parameters: wave-length (λ), transmitter power (P) and aerial gain (G), the line density of electrons in a meteor trail at range R is given by †

$$\alpha = \sqrt{12\pi}\left(\frac{mc^2}{e^2}\right)\frac{1}{G}\sqrt{\frac{\overline{\epsilon R^3}}{P\lambda^3}} \text{ electrons/cm path.} \qquad (1)$$

This only applies to a trail where the volume density is less than the critical density for the radio wave-length employed. Discussions of the situation which arises for higher electron densities have been given by Herlofson‡, Feinstein§, and Kaiser and Closs.‖ From their results it is evident that for the electron densities with which we are concerned in this work, no appreciable error will be introduced by using equation (1) to compute the line densities from the measured signal strengths.

As in Part I a quantity $\gamma = AR^{3/2}/G$ is calculated for each meteor and is given in column 6 of Tables II and IV. Here, A is the amplitude of the radio echo from the first Fresnel zone compared with the receiver noise level, R the range of the meteor and G the effective gain of the aerial system. G depends on the range R and on the azimuth of the meteor with respect to the main beam of the aerial system. The method of computing γ is described in the Appendix to Part I. The only additional information required in this paper is the appropriate sensitivity-range curve for the modified aerial system, which is given in Fig. 5.

The line density α for each meteor is then calculated from

$$\alpha = \sqrt{12\pi}\left(\frac{mc^2}{e^2}\right)\gamma\sqrt{\frac{\overline{\epsilon_0}}{P\lambda^3}},$$

---

* Hawkins, G. S. and Aspinall, A. (unpublished).

† Lovell, A. C. B. and Clegg, J. A., *Proc. Phys. Soc.*, **60**, 491, 1948.

‡ Herlofson, N., *The Observatory*, **68**, 230, 1948; *Arkiv för Fysik*, **3**, 247, 1951.

§ Feinstein, J., *J. Geophys. Res.*, **56**, 37, 1951.

‖ Kaiser, T. and Closs, R. L., *Phil. Mag.*, **43**, 1, 1952.

TABLE III

Details of antapex experiment; spring 1951
(*Wave-length* 8·13 *m*)

Date 1951	Limits of watch U.T.	Total time	No. of echoes	Hourly rate	No. of velocities
	h m h m	h m			
Mar. 29	17 16–17 50	0 34	6	10·6	0
30	17 00–18 58	1 58	27	13·7	0
31	17 03–18 58	1 55	15	7·8	0
Apr. 2	17 10–18 54	1 10	3	2·6	0
4	17 15–18 58	1 43	32	18·6	4
5	17 08–19 02	1 47	21	11·8	2
6	17 00–19 00	2 00	13	6·5	0
9	17 00–19 03	1 55	21	11·0	1
10	17 00–18 57	1 57	19	9·7	1
11	17 21–19 00	1 39	22	13·3	1
12	17 04–19 00	1 31	9	5·9	0
13	17 19–19 03	1 44	49	28·2	6
14	17 10–19 02	1 10	39	33·5	0
16	17 01–18 55	1 54	19	10·0	0
17	17 00–19 00	2 00	75	37·5	3
18	17 00–19 00	1 44	35	20·2	1
19	17 00–19 00	2 00	109	54·5	3
20	17 00–19 00	2 00	71	35·5	0
21	17 28–19 00	1 32	79	51·5	2
24	17 02–18 52	1 50	83	45·3	3
25	17 01–19 01	2 00	76	38·0	4
26	17 03–19 00	1 50	75	41·0	1
May 2	17 09–19 04	1 55	61	31·8	3
3	18 23–19 00	0 37	18	29·2	0
5	17 00–19 00	2 00	86	43·0	5
6	17 17–19 00	1 43	55	32·1	0
7	17 13–19 00	1 45	38	21·7	0
9	17 00–19 05	1 49	54	29·7	3
10	17 00–19 00	1 55	104	54·2	4
11	17 37–19 00	1 14	36	29·2	1
12	17 04–19 00	1 50	60	32·7	2
14	17 32–19 00	1 28	52	35·5	0
17	17 10–19 05	1 44	93	53·7	6
18	17 45–19 00	0 40	31	46·5	1
	Totals	56 33	1586	28·0	57

TABLE IV

Data for velocity measurements during antapex experiment; spring 1951

Date 1951	Time U.T.	Velocity $V \pm dV$ km/sec	Range R km	Amplitude A (Signal to noise ratio)	$\gamma = \frac{AR^{3/2}}{G}$ (R in units of 95 km)	Electron line density (α) $\times 10^{10}$ electrons/cm path
1	2	3	4	5	6	7
	h m					
Apr. 4	17 18	37·4 ± 2·0	435	3	1·0	3·6
	17 25	35·7 ± 0·9	350	7	3·0	10·7
	17 31	35·0 ± 1·6	395	8	2·8	10·0
	18 58	35·8 ± 2·4	450	6	2·1	7·5
5	17 32	23·7 ± 1·2	140	3	...	...
	17 42	27·5 ± 2·6	395	4	1·4	5·0

TABLE IV (*cont.*)

Date 1950	Time U.T.	Velocity $V \pm dV$ km/sec	Range R km	Amplitude A (Signal to noise ratio)	$\gamma = \frac{AR^{3/2}}{G}$ (R in units of 95 km)	Electron line density (α) $\times 10^{10}$ electrons/cm path
1	2 h m	3	4	5	6	7
Apr. 9	18 40	26·5 ± 2·1	320	12	6·5	23·2
10	17 00	24·6 ± 1·9	445	6	2·1	7·5
11	18 29	34·6 ± 3·2	700	8	10·0	35·8
		27·9 ± 0·8	440	3	1·1	3·9
		36·6 ± 2·8	350	10	4·2	15·0
		18·2 ± 1·6	140	10	...	...
13	No clock	15·5 ± 1·0	110	6	...	...
		30·8 ± 1·1	450	14	5·0	17·9
		31·6 ± 1·3	100	10	...	...
17	17 10	39·6 ± 3·0	605	4	2·7	9·7
	17 23	37·6 ± 1·6	540	8	3·8	13·6
	17 35	20·7 ± 0·8	135	4	...	...
18	18 01	24·0 ± 0·6	100	14	...	...
19	17 15	21·1 ± 0·5	90	8	...	...
	18 10	28·8 ± 1·7	360	8	3·3	12·8
	18 16	31·3 ± 2·6	300	13	9·3	33·2
21	18 09	35·5 ± 2·1	390	11	3·9	14·0
	18 25	18·8 ± 0·8	100	8	...	...
24	17 32	19·6 ± 1·4	115	8	...	...
	18 11	33·9 ± 2·5	330	12	2·0	7·2
	18 35	28·9 ± 1·7	120	10	...	...
25	17 50	26·3 ± 1·8	445	11	3·9	14·0
	18 25	24·5 ± 2·0	375	12	4·5	16·1
	18 29	31·5 ± 2·8	140	8	...	...
	18 30	26·6 ± 1·6	100	12	...	...
26	17 17	26·5 ± 0·9	100	12	...	...
May 2	18 31	38·9 ± 1·8	425	12	4·1	14·7
	19 00	25·5 ± 0·9	130	7	...	...
	19 02	20·0 ± 1·3	105	10	...	...
5	17 21	32·9 ± 2·3	420	10	3·4	12·2
	17 35	19·9 ± 0·7	100	9	...	...
	17 55	35·8 ± 3·0	370	12	4·6	16·5
	17 55	35·9 ± 2·2	680	10	11·1	39·8
	18 33	27·2 ± 1·9	380	12	4·4	15·7
9	17 07	30·4 ± 2·2	580	8	4·6	16·5
	18 03	21·1 ± 1·7	310	12	7·5	26·8
	18 24	36·0 ± 1·4	340	13	5·9	21·1
10	17 10	49·8 ± 4·7	430	5	1·7	6·1
	17 40	30·6 ± 1·8	100	8	...	...
	18 41	22·7 ± 0·6	115	14	...	...
	18 46	27·7 ± 1·9	140	15	...	...
11	18 51	32·0 ± 2·3	390	12	4·3	15·4
12	18 10	44·4 ± 2·0	285	14	14·0	50·2
	18 45	37·6 ± 1·4	650	13	11·8	42·3
17	17 15	26·2 ± 2·4	120	7	...	...
	17 32	40·7 ± 3·4	450	8	2·9	10·4
	17 50	35·5 ± 2·9	390	5	1·8	6·4
	18 12	36·5 ± 1·6	530	11	5·0	17·9
	18 55	25·4 ± 0·8	130	7	...	...
	19 05	31·0 ± 0·8	100	15	...	...
18	18 56	40·8 ± 1·0	390	10	3·6	12·9

using the values of λ, P and ϵ_0 given in Section 2; and is given in column 7 of Tables II and IV. The corresponding number distribution against electron density for the apex and antapex experiments is shown in Figs. 3 and 4.

The difficulties in the conversion of these line densities to visual magnitudes have been discussed in Part I. The most recent published data on which the

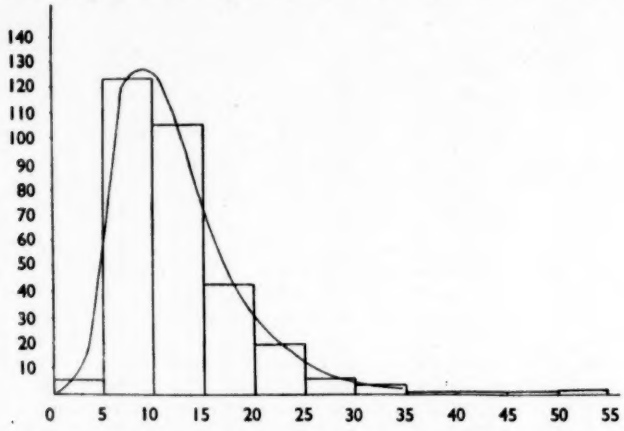

FIG. 3.—*Number distribution of electron line density* (α) *for the* 1950 *apex velocity measurements.* (*Fifteen meteors for which there is no information about* α, *and one meteor for which the only information is* $\alpha > 18{\cdot}6 \times 10^{10}$ *are not included. Eight other meteors with values of* $\alpha = 104$, 109, 125, 165, 193, 238, 247, 286×10^{10} *lie outside the limits of the abscissa.*)

Ordinates : *number of meteors.*

Abscissae : *line density* α *electrons/cm path* ($\times 1{\cdot}57 \times 10^{10}$).

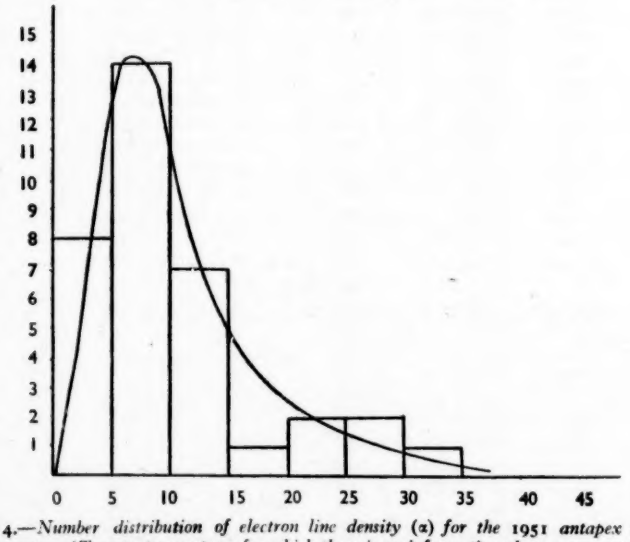

FIG. 4.—*Number distribution of electron line density* (α) *for the* 1951 *antapex velocity measurements.* (*Twenty-two meteors for which there is no information about* α *are not included.*)

Ordinates : *number of meteors.*

Abscissae : *line density* α *electrons/cm path* ($\times 1{\cdot}57 \times 10^{10}$).

conversion may be based are given by Herlofson*, according to whom the peak of the distribution curves in Figs. 3 and 4 lies at zenithal magnitude 3·5. However, recent experimental and theoretical work† has shown that a considerable revision of these estimates is necessary, and that the ionization produced by a meteor of a given magnitude is about 40 times greater than that given by Herlofson. Thus the peak of the distribution curves in Figs. 3 and 4 must lie in the region of magnitude 7.

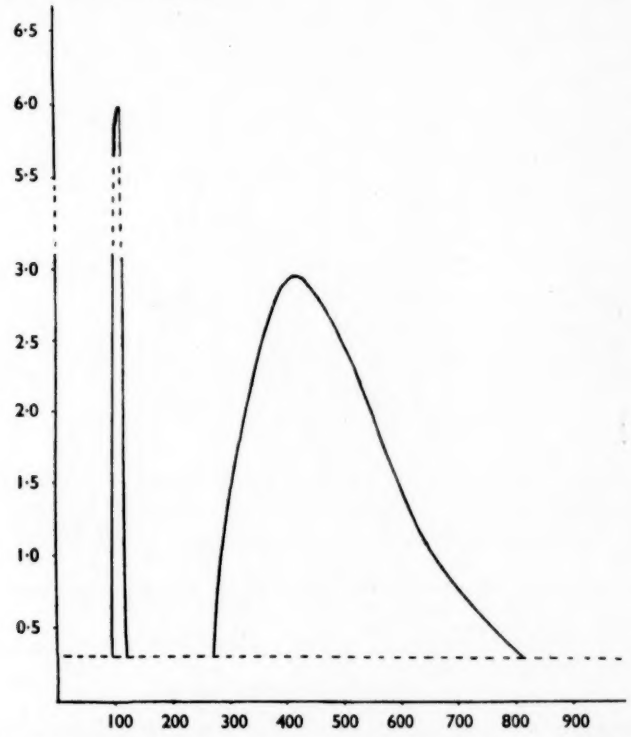

FIG. 5.—*Relation between most probable sensitivity S and range R, for the modified 8-metre aerial system. From these curves the values of γ are calculated for each meteor.*
Ordinates : most probable sensitivity S.
Abscissae : range in kilometres.

In order to examine the velocity distribution for changes related to electron density the 335 velocities comprising Fig. 1 (with the 15 short-range meteors rejected) have been divided into three groups covering different ranges of α. The three distributions are shown in Fig. 6. There is no indication of any change in velocity distribution with magnitude.

(b) *Magnitude estimates by comparison of visual and radio echo rates.*—This method depends on a comparison of the relative collecting areas for meteors of different magnitudes for a visual observer and for the radio equipment. The

* Herlofson, N., *Phys. Soc. Rep. Prog. Phys.*, **11**, 444, 1948.
† Unpublished work at Jodrell Bank.

estimates of the observer's collecting area for various magnitudes have been based on the limiting brightness of a meteor visible at a given angle from the line of vision. The available data on this, taken from the work of Backhouse*, Öpik†, and Hoffmeister‡, are plotted in Fig. 7.§ From these data values have been adopted as given in Table V.

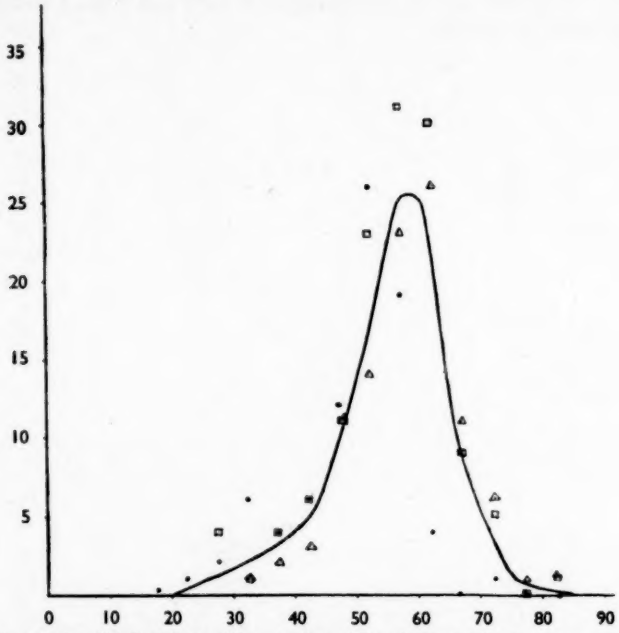

FIG. 6.—*The velocity distribution for different values of line density (α) for the 1950 apex experiment.*

· $\alpha < 14{\cdot}4 \times 10^{10}$ *electrons/cm path (99 velocities).*
⊡ $14{\cdot}4 < \alpha < 22{\cdot}2 \times 10^{10}$ *electrons/cm path (124 velocities).*
△ $\alpha > 22{\cdot}2 \times 10^{10}$ *electrons/cm path (96 velocities).*

All normalized to 100 total.

—— *distribution for all αs.*

Ordinates : number of meteors.
Abscissae : velocity in km/sec.

(One meteor for which the only information is $\alpha > 18{\cdot}6 \times 10^{10}$ *is excluded, together with the 15 short-range meteors for which no values of α are available.)*

If the observer's line of sight is directed upwards at 45°, the intersections of these cones of limiting visibility on the surface 95 km above the Earth can be plotted. These apparent magnitudes are corrected to zenithal magnitude by using data given by Porter‖ and Öpik†, which are in agreement to within a quarter of a magnitude. From the above data the areas in square kilometres over which one observer can see meteors of a given magnitude have been measured graphically. The results are given in column 2 of Table VI. Column 3 gives the relative number of meteors in the various magnitude groups falling on a square kilometre

* Backhouse, T. W., *The Observatory*, **7**, 299, 1884.
† Öpik, E. J., *Publ. Tartu Obs.*, **25**, No. 4, 1923.
‡ Hoffmeister, C. (private communication).
§ In plotting Hoffmeister's data it has been assumed that a meteor of zero magnitude can just be seen at 60° from the line of vision.
‖ Porter, J. G., *Mem. B.A.A.*, **34**, Pt. 4, 1942.

of the sky. These are based on the measurements of Watson* which show that the average increase in numbers of meteors is 2·5 times for each fainter magnitude. Thus the relative numbers (N_1, N_2) between two magnitude groups (m_1, m_2) will be given by

$$N_1/N_2 = (2{\cdot}5)^{(m_1 - m_2)}. \qquad (2)$$

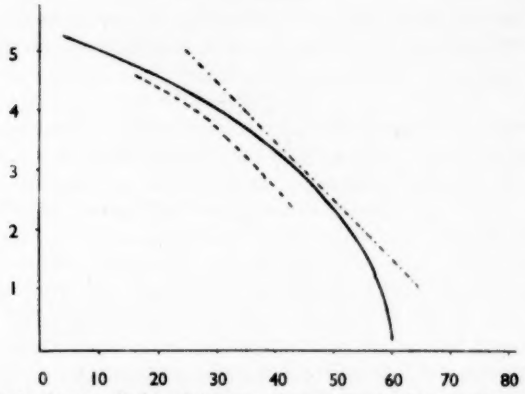

FIG. 7.—*Relation between limiting brightness of a meteor visible at a given angle from an observer's line of vision according to Hoffmeister* (——); *Öpik* (– – –) *and Backhouse* (– · – · –). *Ordinates: meteor magnitude. Abscissae: angle from observer's line of vision.*

TABLE V

Limiting meteor magnitude visible at a given angle from an observer's line of vision

Angle from line of vision	60°	58°	53°	44°	30°	11°	0°
Limiting magnitude	0	1	2	3	4	5	5·5

TABLE VI

Numbers of meteors of different magnitudes seen by a visual observer

Zenithal magnitude	Collecting area (sq. km)	Relative number per sq. km	Relative number seen	True number per sq. km per hour for hourly rate = 1
1	2	3	4	5 ($\times 10^{-4}$)
4½	161	158	25 000	31·8
4	5 160	100	516 000	20·2
3½	9 845	63·1	620 000	12·7
3	16 125	39·8	641 000	8·02
2½	24 200	25·1	607 500	5·05
2	36 150	15·8	571 000	3·18
1½	50 000	10·0	500 000	2·02
1	66 000	6·31	420 000	1·27
½	87 500	3·98	348 000	0·80
0	115 700	2·51	291 000	0·50
− ½	135 800	1·58	214 000	0·32
−1	200 000	1·00	200 000	0·20
		Total	4 953 500	

* Watson, F., *Harv. Ann.*, **105**, 624, 1937; *Proc. Amer. Philos. Soc.*, **81**, 493, 1939.

If one meteor of magnitude -1 falls per sq. km per hour, the number of meteors seen in each magnitude per hour can be calculated, and is given in column 4. Summation of this column gives the total rate seen by the observer. If this is taken to be one meteor per hour, the relative numbers in column 3 can be scaled down to give the actual numbers of meteors falling on a square kilometre per hour, as in column 5.

Assuming that the apex is at an elevation of 45° (its mean elevation during the apex experiments) and that the meteors fall on the Earth from random heliocentric directions with parabolic velocities, it is possible to deduce the numbers of meteors passing per hour through a square kilometre of the 95 km surface from different directions. These true numbers may now be applied in place of the relative numbers given by Clegg* in calculating the theoretical velocity distribution and hence, making the arbitrary assumption that meteors of a certain magnitude are seen to a given sensitivity contour, the number distribution with magnitude can be plotted. This magnitude distribution has a peak at $+0{\cdot}7$.

With the arbitrarily assumed visual rate of one meteor per hour, and for this magnitude distribution, the equivalent radio echo rate derived in this way came to 0·021 per hour for the 1950 apex experiment described in Section 3. If a visual rate of 10 per hour is adopted for the early mornings in autumn when the experiment was performed, the equivalent radio rate becomes 0·21 for this magnitude range. The actual observed magnitude range can now be estimated by comparing this rate with the hourly radio echo rate during the experiment. The total rate observed during the apex experiment was 264 per hour. The shift in the magnitude scale required to bring this rate into line with the above results can be derived from equation (2) which transforms to

$$m_1 - m_2 = 2{\cdot}5 \log_{10}(N_1/N_2).$$

The shift required is therefore given by $\Delta m = 2{\cdot}5 \log_{10}(264/0{\cdot}21) = 7{\cdot}7$. The assumption of a visual rate of 10 per hour is not critical. For example, a doubling of the assumed rate would change the magnitude shift by only 0·75 magnitude. The assumed distribution peaked at magnitude 0·7, so the observed distribution peaked at magnitude 8·4.

Of these echoes only 11 per cent gave velocity measurements; although an additional 29 per cent were of sufficient amplitude and duration they did not yield velocities owing to distortion of the trail or lack of range measurement. Thus the rate of velocity type echoes is 40 per cent of the total and the corresponding magnitude distribution peaks at magnitude 7·4.

The same analysis can be applied to the case of 1949 apex experiment described in Part I. In this case the peak of the magnitude distribution for the velocity type echoes is at magnitude 6·1 and for all echoes is at magnitude 7·1. In the case of the antapex experiments, the calculation has not been attempted because of the difficulty of obtaining a reliable visual rate, and also because a large proportion of echoes occurs outside the main lobe of the aerial.

In Table VII the peaks of the magnitude distributions in the various experiments derived from visual rates are compared with those calculated from the peak electron densities as described in (a) above.

In Part I it was concluded that the 1949–1950 measurements probably referred to meteors of about magnitude 4·5. The estimates now made indicate

* Clegg, J. A., *M.N.*, **112**, No. 4, 1952.

that these meteors were of fifth and sixth magnitudes. In the 1950–1951 experiments described in this paper the meteors are fainter on both estimates by 1·5 magnitudes. The uncertainty in estimating the magnitudes arises on the one hand because of the incomplete state of the meteor evaporation theory, and on the other because of the lack of data on the collecting area of a visual observer for meteors of a given magnitude. It is therefore only possible to conclude that the measurements described in Part I probably referred to meteor magnitudes between 4·5 and 6·0, and in Part II to meteor magnitudes between 6·0 and 7·5.

TABLE VII

Comparison of magnitudes from electron densities and from visual rates

	From visual rate	From electron density at peak of distribution curve	
		(*a*)	(*b*)
1949 apex	6·0	5·5	2·0
1950 apex	7·5	7·0	3·5

(*a*) Assuming the new estimates for electron density (see page 35).
(*b*) Using Herlofson's estimates for the ionization produced by a meteor of given magnitude.

8. *Conclusion.*—The experiments described in this paper and in Part I give no evidence that any appreciable numbers of meteors are moving with velocities in excess of the parabolic limit. This conclusion is in conflict with the work of Öpik*† and Hoffmeister.‡ Although it appears possible to reconcile Hoffmeister's results with this conclusion by abandoning the assumption of uniform distribution (see Part I), there does not appear to be any ground on which the results of Öpik can be aligned with those presented in this paper. The majority of the measurements probably refer to meteors in the magnitude range 6·0 to 7·5, with limits of 7·5 to 9·0. The results therefore cover not only the visual range available to Öpik, but also the telescopic results of Boothroyd.§ Although in his earlier analysis* Öpik concluded that the velocity distribution changed with meteor magnitude, his final decision†, from the analysis of both the Tartu and Arizona work, was that no significant change in velocity distribution with magnitude existed. In this respect only are the present radio echo results in agreement with the work of Öpik.

9. *Acknowledgments.*—The research forms part of the programme of work at the Jodrell Bank Experimental Station of the University of Manchester, to which the Department of Scientific and Industrial Research has contributed substantial financial assistance. One author (M. A.) is also indebted to the Department for the award of a Maintenance Grant during the course of the work.

University of Manchester,
Jodrell Bank Experimental Station,
Cheshire :
1951 *September* 27.

* Öpik, E. J., *Tartu Obs. Publ.*, **30**, No. 5, 1940. † Opik, E. J., *Tartu Obs. Publ.*, **30**, No. 6, 1941.
‡ Hoffmeister, C., *Die Meteore*, Leipzig, 1937.
§ Boothroyd, S. J., *Harv. Circ.*, No. 390, 1934.

ABSORPTION OF RADIATION BY AN ATMOSPHERE OF H, H^+ AND H_2^+—SEMI-CLASSICAL TREATMENT

D. R. Bates

(Received 1951 September 28)

Summary

Calculations are carried out on the absorption of an atmosphere of H, H^+ and H_2^+ using the accurate quantal dipole moment but treating the nuclei as classical particles. Absorption coefficients are tabulated for wave numbers between 500 cm^{-1} and 26 000 cm^{-1}, and for temperatures between 2 500 deg. K and 12 000 deg. K. The relative importance of bound-free and free-free transitions is also determined.

---

1. *Introduction.*—Some time ago Wildt (**1**) suggested that a significant contribution to the opacity of stellar atmospheres might arise from bound-free absorption by H_2^+ ions,

$$H_2^+(1s\sigma) + h\nu \rightarrow (H + H^+)(2p\sigma) \tag{1}$$

and from free-free absorption by colliding H atoms and H^+ ions

$$(H + H^+)(1s\sigma) + h\nu \rightarrow (H + H^+)(2p\sigma). \tag{2}$$

The present paper is devoted to the investigation of these two processes on the assumption that the nuclei behave as classical particles.

2. *Basis of calculations.*—The absorption coefficient $\kappa(\nu, T)$ associated with (1) and (2) together is related to the photon emissivity, $j(\nu, T)$, due to the inverse processes, by the well-known equation

$$\kappa(\nu, T) = (c^2/8\pi\nu^2)\{\exp(h\nu/kT) - 1\}j(\nu, T), \tag{3}$$

ν being the frequency of the radiation, T the temperature, h Planck's constant, and k Boltzmann's constant. Formulae from which $j(\nu, T)$ may be obtained have been developed elsewhere (**2**). On introducing $\gamma(\nu, T)\,d\nu$, the rate coefficient giving the photon emission in the frequency range ν to $\nu + d\nu$, we see that

$$j(\nu, T) = n(H)n(H^+)\gamma(\nu, T), \tag{4}$$

the n's being the concentrations of the substances indicated. Further, if R is the internuclear distance corresponding to the frequency ν, and $\gamma(R, T)\,dR$ is the rate coefficient giving the photon emission from H atoms and H^+ ions whose separation lies between R and $R + dR$, then

$$\gamma(\nu, T) = \gamma(R, T)/(d\nu/dR). \tag{5}$$

Now from the earlier paper (**2**) just mentioned

$$\gamma(R, T) = 4\pi g A(R) R^2 \exp\{-U(2p\sigma|R)/kT\}, \tag{6}$$

where g is the ratio of the statistical weight of the repulsive potential energy curve $U(2p\sigma|R)$ to the sum of the statistical weights of this curve and of the attractive potential energy curve $U(1s\sigma|R)$, and where $A(R)$ is the Einstein

spontaneous transition probability. Denoting the dipole moment involved by $D(R)$, writing

$$x(1s\sigma|R, T)^2 = -U(1s\sigma|R)/kT, \tag{7}$$

$$x(2p\sigma|R, T)^2 = -U(2p\sigma|R)/kT, \tag{8}$$

and using the relations

$$A(R) = \frac{64\pi^4\nu^3}{3hc^3} D(R), \tag{9}$$*

$$h\nu = U(2p\sigma|R) - U(1s\sigma|R), \tag{10}$$

we find

$$\kappa(\nu, T) = \frac{32\pi^4 g}{3hc}\left\{\nu\Big/\frac{d\nu}{dR}\right\}R^2D(R)[\exp\{x(1s\sigma|R, T)^2\} - \exp\{x(2p\sigma|R, T^2\}]n(H)n(H^+). \tag{11}$$

This formula can of course be derived directly using classical statistics to obtain the distribution of internuclear distances. On taking g to equal $\frac{1}{2}$, and substituting for the fundamental physical constants, we have

$$\kappa(\nu, T) = 2{\cdot}51 \times 10^{-42}\{\nu/(d\nu/dR)\}R^2D(R)[\exp\{x(1s\sigma|R, T)^2\} - \exp\{x(2p\sigma|R, T)^2\}]n(H)n(H^+)\,cm^{-1}, \tag{12}$$

where R and $D(R)$ are in the appropriate atomic units (a_0 and $a_0^2e^2$ respectively), $n(H)$ and $n(H^+)$ are particle numbers per cm^3, and the other quantities are in any self-consistent set of units. The stimulated transitions are of course included in $\kappa(\nu, T)$ as negative absorptions.

An asymptotic expression suitable for use at low frequencies can be derived. From elementary perturbation theory (**3**) we have that as R tends to infinity

$$\nu/c \sim (8/3)(R - 3/2R)\exp(-R)\ \text{Rydbergs}\dagger, \tag{13}$$

so

$$\nu/(d\nu/dR) \sim R(2R^2 - 3)/(2R^3 - 2R^2 - 3R - 3). \tag{14}$$

Noting also (**4**) that

$$D(R) \sim \tfrac{1}{4}R^2, \tag{15}$$

we see on expanding the exponentials in (12) that

$$\kappa(\nu, T) \sim 6{\cdot}28 \times 10^{-43}\left(\frac{h\nu}{kT}\right)\left\{\frac{R^5(2R^2 - 3)}{2R^3 - 2R^2 - 3R - 3}\right\}n(H)n(H^+)\,cm^{-1}, \tag{16}$$

the units being as specified above. From (13) R is approximately

$$-\ln(3\nu/8c) + \ln R, \tag{17}$$

so that the value appropriate to any chosen ν can be found rapidly by iteration.

For certain purposes it is desirable to be able to separate the contributions from bound-free and free-free absorption. This can readily be done, for, as can be seen from the earlier paper (**2**), the fraction of the total due to the former is given by

$$r_B(\nu, T) = \Phi\{x(1s\sigma|R, T)\} - 2\pi^{-\frac{1}{2}}x(1s\sigma|R, T)\exp\{-x(1s\sigma|R, T)^2\}, \tag{18}$$

where Φ is the error integral. At low frequencies $r_B(\nu, T)$ is clearly very small. An asymptotic expression can be obtained, but it is of little interest and need not be given.

* The orbital degeneracy factor is omitted as it equals unity for the transition under discussion.

† 1 Rydberg = 109 677·58 cm^{-1}.

All the functions appearing in (12) and (18) are known with some precision; thus the potential energy curves have been evaluated in the course of a recent quantal study of the two-centre problem (**5**), and the dipole moment has been calculated (**6**) from electronic wave-functions made available by this investigation. A number of convenient values of the wave number ν/c covering the range 500 cm^{-1} to 26 000 cm^{-1} were chosen, and the corresponding values of R, $U(1s\sigma|R)$, $U(2p\sigma|R)$, $\nu/(d\nu/dR)$ and $D(R)$ were computed by inverse interpolation and numerical differentiation. The figures obtained (which are displayed in Table I) were then used in (12) and (18) to determine $\kappa(\nu, T)$ and

TABLE I

Data on $1s\sigma-2p\sigma$ *transition of* H_2^+

Wave number ν/c (cm^{-1})	Internuclear distance R (atomic units)	$-\nu/(d\nu/dR)$ (atomic units)	Potentials $-U(1s\sigma\|R)$ (Rydbergs)	$+U(2p\sigma\|R)$ (Rydbergs)	Dipole moment $D(R)$ (atomic units)
500	8·633	1·15	0·00315	0·00141	17·4
1 000	7·839	1·16	·00583	·00329	14·2
1 500	7·367	$1·17_6$	·00843	·00525	12·5
2 000	7·026	$1·18_8$	·01097	·00727	11·3
2 500	6·760	$1·19_7$	·01346	·00933	10·4
3 000	$6·541_6$	$1·20_6$	·01592	·01143	$9·7_7$
3 500	$6·354_8$	$1·21_5$	·01834	·01357	$9·1_8$
4 000	$6·191_9$	$1·22_2$	·02074	·01573	$8·7_0$
5 000	$5·917_8$	$1·23_6$	·02545	·02014	$7·9_2$
6 000	$5·691_2$	$1·24_9$	·03004	·02467	$7·3_1$
7 000	$5·497_8$	$1·26_1$	·03451	·02931	$6·8_0$
8 000	$5·328_6$	$1·27_1$	·03891	·03403	$6·3_7$
9 000	$5·178_3$	$1·28_0$	·04322	·03884	$6·0_0$
10 000	$5·042_9$	$1·28_9$	·04744	·04374	$5·6_8$
12 000	$4·806_6$	$1·30_4$	·05560	·05381	$5·1_4$
14 000	$4·604_8$	$1·31_5$	·06347	·06418	$4·7_1$
16 000	$4·428_8$	$1·32_5$	·07100	·07488	$4·3_6$
18 000	$4·272_0$	$1·33_3$	·07828	·08584	$4·0_5$
20 000	$4·131_2$	$1·34_0$	·08527	·09708	$3·7_9$
22 000	$4·003_2$	$1·34_5$	·09200	·10859	$3·5_6$
24 000	$3·885_9$	$1·35_1$	·09847	·12035	$3·3_6$
26 000	$3·777_6$	$1·35_6$	0·10470	0·13236	$3·1_8$

$r_B(\nu, T)$ at various temperatures between 2 500 deg. K and 12 000 deg. K. Tables II and III contain the final results. Those in the former table may be a few per cent in error (particularly at the lower wave numbers) because of possible slight inaccuracies in the original data; those in the latter should be correct to the number of decimal places given. It is difficult to assess the extent of the uncertainties introduced by the assumption that the movement of the nuclei is strictly classical. The de Broglie wave-length of a proton near the maximum of the Maxwellian distribution at 2 500 deg. K (the lowest temperature considered) is about one atomic unit, which is certainly not negligible compared with the internuclear separations of importance; but in spite of this the classical treatment of the free states should actually be quite successful since the use of the Winans–Stueckelberg δ-function (**7**) gives a fair representation of the photodissociation of even light molecules (**8**). The quantization of the bound states is unlikely to be very important owing to the large number involved. We consider

TABLE II *

Absorption coefficient in units 10^{-39} cm^{-1}/(H atom/cm^3)/(H^+ ion/cm^3)

ν/c	Temperature in 10^3 deg. K									
(cm^{-1})	2·5	3	3·5	4	5	6	7	8	10	12
500	1·14	0·94	0·80	0·69	0·55	0·46	0·39	0·34	0·270	0·226
1 000	1·61	1·32	1·12	0·97	0·77	·63	·54	·47	·38	·31
1 500	1·97	1·60	1·35	1·17	0·92	·76	·64	·56	·44	·37
2 000	2·28	1·83	1·53	1·32	1·03	·85	·72	·63	·50	·41
2 500	2·56	2·04	1·69	1·45	1·13	·92	·78	·68	·54	·44
3 000	2·84	2·23	1·84	1·56	1·21	0·99	·83	·72	·57	·47
3 500	3·1	2·42	1·97	1·67	1·28	1·04	·88	·76	·60	·49
4 000	3·4	2·60	2·10	1·77	1·35	1·09	·92	·79	·62	·51
5 000	4·0	2·98	2·36	1·96	1·47	1·17	·98	·84	·66	·54
6 000	4·8	3·4	2·63	2·15	1·57	1·25	1·04	·89	·69	·57
7 000	5·6	3·9	2·91	2·33	1·67	1·31	1·08	·92	·71	·58
8 000	6·7	4·4	3·2	2·53	1·77	1·37	1·12	·95	·73	·59
9 000	7·9	5·0	3·5	2·74	1·87	1·43	1·16	·97	·74	·60
10 000	9·3	5·6	3·9	2·95	1·97	1·48	1·19	0·99	·75	·61
12 000	13·0	7·2	4·7	3·4	2·18	1·58	1·25	1·03	·77	·62
14 000	18·1	9·3	5·7	4·0	2·40	1·69	1·30	1·06	·78	·62
16 000	25·1	11·9	7·0	4·7	2·64	1·80	1·36	1·09	·78	·62
18 000	35	15·2	8·4	5·4	2·91	1·91	1·41	1·11	·79	·61
20 000	47	19·3	10·2	6·3	3·2	2·03	1·46	1·14	·79	·61
22 000	64	24·3	12·2	7·3	3·5	2·16	1·52	1·16	·79	·60
24 000	86	31	14·6	8·4	3·8	2·29	1·57	1·18	·79	·59
26 000	114	38	17·3	9·6	4·2	2·42	1·63	1·21	0·79	0·58

* At wave numbers below 500 cm^{-1} the asymptotic formula (16) may be used.

TABLE III

Fraction of total absorption due to bound-free transitions

ν/c	Temperature in 10^3 deg. K									
(cm^{-1})	2·5	3	3·5	4	5	6	7	8	10	12
500	0·059	0·046	0·037	0·031	0·022	0·017	0·014	0·011	0·008	0·006
1 000	·135	·107	·087	·072	·053	·041	·033	·027	·020	·015
1 500	·214	·171	·141	·118	·088	·069	056	·046	·034	·026
2 000	·291	·236	·196	·166	·125	·098	·080	·067	·049	·038
2 500	·363	·298	·250	·214	·162	·129	·105	·088	·065	·050
3 000	·430	·357	·303	·260	·200	·159	·131	·110	·082	·064
3 500	·490	·413	·353	·305	·237	·190	·157	·132	·099	·077
4 000	·546	·464	·400	·349	·273	·221	·183	·155	·116	·091
5 000	·640	·556	·486	·429	·342	·280	·234	·200	·151	·120
6 000	·715	·632	·561	·501	·406	·336	·284	·243	·186	·148
7 000	·775	·696	·625	·564	·464	·388	·331	·285	·220	·176
8 000	·822	·748	·680	·619	·517	·437	·375	·326	·254	·204
9 000	·859	·792	·727	·667	·564	·482	·417	·364	·286	·232
10 000	·888	·827	·767	·709	·607	·524	·456	·400	·317	·258
12 000	·929	·881	·829	·777	·680	·597	·526	·467	·375	·309
14 000	·954	·917	·874	·829	·739	·658	·586	·525	·428	·356
16 000	·970	·942	·906	·867	·786	·708	·638	·577	·476	·400
18 000	·980	·959	·930	·897	·824	·751	·683	·622	·519	·440
20 000	·987	·970	·947	·919	·854	·786	·721	·661	·558	·476
22 000	·991	·978	·960	·936	·879	·816	·754	·695	·593	·510
24 000	·994	·984	·969	·949	·898	·841	·782	·726	·625	·541
26 000	0·996	0·988	0·976	0·959	0·914	0·862	0·806	0·752	0·653	0·569

therefore that the results presented are probably accurate at the higher temperatures and lower frequencies and that they are probably correct to well within one part in ten even at the lower temperature and higher frequencies. Quantal calculations in the former region would be very laborious. Though still very formidable in the latter region they have, nevertheless, been undertaken by Dr R. A. Buckingham* and Mr S. Reed and should show clearly the range of validity of the classical approximation. The two investigations are essentially supplementary and together should provide reliable data at all temperatures and frequencies of interest.

The application of the absorption cross-section data to stellar atmospheres is being carried out by Professor B. Strömgren.

Dept. of Applied Mathematics,
Queen's University,
Belfast, N. Ireland:
1951 *September* 26.

References

(1) Wildt, R., *Relations entre les phénomènes solaires et géophysiques*, p. 7, Centre National de la Recherche Scientifique, Paris, 1947.
(2) Bates, D. R., *M.N.*, **111**, 303, 1951.
(3) *Cf.* Eyring, H., Walter, J. and Kimball, G. E., *Quantum Chemistry*, Chapman & Hall, London, 1944.
(4) Mulliken, R. S., *J. Chem. Phys.*, **7**, 20, 1939.
(5) Bates, D. R., Ledsham, K. and Stewart, A. L. (in course of preparation).
(6) Bates, D. R., *J. Chem. Phys.*, **19**, 1122, 1951.
(7) Winans, J. G. and Stueckelberg, E. C. G., *Proc. Nat. Acad. Sci.*, **14**, 867, 1928.
(8) Coolidge, A. S., James, H. M. and Present, R. D., *J. Chem. Phys.*, **4**, 193, 1936.

* I wish to thank Dr Buckingham for informing me of this work and for helpful discussions.

ON EMISSION LINES IN STELLAR SPECTRA

Ida W. Busbridge

(Received 1951 October 27)

Summary

Conditions are investigated for the formation of absorption lines when the fraction ξ of the line absorption coefficient l_ν is due to absorption and the fraction $1-\xi$ is due to scattering, continuous absorption and continuous isotropic scattering being taken into account when estimating the flux of continuous radiation. It is shown that if $\xi<\lambda_c=\kappa_\nu/(\kappa_\nu+\sigma)$ the line must be dark, but that if $\xi>\lambda_c$ the line may be bright. The case $\xi=1$, in which the line is formed by pure absorption, is considered in detail. It is shown that the line will be bright if $f(\lambda_\nu, \beta_\nu)>f(\lambda_c, \beta_\nu)$, where $f(\lambda, \beta)$ is a certain function, $\lambda_\nu=(\kappa_\nu+l_\nu)/(\kappa_\nu+\sigma+l_\nu)$, and β_ν is a constant depending on the constitution of the star and the frequency ν considered. Some numerical examples are discussed.

1. *Introduction.*—In a recent paper (**3**) Miss Underhill has considered the formation of absorption lines when continuous absorption and continuous isotropic scattering are both taken into account in estimating the flux of continuous radiation, and when the lines are formed (*a*) by absorption and (*b*) by scattering. Assuming that σ, the coefficient of continuous scattering, is independent of both the frequency ν and the depth, and that the coefficient of absorption κ_ν is independent of the depth, she has shown that lines formed by scattering must be dark. She has also shown by an extreme case that lines formed by absorption may be bright, but she merely says that in other cases "the appearance of emission becomes more stringent".

The main object of this paper is the investigation of these more stringent conditions, but I have begun by considering what happens when the line is formed partly by absorption and partly by scattering.

2. *The residual intensity.*—Let $\xi l_\nu (0 \leqslant \xi \leqslant 1)$ be the part of the line absorption coefficient l_ν which is due to absorption and let the remainder $(1-\xi)l_\nu$ be due to scattering. Then the equation of transfer is (with the usual notation)

$$\mu \frac{dI_\nu}{\rho\, dx} = (\kappa_\nu+\sigma+l_\nu)I_\nu - \tfrac{1}{2}[\sigma+(1-\xi)l_\nu]\int_{-1}^{1} I_\nu\, d\mu - (\kappa_\nu+\xi l_\nu)B_\nu, \tag{2.1}$$

where x is the depth below the surface of the star of the layer considered.

On writing

$$\lambda_\nu^{(\xi)} = \frac{\kappa_\nu+\xi l_\nu}{\kappa_\nu+\sigma+l_\nu} \tag{2.2}$$

and

$$t_\nu = \int_0^x \rho(\kappa_\nu+\sigma+l_\nu)\, dx, \tag{2.3}$$

(2.1) takes the standard form

$$\mu \frac{dI_\nu}{dt_\nu} = I_\nu - \tfrac{1}{2}(1-\lambda_\nu^{(\xi)})\int_{-1}^{1} I_\nu\, d\mu - \lambda_\nu^{(\xi)} B_\nu. \tag{2.4}$$

Following previous writers, Underhill assumed that, for the surface layers, a linear approximation for the Planck function B_ν is sufficiently good. Accepting this, though remembering that the exact solution of (2.4) depends on the values taken by B_ν for all values of t_ν from 0 to ∞, we write

$$B_\nu = b_\nu^{(0)} + b_\nu^{(1)}\tau_\nu, \tag{2.5}$$

where

$$\tau_\nu = \int_0^x (\kappa_\nu + \sigma)\rho\, dx.$$

If l_ν, κ_ν and σ are all independent of the depth, then

$$\tau_\nu = n_\nu t_\nu, \tag{2.6}$$

where

$$n_\nu = \frac{\kappa_\nu + \sigma}{\kappa_\nu + \sigma + l_\nu}. \tag{2.7}$$

Subject to these conditions, (2.4) can be solved exactly (**2**) and the emergent flux is

$$F_\nu = 2b_\nu^{(1)}\{n_\nu R_1(\lambda_\nu^{(\xi)}) + (b_\nu^{(0)}/b_\nu^{(1)})R_2(\lambda_\nu^{(\xi)})\}, \tag{2.8}$$

where

$$R_1(\lambda) = \lambda^{1/2}\alpha_2 + \tfrac{1}{2}(1-\lambda)\alpha_1^2, \tag{2.9}$$

$$R_2(\lambda) = \lambda^{1/2}\alpha_1, \tag{2.10}$$

and α_1, α_2 are the first and second moments of $H(\mu)$, the solution of the equation

$$H(\mu) = 1 + \tfrac{1}{2}(1-\lambda)\mu H(\mu)\int_0^1 \frac{H(\mu')}{\mu+\mu'}\,d\mu'. \tag{2.11}$$

By a theorem of Chandrasekhar*, α_1 and α_2 are related by the equation

$$\lambda^{1/2}\alpha_2 + \tfrac{1}{4}(1-\lambda)\alpha_1^2 = \tfrac{1}{3}, \tag{2.12}$$

so that $R_1(\lambda)$ can also be written

$$R_1(\lambda) = \tfrac{1}{4}(1-\lambda)\alpha_1^2 + \tfrac{1}{3}. \tag{2.13}$$

Tables for $R_1(\lambda)$ and $R_2(\lambda)$ are given by Underhill (**3**) and tables for α_1 and α_2 by Chandrasekhar (**2**).

The emergent flux of ν-radiation in the continuum is obtained by putting $l_\nu = 0$ in the preceding equations. Writing

$$\lambda_c = \kappa_\nu/(\kappa_\nu + \sigma), \tag{2.14}$$

this is

$$F_{\text{cont.}} = 2b_\nu^{(1)}\{R_1(\lambda_c) + (b_\nu^{(0)}/b_\nu^{(1)})R_2(\lambda_c)\}.$$

The residual intensity $\boldsymbol{R}_\nu$ in the absorption line is

$$\boldsymbol{R}_\nu = \frac{F_\nu}{F_{\text{cont.}}} = \frac{n_\nu R_1(\lambda_\nu^{(\xi)}) + (b_\nu^{(0)}/b_\nu^{(1)})R_2(\lambda_\nu^{(\xi)})}{R_1(\lambda_c) + (b_\nu^{(0)}/b_\nu^{(1)})R_2(\lambda_c)}. \tag{2.15}$$

This is identical with the expression obtained by Underhill (though her λ_ν and λ_ν' are obtained by taking $\xi = 1$ and $\xi = 0$ in (2.2)). The form (2.15) is, however, not the most useful form for $\boldsymbol{R}_\nu$ and we proceed to transform it.

By (2.2), (2.7) and (2.14),

$$n_\nu = (\xi - \lambda_\nu^{(\xi)})/(\xi - \lambda_c) \tag{2.16}$$

* (**1**), theorem 2. Here $\Psi(\mu) = \tfrac{1}{2}(1-\lambda)$.

except when $\xi=\lambda_c$. Then $\xi=\lambda_\nu^{(\xi)}$ also. Hence $\boldsymbol{R}_\nu$ can be written, when $\xi\neq\lambda_c$, in the form

$$\boldsymbol{R}_\nu=\frac{(\xi-\lambda_\nu^{(\xi)})R_1(\lambda_\nu^{(\xi)})+\beta_\nu^{(\xi)}R_2(\lambda_\nu^{(\xi)})}{(\xi-\lambda_c)R_1(\lambda_c)+\beta_\nu^{(\xi)}R_2(\lambda_c)}, \tag{2.17}$$

where

$$\beta_\nu^{(\xi)}=(\xi-\lambda_c)b_\nu^{(0)}/b_\nu^{(1)}. \tag{2.18}$$

We shall first show that if $\xi<\lambda_c$, then $\boldsymbol{R}_\nu<1$ and the line must be dark, but that if $\xi>\lambda_c$ the line may be bright.

Since $0<n_\nu<1$, it follows from (2.16) that if $\xi<\lambda_c$, then $\xi<\lambda_\nu^{(\xi)}$ and

$$\xi<\lambda_\nu^{(\xi)}<\lambda_c. \tag{2.19}$$

If $\xi>\lambda_c$, then $\xi>\lambda_\nu^{(\xi)}$ and

$$\xi>\lambda_\nu^{(\xi)}>\lambda_c. \tag{2.20}$$

When $\xi<\lambda_c$, $\beta_\nu^{(\xi)}$ is negative and $\boldsymbol{R}_\nu$ can be written

$$\boldsymbol{R}_\nu=\frac{(\lambda_\nu^{(\xi)}-\xi)R_1(\lambda_\nu^{(\xi)})+|\beta_\nu^{(\xi)}|R_2(\lambda_\nu^{(\xi)})}{(\lambda_c-\xi)R_1(\lambda_c)+|\beta_\nu^{(\xi)}|R_2(\lambda_c)}.$$

From the tables given by Underhill for $R_1(\lambda)$ and $R_2(\lambda)$ it is at once seen that $R_1(\lambda)$ is a decreasing function in $(0,1)$ and that $R_2(\lambda)$ is an increasing function. Moreover a simple calculation shows that $\lambda R_1(\lambda)$ is increasing in $(0,1)$. It follows that

$$(\lambda-\xi)R_1(\lambda)+|\beta_\nu^{(\xi)}|R_2(\lambda)$$

is increasing in $(0,1)$ and, since $\xi<\lambda_\nu^{(\xi)}<\lambda_c$, that $\boldsymbol{R}_\nu<1$. Thus when $\xi<\lambda_c$ the absorption line is dark. In particular, lines formed by pure scattering ($\xi=0$) are necessarily dark. This is the result established by Underhill.

When $\xi>\lambda_c$ we return to the form (2.17) for $\boldsymbol{R}_\nu$, since $\beta_\nu^{(\xi)}$ is now positive. Since $(\xi-\lambda)R_1(\lambda)$ is a decreasing function of λ while $R_2(\lambda)$ is increasing,

$$(\xi-\lambda)R_1(\lambda)+\beta_\nu^{(\xi)}R_2(\lambda)$$

will be increasing or decreasing in $(0,1)$ according to the values of ξ and $\beta_\nu^{(\xi)}$. Thus it is possible to have $\boldsymbol{R}_\nu>1$, so that the line is bright.

We shall discuss only the case of pure absorption ($\xi=1$) in detail. Let

$$f(\lambda,\beta)=(1-\lambda)R_1(\lambda)+\beta R_2(\lambda). \tag{2.21}$$

By (2.10) and (2.13), this can be written

$$f(\lambda,\beta)=\tfrac{1}{4}(1-\lambda)^2\alpha_1{}^2+\tfrac{1}{2}(1-\lambda)+\beta\lambda^{1/2}\alpha_1. \tag{2.22}$$

From (2.17) with $\xi=1$ and (2.21) we see that

$$\boldsymbol{R}_\nu=f(\lambda_\nu^{(1)},\beta_\nu^{(1)})/f(\lambda_c,\beta_\nu^{(1)}).$$

Since, by (2.20), $1>\lambda_\nu^{(1)}>\lambda_c$, the condition for the formation of an emission line can be written

$$f(\lambda_\nu,\beta_\nu)>f(\lambda_c,\beta_\nu)\quad(\lambda_\nu>\lambda_c), \tag{2.23}$$

where, by (2.2), (2.14) and (2.18),

$$\lambda_\nu=\lambda_\nu^{(1)}=\frac{\kappa_\nu+l_\nu}{\kappa_\nu+\sigma+l_\nu},\quad \lambda_c=\frac{\kappa_\nu}{\kappa_\nu+\sigma} \tag{2.24}$$

and

$$\beta_\nu=\beta_\nu^{(1)}=(1-\lambda_c)b_\nu^{(0)}/b_\nu^{(1)}. \tag{2.25}$$

Note that α_1 in (2.22) is a function of λ, since $H(\mu)$ is a function of μ and λ.

3. *The constant* β_ν.—The usual definition of $b_\nu^{(0)}/b_\nu^{(1)}$ is

$$\frac{b_\nu^{(0)}}{b_\nu^{(1)}} = [1-\exp(-h\nu/kT_0)]\frac{kT_0^2}{h\nu}\left(\frac{dT}{d\tau}\right)_{\tau=0}^{-1} \times \frac{\kappa_\nu+\sigma}{\bar{\kappa}+\sigma},$$

where $\bar{\kappa}$ is a mean absorption coefficient and

$$\tau = \int_0^x \bar{\kappa}\rho\, dx.$$

Assuming the approximate formula

$$T^4 = T_0^4(1+a\tau), \tag{3.1}$$

where, for a grey atmosphere, $a = 3/2$, we have

$$\left(\frac{dT}{d\tau}\right)_{\tau=0} = \tfrac{1}{4}aT_0.$$

Hence, if $x = h\nu/kT_0$,

$$\beta_\nu = (1-\lambda_e)\frac{b_\nu^{(0)}}{b_\nu^{(1)}} = \frac{\sigma}{\kappa_\nu+\sigma}\cdot\frac{1-e^{-x}}{x}\cdot\frac{4}{a}\cdot\frac{\kappa_\nu+\sigma}{\bar{\kappa}+\sigma},$$

i.e.

$$\beta_\nu = \frac{1-e^{-x}}{x}\cdot\frac{4}{a}\cdot\frac{\sigma}{\bar{\kappa}+\sigma}, \qquad x = \frac{h\nu}{kT_0}. \tag{3.2}$$

In this form β_ν is completely determined by the frequency ν considered and by the constitution of the star, subject to the assumptions made above.

It is easy to see that β_ν lies between 0 and 4, assuming that a, which is $\frac{3}{2}$ for a grey atmosphere, cannot be less than unity. Since

$$x^{-1}(1-e^{-x}) = 1 - \frac{x}{2!} + \frac{x^2}{3!} - \ldots \to 1 \quad \text{as} \quad x \to 0$$

and

$$\frac{d}{dx}\{x^{-1}(1-e^{-x})\} = -x^{-2}e^{-x}(e^x-1-x) < 0 \quad \text{for} \quad x > 0,$$

therefore $(1-e^{-x})/x$ decreases steadily from 1 to 0 as x increases from 0 to ∞. The ratio $\sigma/(\bar{\kappa}+\sigma)$ of the continuous scattering to the total continuous absorption can take any value between 0 and 1, and therefore β_ν lies in the stated range.

We have to discover the range of values of β_ν for which (2.23) can be true.

Since x (i.e. $h\nu/kT_0$) decreases with increasing wave-length, for a given star β_ν will increase with increasing wave-length, and the largest value of β_ν for visible light will be that corresponding to the red end of the spectrum. From this it will subsequently appear that emission lines in high-temperature stars are more likely to appear in the red part of the spectrum, a result which accords with observation.

4. *The function* $f(\lambda,\beta)$.—The values of $f(\lambda,\beta)$ for values of λ lying between 0 and 1 and for certain values of β are given in Table I and are shown by the full lines in Fig. 1.

When $\beta < 1$, the behaviour near $\lambda = 0$ needs careful investigation, and for this we have to go back to the behaviour of $H(\mu)$ for small λ.

Let $H_0(\mu)$ be the solution of (2.11) when $\lambda = 0$. The exact solution of Milne's problem in the grey case is $I(0,\mu) = \frac{1}{4}\sqrt{3}FH_0(\mu)$ and for this reason the second moment of $H_0(\mu)$ is known with great precision, while the first is known exactly. These are

$$\alpha_1^{(0)} = 2/\sqrt{3}, \quad \alpha_2^{(0)} = 0{\cdot}820\,352. \tag{4.1}$$

TABLE I

Values of $f(\lambda, \beta)$

λ \ β	0·710446	1·0	1·5	2·0	2·5	3·0	3·258889
0·0	0·666...	0·666...	0·666...	0·666...	0·666...	0·666...	0·666...
0·025	·65442	·69857	·77482	·85107	0·92732	1·00357	1·04305
0·05	·64343	·70182	·80265	·90348	1·00431	1·10515	1·15735
0·075	·63314	·70124	·81883	·93641	1·05400	1·17159	1·23247
0·1	·62336	·69893	·82943	0·95992	1·09042	1·22091	1·28848
0·2	·58707	·68235	·84688	1·01141	1·17594	1·34047	1·42566
0·3	·55385	·66148	·84734	1·03320	1·21907	1·40493	1·50116
0·4	·52254	·63913	·84045	1·04177	1·24310	1·44442	1·54866
0·5	·49261	·61617	·82954	1·04291	1·25628	1·46964	1·58012
0·6	·46371	·59295	·81611	1·03928	1·26244	1·48561	1·60116
0·7	·43566	·56966	·80105	1·03244	1·26382	1·49521	1·61502
0·8	·40830	·54639	·78481	1·02325	1·26168	1·50012	1·62357
0·9	·38151	·52315	·76772	1·01229	1·25687	1·50144	1·62808
1·0	0·35522	0·50000	0·75000	1·00000	1·25000	1·50000	1·62944

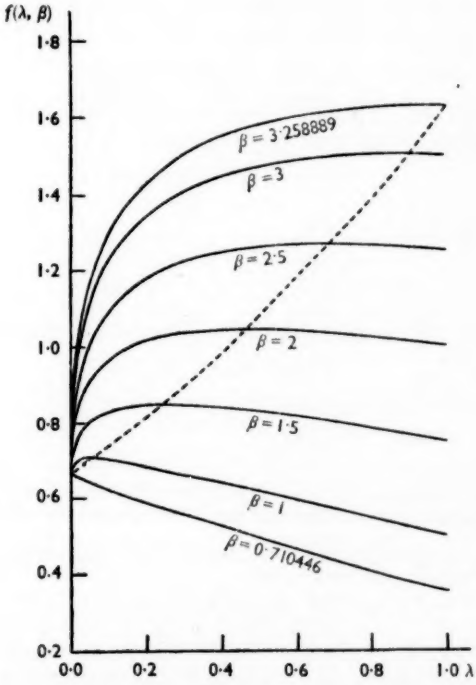

FIG. 1.—*The function* $f(\lambda, \beta)$. *The full curves represent the function for different values of* β. *The maxima lie in the dotted curve.*

The equation (2.11) can be expressed in the alternative form (1)

$$\frac{1}{H(\mu)} = \lambda^{1/2} + \tfrac{1}{2}(1-\lambda)\int_0^1 \frac{\mu' H(\mu')}{\mu+\mu'}\,d\mu', \tag{4.2}$$

and putting $\lambda = 0$, we have

$$\frac{1}{H_0(\mu)} = \tfrac{1}{2}\int_0^1 \frac{\mu' H_0(\mu')}{\mu+\mu'}\,d\mu'. \tag{4.3}$$

An iteration starting from $H_0(\mu)$ as a first approximation suggests that, when λ is small, $H(\mu)$ can be expressed in the form

$$H(\mu) = H_0(\mu) - \lambda^{1/2}H_1(\mu) + \lambda H_2(\mu) - \ldots,$$

but it is doubtful whether the sequence of iterations converges. If, however, we substitute for $H(\mu)$ in (4.2)

$$H(\mu) = H_0(\mu) - \lambda^{1/2}H_1(\mu) + \lambda h_\lambda(\mu), \tag{4.4}$$

where $H_1(\mu)$ is the solution of the integral equation

$$H_1(\mu) = H_0{}^2(\mu)\left\{1 - \tfrac{1}{2}\int_0^1 \frac{\mu' H_1(\mu')}{\mu+\mu'}\,d\mu'\right\}, \tag{4.5}$$

it can be shown that $h_\lambda(\mu)$ is bounded* as $\lambda \to 0$, so that the last term on the right-hand side of (4.4) is $O(\lambda)$.

Let $\alpha_1{}^{(1)}$, $\alpha_2{}^{(1)}$ be the first and second moments of $H_1(\mu)$. Then multiplying (4.4) by μ and μ^2 in turn and integrating over $(0, 1)$, we get

$$\alpha_1 = \alpha_1{}^{(0)} - \lambda^{1/2}\alpha_1{}^{(1)} + O(\lambda) = 2/\sqrt{3} - \lambda^{1/2}\alpha_1{}^{(1)} + O(\lambda), \tag{4.6}$$

$$\alpha_2 = \alpha_2{}^{(0)} - \lambda^{1/2}\alpha_2{}^{(1)} + O(\lambda), \tag{4.7}$$

and substituting these into (2.12) we have the identity

$$\lambda^{1/2}\alpha_2{}^{(0)} - \lambda\alpha_2{}^{(1)} + O(\lambda^{3/2}) + (1-\lambda)\{\tfrac{1}{3} - \lambda^{1/2}\alpha_1{}^{(1)}/\sqrt{3} + O(\lambda)\} = \tfrac{1}{3}.$$

In this the coefficient of $\lambda^{1/2}$ must vanish and so†

$$\alpha_1{}^{(1)} = \sqrt{3}\alpha_2{}^{(0)} = 1{\cdot}420\,892 \tag{4.8}$$

by (4.1).

Differentiating (4.6), we have

$$d\alpha_1/d\lambda = -\tfrac{1}{2}\alpha_1{}^{(1)}\lambda^{-1/2} + O(1). \tag{4.9}$$

From (2.22)

$$\frac{d}{d\lambda}f(\lambda,\beta) = -\tfrac{1}{2}(1-\lambda)\alpha_1{}^2 + \tfrac{1}{2}(1-\lambda)^2\alpha_1\frac{d\alpha_1}{d\lambda} - \tfrac{1}{3} + \tfrac{1}{2}\beta\lambda^{-1/2}\alpha_1 + \beta\lambda^{1/2}\frac{d\alpha_1}{d\lambda} \tag{4.10}$$

and by (4.6) and (4.9)

$$\frac{d}{d\lambda}f(\lambda,\beta) = \frac{1}{2\sqrt{3}}(2\beta - \alpha_1{}^{(1)})\lambda^{-1/2} + O(1).$$

---

* From (4.4) it is only known that $\lambda h_\lambda(\mu)$ is bounded as $\lambda \to 0$ for $0 \leqslant \mu \leqslant 1$. From this and from the integral equation which $h_\lambda(\mu)$ is found to satisfy, it can be shown that $h_\lambda(\mu)$ is itself bounded as $\lambda \to 0$.

† An alternative way of establishing (4.8) which provides an independent check of (4.4) is as follows. By means of (4.3), (4.5) can be written

$$H_0(\mu) = \tfrac{1}{2}\int_0^1 \frac{\mu'}{\mu+\mu'}\{H_0(\mu)H_1(\mu') + H_0(\mu')H_1(\mu)\}\,d\mu'.$$

Multiplying by μ^2 and integrating over (0, 1), we have

$$\alpha_2{}^{(0)} = \tfrac{1}{2}\int_0^1\int_0^1 \frac{\mu^2\mu'}{\mu+\mu'}\{H_0(\mu)H_1(\mu') + H_0(\mu')H_1(\mu)\}\,d\mu\,d\mu'.$$

In this μ and μ' can be interchanged and the two equations added. This gives

$$2\alpha_2{}^{(0)} = \tfrac{1}{2}\{\alpha_1{}^{(0)}\alpha_1{}^{(1)} + \alpha_1{}^{(0)}\alpha_1{}^{(1)}\} = \alpha_1{}^{(0)}\alpha_1{}^{(1)} = 2\alpha_1{}^{(1)}/\sqrt{3}$$

by (4.1).

It follows that the graph of $f(\lambda, \beta)$ has a finite gradient at $\lambda = 0$ only if

$$\beta = \tfrac{1}{2}\alpha_1^{(1)} = 0{\cdot}710\,446.$$

If $\beta > 0{\cdot}710\,446$, $f(\lambda, \beta)$ has an infinite positive gradient at $\lambda = 0$; if $\beta < 0{\cdot}710\,446$ it has an infinite negative gradient. Thus, provided that $\beta_r > 0{\cdot}710\,446$, it is possible to satisfy (2.23) for sufficiently small λ_r and λ_c.

From the graphs in Fig. 1 it is seen that, when $\beta > 0{\cdot}710\,446$, $f(\lambda, \beta)$ has a single maximum for $0 \leqslant \lambda \leqslant 1$. As β increases, the abscissa of this maximum also increases and it is important to determine the value of β for which it is exactly at $\lambda = 1$. For all greater values of β, $f(\lambda, \beta)$ is steadily increasing in (0, 1) and the condition (2.23) for emission lines (with $\beta_r = \beta$) will always be satisfied since $\lambda_r > \lambda_c$.

From (4.10), with $\lambda = 1$, we have

$$\left[\frac{d}{d\lambda} f(\lambda, \beta)\right]_{\lambda=1} = -\tfrac{1}{3} + \beta\left[\tfrac{1}{2}\lambda^{-1/2}\alpha_1 + \lambda^{1/2}\frac{d\alpha_1}{d\lambda}\right]_{\lambda=1}.$$

When $\lambda = 1$, $\alpha_1 = \frac{1}{2}$ (see (**2**)), and so

$$\left[\frac{d}{d\lambda} f(\lambda, \beta)\right]_{\lambda=1} = -\tfrac{1}{3} + \beta\left[\tfrac{1}{4} + \left(\frac{d\alpha_1}{d\lambda}\right)_{\lambda=1}\right]. \tag{4.11}$$

Differentiating (2.11) with respect to λ and putting $\lambda = 1$ we have, since $H(\mu) = 1$ when $\lambda = 1$,

$$\left[\frac{\partial}{\partial\lambda} H(\mu)\right]_{\lambda=1} = -\tfrac{1}{2}\mu \int_0^1 \frac{d\mu'}{\mu + \mu'} = -\tfrac{1}{2}\mu \ln(1 + \mu^{-1}).$$

Hence

$$\begin{aligned}\left(\frac{d\alpha_1}{d\lambda}\right)_{\lambda=1} &= \int_0^1 \left[\frac{\partial}{\partial\lambda} H(\mu)\right]_{\lambda=1} \mu\, d\mu \\ &= -\tfrac{1}{2}\int_0^1 \mu^2 \ln(1 + \mu^{-1})\, d\mu \\ &= \tfrac{1}{12} - \tfrac{1}{3}\ln 2.\end{aligned}$$

Substituting into (4.11), we have

$$\left[\frac{d}{d\lambda} f(\lambda, \beta)\right]_{\lambda=1} = -\tfrac{1}{3} + \beta(\tfrac{1}{3} - \tfrac{1}{3}\ln 2),$$

and this is zero when

$$\beta = 1/(1 - \ln 2) = 3{\cdot}258\,889.$$

Thus for $\beta_r \geqslant 3{\cdot}258\,889$ the condition (2.23) for emission will always be satisfied; if

$$0{\cdot}710\,446 < \beta_r < 3{\cdot}258\,889, \tag{4.12}$$

the condition will be satisfied if λ_r and λ_c both lie to the left of the maximum, and it is possible for it to be satisfied if they are separated by the maximum. The maxima of $f(\lambda, \beta)$ as β varies lie on the dotted curve in Fig. 1.

5. *Some numerical examples.*—(i) If $T_0 = 5\,000$ deg., then for visible light $x = h\nu/kT_0$ varies between about 3·6 and 7·2; hence $(1 - e^{-x})/x$ varies between 0·271 and 0·139. Taking $a = \frac{3}{2}$ in (3.2) we see that β_r varies between $0{\cdot}723\sigma/(\bar{\kappa} + \sigma)$ (corresponding to the red end of the spectrum) and $0{\cdot}367\sigma/(\bar{\kappa} + \sigma)$ (corresponding to the violet end). Even the largest value of β_r will not fall within the range given by (4.12) unless $\sigma/(\bar{\kappa} + \sigma) > 0{\cdot}9826$ making the ratio $\sigma : \bar{\kappa}$ greater than 70 : 1—an impossible value because there are very few free electrons at this

temperature to produce the continuous scattering. Thus emission lines will not be formed by pure absorption.

Without investigating (2.17) in detail when $\xi<1$, it is possible to see that emission lines cannot be formed in such a star partly by absorption and partly by scattering. Since σ is small, it follows from (2.14) that λ_c is very nearly unity. But we have shown that the formation of emission lines is impossible unless $\xi>\lambda_c$ and so $\xi\simeq 1$. This brings us back to the case which we have already dismissed as impossible. There is strong evidence, however, that scattering plays an important part in line formation in such a star, so that ξ is, in fact, small, and certainly $\xi<\lambda_c$. Thus lines formed in this way must be dark, and an explanation of any bright lines which do occur must be based on some other hypothesis (see Section 6).

(ii) If $T_0=30\,000$ deg., then for visible light x varies between 0·6 and 1·2, and $(1-e^{-x})/x$ varies between 0·752 and 0·582. Again taking $a=\frac{3}{2}$, we see that β_ν varies between $2{\cdot}005\sigma/(\bar{\kappa}+\sigma)$ and $1{\cdot}552\sigma/(\bar{\kappa}+\sigma)$. These values of β_ν all lie within the range (4.12) if $\sigma/(\bar{\kappa}+\sigma)>0{\cdot}457\,8$, i.e. if $\sigma/\bar{\kappa}>0{\cdot}844\,3$.

(iii) Underhill has recently published details of a model for an early O-type star (**4**), which she has classified as O9·5. For this $T_0=30\,000$ deg. The coefficients* σ and $\bar{\kappa}$ vary with depth, but the average value of $\sigma/(\bar{\kappa}+\sigma)$ over the range $0\leqslant\tau\leqslant 5$ is 0·327. With this value, together with the results of (ii), we find that the greatest value of β_ν for visible light is $0{\cdot}655\,6$; hence emission lines are not likely to occur.

(iv) It is unlikely that the upper value $3{\cdot}258\,889$ will be exceeded by the β_ν of any star. If, for example, $T_0=40\,000$ deg., the largest value of $(1-e^{-x})/x$ for visible light is about 0·806 ($x=0{\cdot}448$). With this value, $\beta_\nu\geqslant 3{\cdot}258\,889$ only if

$$\frac{1}{a}\cdot\frac{\sigma}{\bar{\kappa}+\sigma}\geqslant\frac{3{\cdot}258\,889}{4\times 0{\cdot}806}\simeq 1{\cdot}01,$$

an inequality which is impossible unless $a<1$ and σ is very large compared with $\bar{\kappa}$.

6. *Discussion.*—From the examples just considered we can see that conditions favourable for the formation of emission lines are to be expected in a star of high surface temperature with an atmosphere in which electron scattering is of greater importance than continuous absorption. The conditions will, moreover, be more favourable in the longer wave-lengths, so that emission lines are likely to appear first in the red.

Unsöld, in his investigations of the B-type star τ Scorpii (**5**), concluded from the observed central intensities of the absorption lines that the lines are formed by pure absorption. The fact that emission lines in a high-temperature star can be explained theoretically on the hypothesis of pure absorption but not on that of pure scattering gives independent support for Unsöld's inference. If this hypothesis is indeed correct, that of detached shells, which has been evoked as an explanation of emission lines in a hot star, becomes unnecessary.

In low-temperature stars the formation of emission lines is impossible according to the theory developed here. The theory depends upon assumptions, such as the independence of depth of the coefficients σ and κ_ν, which are known to be untrue, but it should provide a first approximation to the stellar reality. The figures given in Section 5(i) are sufficient to show that no refinements of

* Underhill uses the Chandrasekhar-mean absorption coefficient for $\bar{\kappa}$.

the theory are likely to account for bright lines in the spectrum of a star whose surface temperature is 5 000 deg. or less. It follows that we must look for an entirely different hypothesis to account for the emission lines in the spectra of some long-period variables of low surface temperature. This must take into account the peculiar conditions obtaining near the surface of the variable at times of maximum and minimum brightness.

7. *Mixed absorption and scattering.*—In Section 4 we have only considered lines formed by pure absorption. We can, however, show that, if a line is found to be dark on a hypothesis of pure absorption, it will be dark if it is formed partly by absorption and partly by scattering. In other words, no hypothesis intermediate between pure absorption and pure scattering will account for the formation of bright lines, if they cannot be explained on the hypothesis of pure absorption.

We have seen that a line is dark if $\xi<\lambda_c$ and we must therefore consider values of ξ for which $\lambda_c\leqslant\xi<1$, or values of $\lambda_\nu^{(\xi)}$ for which

$$\lambda_c\leqslant\lambda_\nu^{(\xi)}<\lambda_\nu, \tag{7.1}$$

where $\lambda_\nu^{(\xi)}$ and λ_ν are given by (2.2) and (2.24) respectively.

From (2.7), (2.14) and (2.24) we have

$$n_\nu=(1-\lambda_\nu)/(1-\lambda_c)$$

and (2.15) can therefore be written

$$\boldsymbol{R}_\nu=\frac{(1-\lambda_\nu)R_1(\lambda_\nu^{(\xi)})+\beta_\nu R_2(\lambda_\nu^{(\xi)})}{(1-\lambda_c)R_1(\lambda_c)+\beta_\nu R_2(\lambda_c)}, \tag{7.2}$$

where β_ν is given by (2.25) or by (3.2). From (2.21),

$$\boldsymbol{R}_\nu=\frac{f(\lambda_\nu^{(\xi)},\beta_\nu)-(\lambda_\nu-\lambda_\nu^{(\xi)})R_1(\lambda_\nu^{(\xi)})}{f(\lambda_c,\beta_\nu)}<\frac{f(\lambda_\nu^{(\xi)},\beta_\nu)}{f(\lambda_c,\beta_\nu)}. \tag{7.3}$$

We have now to distinguish two cases: $\beta_\nu\leqslant 0{\cdot}710\,446$ and $\beta_\nu>0{\cdot}710\,446$. In Section 4 we have shown that $f(\lambda,\beta_\nu)$ is steadily decreasing in $(0,1)$ when $\beta_\nu\leqslant 0{\cdot}710\,446$. In that case

$$f(\lambda_\nu^{(\xi)},\beta_\nu)\leqslant f(\lambda_c,\beta_\nu),$$

since $\lambda_\nu^{(\xi)}\geqslant\lambda_c$, and it follows from (7.3) that $\boldsymbol{R}_\nu<1$. Thus when $\beta_\nu\leqslant 0{\cdot}710\,446$ lines are necessarily dark whether formed by pure absorption or by part absorption and part scattering.

Now suppose that $\beta_\nu>0{\cdot}710\,446$ and consider the numerator $N(\lambda_\nu^{(\xi)})$ of (7.2), where

$$N(\lambda)=(1-\lambda_\nu)R_1(\lambda)+\beta_\nu R_2(\lambda). \tag{7.4}$$

We shall show that $N(\lambda)$ is an increasing function of λ in $(0,1)$. From this it will follow that, when $\lambda_\nu^{(\xi)}<\lambda_\nu$,

$$N(\lambda_\nu^{(\xi)})<N(\lambda_\nu)=f(\lambda_\nu,\beta_\nu)$$

and hence that

$$\boldsymbol{R}_\nu<\frac{f(\lambda_\nu,\beta_\nu)}{f(\lambda_c,\beta_\nu)}.$$

If a line is found to be dark on the hypothesis of pure absorption, then

$$f(\lambda_\nu,\beta_\nu)<f(\lambda_c,\beta_\nu)$$

and it will follow that $\boldsymbol{R}_\nu<1$ and that the line is dark on a hypothesis of part absorption and part scattering.

In order to establish that $N(\lambda)$ is an increasing function of λ in $(0, 1)$, we write (7.4) in the form

$$N(\lambda) = h(\lambda) - \lambda_* R_1(\lambda), \tag{7.5}$$

where

$$h(\lambda) = R_1(\lambda) + \beta_* R_2(\lambda). \tag{7.6}$$

Since $R_1(\lambda)$ is steadily decreasing in $(0, 1)$, the result will follow if $h(\lambda)$ is steadily increasing. Now from (2.12) and (2.13) we have

$$R_1(\lambda) = \tfrac{2}{3} - \lambda^{1/2}\alpha_2,$$

and so, by (2.10),

$$\begin{aligned} h(\lambda) &= \tfrac{2}{3} + \lambda^{1/2}(\beta_*\alpha_1 - \alpha_2) \\ &= \tfrac{2}{3} + R_2(\lambda)(\beta_* - \alpha_2/\alpha_1). \end{aligned} \tag{7.7}$$

From the tables for α_1 and α_2 given in (**2**) it is found that α_2/α_1 decreases steadily from the value 0·710 446 when $\lambda = 0$ to the value $\frac{2}{3}$ when $\lambda = 1$. It follows that $\beta_* - \alpha_2/\alpha_1$ is positive and steadily increasing when $\beta_* > 0{\cdot}710\,446$. Since the same is true of $R_2(\lambda)$, it follows from (7.7) that $h(\lambda)$ is also steadily increasing in $(0, 1)$. This completes the proof.

In conclusion I should like to thank Professor H. H. Plaskett for drawing my attention to Unsöld's paper on τ Scorpii and for some valuable criticisms.

St. Hugh's College,
Oxford :
1951 *October* 20.

References

(1) S. Chandrasekhar, *Radiative Transfer*, chap. V, Oxford, 1950.
(2) S. Chandrasekhar, *loc. cit.*, Section 84.
(3) A. B. Underhill, *Ap. J.*, **110**, 350, 1949.
(4) A. B. Underhill, *Publ. D.A.O.*, **8**, No. 12, 357, 1951.
(5) A. Unsöld, *Zs. f. Ap.*, **21**, 22, 1941.

STUDIES OF Hα LINE PROFILES IN PROMINENCES

Mary T. Conway

(Communicated by the Astronomer Royal for Scotland)

(Received 1951 October 2)

Summary

An account is given of observations made on quiescent prominences in the Hα line with the combined spectrograph and spectrohelioscope at the Royal Observatory, Edinburgh. Prominences were photographed in emission on the limb and in absorption on the disk. Corrections were determined and applied for the effect of grating ghosts, scattered light and limited resolving power. The average corrected intensity for prominences observed in emission on the limb was 10·4 per cent of the continuous spectrum of the centre of the Sun's disk 13 A outside Hα. The half-width of the Hα emission line ranges between 0·64 and 1·30 A.

---

1. *Introduction.*—Line profiles of Hα in quiescent prominences have been measured previously by Woolley and Newton (**1**) at Greenwich and by Unsöld (**2**) at Mount Wilson. The measurements of Woolley and Newton were made visually with a spectrohelioscope. Intensities were found by means of a wedge photometer, prominence intensities being compared with the brightness of a lamp, which in turn was compared with the Sun's continuous spectrum 15 A outside Hα at the centre of the disk. Observed profiles were corrected for the finite width of the spectrohelioscope slits, and for the effect of heterochromatic light in the instrument.

Unsöld measured profiles photographically but applied no corrections. Only three plates were obtained, and two of these show a considerable background of scattered light.

The present work was undertaken with a view to determining line profiles to a greater degree of accuracy than has been attained by either of the above methods. The improvements may be summed up as follows.

(*a*) By using the photographic method, only one slit was used. In Woolley and Newton's visual method, corrections had to be made for the slits of the spectrohelioscope. Further, their correction was for finite slit-width only; thus they assumed that the optical performance of the instrument was limited only by the slit. In this present work the instrumental profile was measured directly, so that the errors due to the imperfect performance of the instrument, as well as those due to the finite width of the slit, have been accounted for.

(*b*) Scattered light was measured directly.

(*c*) A correction was made for grating ghosts.

(*d*) In the photographic method, the spectrograph slit could be set to gather light from any desired part of the prominence, therefore intensity and profile measurements made on such a plate represent the conditions at a particular region in the prominence. The intensity of a prominence is by no means uniform over its whole area, though it may appear uniformly bright when observed in the

spectrohelioscope. By Woolley and Newton's visual method the whole prominence was observed at one time.

(*e*) When making exposures on limb prominences, an image rotator was used to orient the Sun's image until the limb near the prominence was brought parallel to the slit. In this way all photospheric light was excluded from the spectrograph during prominence exposures, thus avoiding a background of scattered light which may be as great as 60 per cent of the maximum brightness of the prominence, as was the case in one of Unsöld's prominences.

2. *Procedure.*—The observations described here were carried out with the combined spectrograph and spectrohelioscope at the Royal Observatory, Edinburgh. This combined instrument was constructed by Dr M. A. Ellison and is designed for the photography of the spectra of flares and other transient phenomena. It is shown diagrammatically in Fig. 1. The Sun's light is directed by a siderostat through a 5-inch achromatic lens of 18 feet focal length, which forms an image of the Sun 2 inches in diameter on the primary slit S_1. The instrument, which is autocollimating, uses a $5\frac{1}{2}$-inch Rowland plane grating G of 80 000 lines. The achromatic lens L, which has a focal length of 16 feet, fills the grating with parallel light and also serves to focus the spectrum either on the viewing slit S_2 or on the plate in the camera at P. The Sun's image may be

FIG. 1.—*Combined spectrohelioscope and spectrograph.*

viewed in Hα light in the spectrohelioscope. For photography, the grating may be rotated until the required part of the spectrum is brought on to the plate; this is easily done by means of a handle at the eye end. The primary slit is 0·1 mm wide, a suitable width for spectrohelioscope work, which is the main function of this instrument. This width is, however, greater than the optimum value for a spectrograph of this type, which from simple theory (**3**) is 0·02 mm. The slit jaws were adjusted to parallelism by closing them against a steel shim, previously tested for uniformity of thickness with a micrometer. The jaws were clamped in this position and have not been altered throughout the course of the work presented in this paper.

Each prominence to be photographed was first located visually in the spectrohelioscope, and its dimensions and characteristics noted and entered on a drawing of the Sun's disk. During exposure an image rotator was mounted directly in front of the slit on an optical bench (B in Fig. 1). This image rotator (constructed by Dr Ellison) uses a right-angled prism with sides of 2 inches mounted with its hypotenuse face parallel to the axis of the incoming beam. A weak positive lens is fixed in front of the prism to compensate for the change in focus. During exposures the image was accurately guided on the slit by tilting a plane parallel plate of glass in front of the slit. For each exposure the height above the limb could be estimated to the nearest ten thousand kilometres by means of two pairs

of lines ruled on the faces of the slit jaws at distances corresponding to distances of thirty and sixty thousand kilometres on the Sun. For small prominences exposures at one height only were made; for large prominences a series of exposures was taken at different heights above the limb, ranging from ten to seventy thousand kilometres.

In the case of prominences photographed on the disk, it was not possible to eliminate scattered light, since the slit was fully illuminated. There was, therefore, no point in using the image rotator for disk prominences.

Exposures were made in both first and second orders. Exposure times varied from 5 to 30 seconds, and were in the majority of cases about 20 seconds. The camera shutter was operated by hand, timing being done with an electric clock with centre seconds hand.

All prominence spectra were standardized by photographing, on another part of the same plate and through a Hilger step wedge, the spectrum of the centre of the Sun's disk. The wedge has six steps and a clear glass portion, the transmissions of successive steps being in the approximate ratio of 2 : 1. The transmissions were accurately measured with a rectifier photocell in the red end of the spectrum. The intensity at any wave-length in the profile of a prominence could thus be found in terms of the intensity of the Hα continuum at the centre of the Sun's disk. This intensity was considerably higher than that of the prominence, and therefore it was necessary to reduce the light from the disk during standardization by means of neutral screens, in order that the exposure times on prominence and disk be the same. The transmissions of the screens were measured (in the red end of the spectrum) with the rectifier photocell. Plates were standardized as far as possible immediately after exposure, to avoid any error due to changing sky conditions. Where the image rotator was used for an exposure, it was left in position during standardization. The plates used throughout were Kodak type IIIF; they were always developed in M.Q. developer at 18 deg. C for five minutes.

The majority of plates were measured with the Kipp and Zonen recording microphotometer which was brought into use in the Observatory at the beginning of 1949. A few of the plates obtained before this date were measured with the non-recording microphotometer of the Observatory. The recording microphotometer gives a magnification of 50 between plate and bromide tracing. Distance lines impressed on the tracings every 5 mm correspond to distances of 0·1 mm on the plate. The full deflection between clear glass and infinite density was kept as near as possible to 10 cm. It was found that, with the particular dispersion and resolution of the spectrograph, a width of up to 20 μ was permissible for the analysing slit. It was thus possible to adjust the full-scale deflection to 10 cm by varying the slit width between 16 μ and 20 μ. The width was never allowed to exceed 20 μ, so in the case of very short prominence images a full-scale deflection was not possible. The illuminating slit was always set so that the width of the exploring beam was double that of the analysing slit.

The standardization spectrum was measured in two regions free from Fraunhofer lines and equidistant from Hα. The wave-lengths chosen were λ6550 and λ6576. A short run on each step of the standardization spectrum at both these wave-lengths was made. Two clear-glass records were also made, one near the prominence spectrum and one near the standardization spectrum and near the centre of the plate to avoid edge effects.

Fig. 2 (Plate 1) shows a specimen of microphotometer tracings for a prominence Hα profile and its standardization.

Deflections on the tracings were converted to Δ-values, where the function Δ, known as the blackening, is $\log_{10}\{(1-T)/T\}$, T being the transparency, or fraction of light transmitted. For the standardization spectra, the Δ-values corresponding to the wave-length of Hα were taken to be the mean of the Δ-values measured at λ6550 and λ6576. Δ-values were plotted against wedge "magnitudes" (magnitude $m = 2{\cdot}5 \log_{10}(1/t)$, where t is the transmission of a step of the wedge), to give calibration curves which are approximately linear and of about unit slope. This procedure was adopted on the suggestion of Dr E. A. Baker, who first introduced the Δ-function into spectrophotometry (**4**).

3. *Correction for grating ghosts.*—The grating used in the Edinburgh spectrograph had been ruled by Schneider on Professor Rowland's engine and therefore it was expected to be comparatively free from ruling errors. The ghosts were photographed in both orders for the green line of mercury λ5461. As the first ghosts on either side of the line seemed to have an intensity of less than 1 per cent of the main line, a very narrow strip of neutral glass of measured transmission about 1 per cent was mounted directly in front of the plate so as to intercept and transmit the light from the main line. This had the effect of reducing the intensity of the main line so as to be comparable with that of its ghosts. The ghosts were found to be symmetrically placed about the main line at distances from it of nd, where $n(=1, 2, 3, \text{etc.})$ is the order of the ghost, $d = 7$A for the first order and $d = 3{\cdot}5$ A for the second order. They were somewhat brighter on the red side of the line than on the violet side. Exposures of 15 to 30 minutes were given on the ghosts and the plates were standardized for the same length of time, using light from the centre of the Sun's disk. It was necessary to reduce the intensity of the Sun's light by stopping down the aperture of the objective to 1 or 2 inches. Four plates were obtained in each order. One of the first-order plates was exposed without the 1 per cent screen; this plate gave the relative intensities of the ghosts but not their absolute values. The plates show a background of scattered light, which is termed linear scattering and which will be discussed later. This background of scattered light had to be subtracted from the apparent ghost intensities to give true values. It is fortunate that the ghosts are weak, so that the errors in the estimation of their intensity due to the presence of scattered light are without importance.

Though seven or eight ghosts are visible on either side of the line, only four were measurable on the plates. The intensities of these four are given in Table I. The totals given include contributions of the fainter ghosts which were found by extrapolation.

TABLE I

Intensities of Grating Ghosts in Percentages of the Main Line

	Red				Violet				
Ghost	1	2	3	4	1	2	3	4	Total
First Order	0·20	0·07	0·04	0·03	0·10	0·05	0·03	0·02	0·60
Second Order	0·62	0·23	0·14	0·09	0·52	0·26	0·14	0·09	2·34

The ratio of the total ghost intensities in the first and second orders is in good agreement with Minnaert's theory (**5**) which predicts a ratio of 1 : 4.

The intensities of the ghosts in the Edinburgh spectrograph may be compared with those of the Mount Wilson 150-foot tower telescope which is equipped with

FIG. 2.—*Microphotometer tracing of the Hα line in emission in a prominence, showing standardization of λ 6550 and λ 6576. The values of the steps of the calibrating wedge are given in magnitudes.*

a Michelson plane grating. The total ghost intensities for this spectrograph, as measured by Minnaert, Mulders and Houtgast (**6**), are 0·61 per cent in the first and 2·34 per cent in the second order, though the relative intensities of the individual ghosts are different from ours. For the Utrecht spectrograph, which is similar to the Edinburgh instrument and which has an 8-cm plane Rowland grating of 45 000 lines, the total ghost intensities found by Houtgast (**7**) are 1·25 per cent in the first and 5·1 per cent in the second order.

If the total ghost intensity is g, that is, if each part of the spectrum loses a fraction g of its light to its ghosts, then the true intensity i of an emission line is found from the observed intensity i' from the relation

$$i = i'/(1-g). \tag{1}$$

The value for the ghost intensities derived in Table I are the intensities of the ghosts compared with the residual line. The last column of the table, therefore, does not represent g but $g/(1-g)$. The difference between the two is of the order g^2, and in practice it is sufficient to take g to be 0·006 in the first order, and 0·023 in the second order.

The correction of absorption lines for ghosts depends on how the intensities have been measured in the first instance. Normally, the intensity of an absorption line is measured as a fraction of the continuous spectrum outside its own wings, and when this is the case the correction is the usual one (**6,7**),

$$r = (r'-g)/(1-g), \tag{2}$$

where r is the true intensity of the line and r' is the observed intensity, the intensity of the continuous spectrum on this scale being 1. Intensities measured in terms of the local continuum in this way will be referred to in this paper as "relative" intensities.

In measuring the intensity of a prominence which is not located on the centre of the Sun's disk, the intensity may also be given in terms of the continuous spectrum for the centre of the Sun's disk as unit. The value of this intensity is found directly from the standardization spectrum, and will be referred to as the "absolute" intensity. In this case the intensity of the continuous spectrum at the centre of the Sun's disk is put equal to 1, and the intensity of the continuous spectrum at the position of the prominence is now not 1 but σ, the limb-darkening coefficient. The quantity σ was known for each prominence, as will be described in Section 9. The centre of the absorption line whose true intensity is i loses therefore an amount of light gi and gains an amount $g\sigma$ from the local continuous spectrum. Hence the observed intensity i' is given by $i' = (i-gi) + \sigma g$ or

$$i = (i'-\sigma g)/(1-g). \tag{3}$$

4. *Correction for heterochromatic light.*—It is well known that one of the main sources of error in spectrophotometry arises from heterochromatic light being scattered from the walls and surfaces of the instrument on to the plate. General precautions were taken to reduce this scattering to a minimum.

(*a*) The walls of the spectrograph were covered throughout with black velvet.

(*b*) A stop O_1 (Fig. 1) was placed at the effective focus of the outer concave surface of the spectrograph lens to eliminate the real image of the first slit formed by reflection from this surface. This stop (a black rectangle 10 mm × 5 mm) is placed 30 inches in front of the lens on the axis of the spectrograph. Another stop O_2 in the form of a horizontal strip 6 mm wide, mounted at the level of the

centre of the lens, cuts out the light from the virtual images of the first slit formed behind the lens by reflection from the other lens surfaces.

(*c*) A red filter (Schott and Gen. R.G. 2) which transmits only wave-lengths greater than $\lambda 6200$ was mounted in front of the slit. Since the amount of scattered light depends on the total light entering the instrument, this had the effect of reducing scattered light as well as preventing overlapping of orders.

The intensity of the scattered light reaching the plate was determined by experiment. A metal strip a few millimetres wide was fixed horizontally across the centre of the (vertical) slit of the spectrograph. When an exposure was made on the centre of the Sun's disk, it was found that a certain amount of light had been scattered into the unexposed band across the centre of the spectrum corresponding to the part of the slit which had been occulted. Exposures of ten times the normal exposure time had to be given in order to show up the scattered light, and the plates were standardized in the usual way, using the centre of the Sun's disk.

On examining the occulted region on the plates it was found that Fraunhofer lines could be traced to distances of 1·2 mm from either edge. This effect is astigmatism, which causes the spectrum to be spread in a direction perpendicular to the dispersion. Beyond 1·2 mm the scattered light was uniform both with distance from the edges and along the dispersion. This indicates that the scattered light which we want to measure is spread uniformly over the spectrum. In order to measure the intensity of this uniformly scattered light, it is obvious that the minimum width of occulting strip must exceed 2·4 mm. In these experiments two strips were used of widths 3 mm and 6·5 mm. The exact width of the occulted region was measured on each plate with a travelling microscope. A series of plates was taken in both orders, the total length of slit being varied by means of a pair of horizontal jaws mounted in front of it.

The results found are plotted in Fig. 3. Each point on the curves represents the mean of two plates taken under identical conditions. The length of slit illuminated is the total length minus the width of the occulting strip, and the intensities are measured in terms of the continuous spectrum outside Hα at the centre of the disk. Scattered light was assumed by Shane (**8**) for the Mount Wilson spectrograph to be proportional to the length of slit illuminated, but the curves in Fig. 3 show that this is only approximately true for our spectrograph.

A somewhat similar method for the determination of scattered light was used by Shane (**8**) in his study of absorption lines made with the Mount Wilson spectrograph. In Shane's experiments over-exposed plates were taken of the Sun's spectrum and the light scattered beyond the edges of the spectrum was measured. This light is made up of two components—general scattered light which is the quantity required, and light scattered by astigmatism in a direction perpendicular to the spectrum. Perpendicular scattering was measured separately from an over-exposed plate of a single emission line, which was, of course, free from general scattering. The difference between the total scattering and the perpendicular scattering gave the general scattering. The advantage of the occulting strip method used here is that the general scattering could be measured directly, independently of astigmatism. Moreover, the scattering was measured at the centre of the field, just where we require to know its value, and not beyond the edge of the spectrum, where its effect may be appreciably different.

A certain amount of inaccuracy arises in estimating the scattered light correction to be applied when the full slit is illuminated. The total slit length is 26 mm,

and, as has been explained before, the minimum occulting strip which could be used in our experiments had to exceed 2·4 mm in width. Hence the last point on the curves in Fig. 3 corresponds to only 23 mm length of illuminated slit, so that the scattered light for the total slit must be found by extrapolation. The obvious way to avoid this is to use a shorter slit for exposures on the Sun's disk.

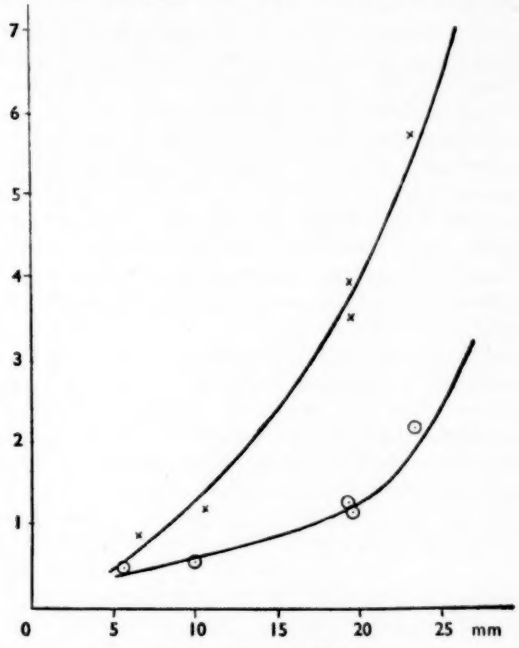

FIG. 3.—*Scattered light.*
Ordinates : *Intensity (percentage of continuum).*
Abscissae : *Length of slit illuminated.*
○ : *First order.*
× : *Second order.*

Since the image rotator was used in photographing prominences on the limb, and no direct photospheric light was allowed to enter the instrument, there is for such emission prominences no appreciable heterochromatic light scattered on to the plate. The standardization spectrum, however, is enhanced by heterochromatic light, and the intensities measured from it must be corrected accordingly. The total effective length of slit illuminated during standardization is 9·4 mm. If the intensity of the scattered light corresponding to a slit length of 9·4 mm is α times the intensity of the Hα continuum, then the apparent intensities found from the standardization must be increased by α times the intensity of the Hα continuum for the light incident on the slit. The intensities of scattered light plotted in Fig. 3 were found, using the uncorrected standardization (as given by the photoelectrically determined transmissions of the wedge steps), and so they need correction, with the result that the value of α is not that corresponding to 9·4 mm on the appropriate graph in Fig. 3. In the first order, exposures for scattered light were standardized through a neutral screen of transmission

0·25, so that all intensities on the first-order graph are too small by an amount $0{\cdot}25\alpha$. From the curve we find the apparent scattering at 9·4 mm to be 0·56 per cent, giving $\alpha = 0{\cdot}56 + 0{\cdot}25\alpha$, so that $\alpha = 0{\cdot}75$ per cent. Similarly, in the second order the screen used for standardization was of transmission 0·364. The apparent intensity of the scattered light at 9·4 mm is 1·20 per cent, giving $\alpha = 1{\cdot}20 + 0{\cdot}364\alpha$, or $\alpha = 1{\cdot}89$ per cent.

In general, then, where a screen of transmission T is used to reduce the intensity of the standardization spectrum, the corrected intensity I is found from the apparent intensity I' by using the formula $I = I' + \alpha T$, the unit of intensity in this formula being the intensity of the Hα continuum at the centre of the disk. This correction affects every point on the line profile and is proportionally greatest at the low-intensity values. The best method of procedure would have been to adopt new effective transmission values for the steps of the calibrating wedge and thus avoid completely the necessity of correcting each intensity measurement made, but as most of the reductions of plates were done before the scattered light was accurately measured, this was not practicable. The intensity measurements set down as "observed" intensities in Tables III and V incorporate this standardization correction.

When measured intensities in an *absorption* line have been corrected for the standardization effect described above, a further correction is necessary for the light scattered over the spectrum itself. In photographing prominences on the disk, the whole slit was always fully illuminated. If the scattered light corresponding to the total slit is βI (where I denotes the intensity of the continuum), then each part of the spectrum is enhanced by an amount of light βI. Therefore, if r is the true relative (see Section 3) intensity, the observed relative intensity r' is given by $r' = (r + \beta)/(1 + \beta)$ or

$$r = r'(1 + \beta) - \beta. \tag{4}$$

The absolute (see Section 3) intensity is affected in a different way. If i is the true absolute intensity, i' the observed intensity and σ the intensity of the local continuum, then

$$i = i' - \beta\sigma. \tag{5}$$

The value of β is 2·8 per cent in the first and 7·7 per cent in the second order. These values were found by reading off the graph in Fig. 3 the percentage scattered light corresponding to 26 mm, which is the total length of the slit, and adding the correction αT.

5. *Discussion of other forms of scattered light*

(*a*) *Astigmatism.*—Light scattered in a direction perpendicular to the dispersion by astigmatism does not affect profile measurements at all and affects absolute intensity measurements only if the object photographed is very small. It has been stated above that the effect of astigmatism can be traced out to 1·2 mm from the edge of the spectrum. Its actual intensity has been measured from the plates used for measuring scattered light, and is found to fall off rapidly with distance from the edge of the spectrum. At a distance of 0·3 mm from the spectrum the effect of perpendicular scattering (found by subtracting the known general scattering from the total scattering) is only 0·5 per cent. As the length of the Hα line of a prominence is usually a few millimetres on the plate, there will be no change of the density of the central part of the image due to this effect.

(*b*) *Linear scattering.*—The light of a particular wave-length scattered by the grating along the dispersion into other wave-lengths is termed linear scattering. It arises from random irregularities in the ruling of the grating in the same way as periodic ruling errors give rise to ghosts. Its magnitude was estimated by Shane (**8**) from highly exposed plates of the mercury green line used for measuring ghosts. The effect is apparent on our ghost plates as well, but, as Thackeray (**9**) has pointed out, it is impossible to distinguish true linear scattering from the extended wings of a broad line such as the mercury line. No attempt was made to measure linear scattering in this way, because since it falls off with the distance from the centre of the line, it is included in the wings of the instrumental profile. For this reason it was not necessary to investigate linear scattering separately.

(*c*) *Scattered light due to indirect photospheric light.*—It has been pointed out already that no direct photospheric light was allowed to enter the spectrograph during exposures on limb prominences. Photospheric light enters the slit indirectly, however, as a result of diffusion in the atmosphere and of scattering by the telescope lens and the siderostat mirror. Atmospheric scattering has been measured by Fracastoro (**10**) and found to be 10^{-3} times the intensity of the Sun's photosphere at 2′ beyond the limb under normal seeing conditions at a level of 2 700 metres. The same figure has been obtained by Kienle (**11**) for the minimum sky brightness at a distance of $0{\cdot}1R$ from the Sun's limb. Under normal conditions he estimated the intensity to be at least ten times this value, or equal to 10^{-2} times the photospheric brightness. Though this effect is too small to show up on the photographic plate in the exposure time given to the prominences, it means, nevertheless, that the intensity values measured for prominences are all systematically too great by an amount which may be up to 1 per cent. The amount varies with the sky conditions and with distance from the limb, so that ideally it should be measured for each individual exposure.

Scattering by the lens and mirror can be estimated from measurements made by Lyot (**12**) on an 8-inch lens of focal length 12 feet and of medium quality. He found the scattering in this lens to be of the order of 10^{-3} at 2′ beyond the Sun's limb, a distance which corresponds approximately to 100 000 kilometres on the Sun. The object glass which forms the Sun's image at Edinburgh has a very perfect polish and is free from bubbles, so that the scattered light intensity probably does not exceed Lyot's figure. A similar source of scattering is the siderostat mirror, whose aluminized surface was kept in good condition so that it probably scatters light to the same small degree as the lens. The total effect, therefore, appears to be small, and as it decreases rapidly with height above the limb, it will be negligible at distances of, say, 20 000 kilometres upwards.

6. *Correction for limited resolving power.*—The instrumental profile was measured for the krypton green line λ5571, which has a natural half-width of 0·01 A (**13**). Three plates were obtained in each order; exposure times were 30 minutes in the first order and 2 to 2½ hours in the second order. These exposures were too long to allow the plates to be standardized in the usual way, using the centre of the Sun's disk; they were therefore standardized on the multiple-slit calibration spectrograph of the Observatory. The wings of the profile (intensities below 7 per cent of the centre of the line) were found from over-exposed plates, one in each order, which gave the intensity down to 1 per cent. The exposures which had to be given were 4 hours in the first and 7 hours in the second order. Exposures over a longer period, to show up the wings farther out, were

not made as it was considered that such long exposures would result in loss of accuracy due to temperature changes in the spectrograph, or shifts in the plate. The line profiles reproduced in Fig. 4 show that most of the broadening is due to the finite width of the slit (the slit width is marked on the figure). The profiles

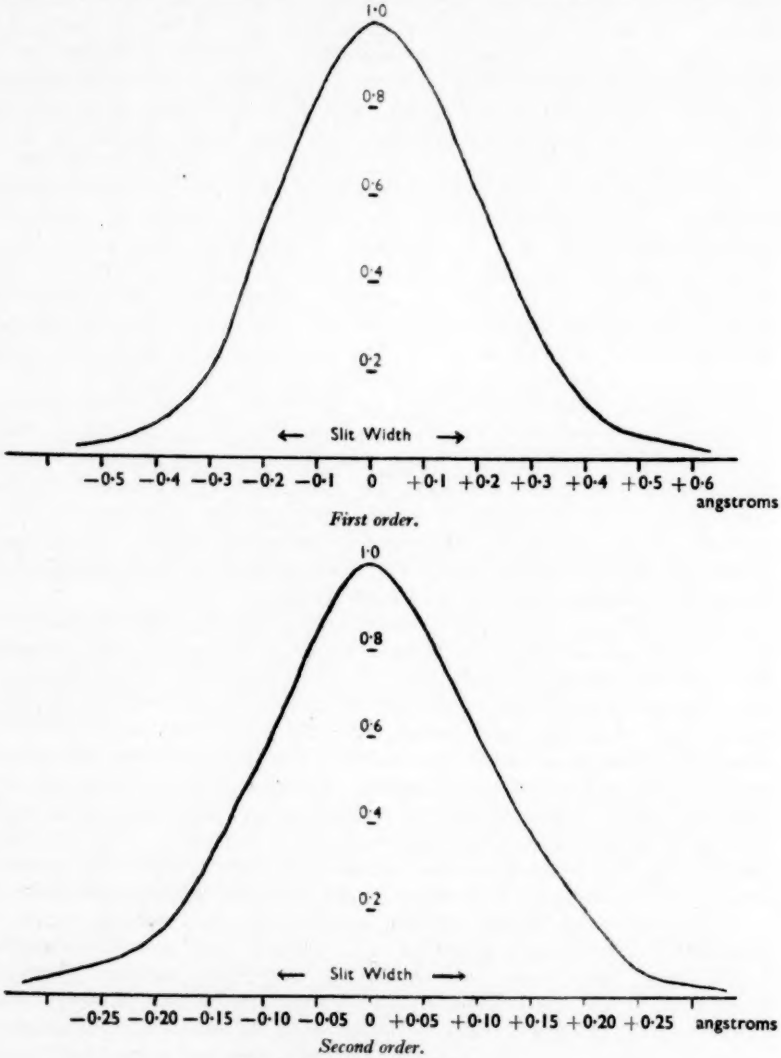

FIG. 4.—*Instrumental profile.*

are not perfectly symmetrical at the wings, but it was sufficient for purposes of reduction to take the mean of the two wings for the standard profile. This also simplified the working out of corrections.

The observed profiles were corrected by Burger and van Cittert's method of successive approximations as outlined by van Albada (**14**). If the true profile

is W, the instrumental profile A, and $W(A)$ the profile W broadened by the instrument, the problem is to solve the equation $W(A)=I$, I being the observed profile. A is normalized so that $\int_{-\infty}^{+\infty} A\,dx = 1$, where x represents the distance from the centre of the line in arbitrary units. In this case the units chosen were 0·10 A in the first order and 0·05 A in the second order. Table II shows the correction to a typical prominence in the second order and will serve as an illustration of the method. Column 1 gives distances from the centre of the line in angstroms. Since both the prominence and the instrumental profiles are taken to be symmetrical, only one-half of the prominence profile has been tabulated. The intensities at the various points along the observed prominence profile, corresponding to the displacements in column 1, are set down in column 2. All intensities have been multiplied by a constant factor which reduces the intensity of the central maximum to 1·00. Intensities which were too low to be measured on the plate were extrapolated and are given in brackets.

TABLE II

Correction of an Emission Line for Instrumental Profile

1	2	3	4	5	6
$\Delta\lambda$	I	$I(A)$	$D_1=I(A)-I$	W_2	$W_2(A)$
0	1·00	0·98	−0·02	1·02	1·00
0·05	0·99	0·97	−0·02	1·01	0·99
0·10	0·98	0·96	−0·02	1·00	0·99
0·15	0·96	0·94	−0·02	0·98	0·98
0·20	0·94	0·90	−0·04	0·98	0·94
0·25	0·89	0·85	−0·04	0·93	0·89
0·30	0·84	0·77	−0·07	0·91	0·82
0·35	0·73	0·68	−0·05	0·78	0·73
0·40	0·58	0·57	−0·01	0·59	0·58
0·45	0·43	0·46	+0·03	0·40	0·44
0·50	0·30	0·35	+0·05	0·25	0·29
0·55	0·21	0·25	+0·04	0·17	0·21
0·60	0·13	0·17	+0·04	0·09	0·13
0·65	(0·08)	0·11	+0·03	0·05	0·07
0·70	(0·04)	0·07	+0·03	0·01	0·04

The observed profile I was taken as the first approximation. Under the influence of instrumental broadening this becomes $I(A)$. The difference $D_1=I(A)-I$ (column 4) is subtracted from I to give the second approximation W_2 (column 5). W_2 is now broadened to $W_2(A)$ and the difference $D_2=W_2(A)-I$ is subtracted from W_2 to give the third approximation $W_3=W_2-D_2$. This process is continued until W_n is reached, where $W_n(A)=I$. The calculation of the $W(A)$ values involves integrating the contributions to intensity made by every part of the profile W. To avoid plotting several series of points and measuring areas in every case, the integration was carried out by Simpson's rule, using intervals of 1 unit (0·1 A in the first order and 0·05 A in the second order). As a final check, areas could be plotted and measured with an Amsler planimeter. It was important to verify occasionally during the approximations that the areas under the curves I and W were the same, as the area represents the total amount of light emitted and cannot be changed.

The number of successive approximations which had to be made depended on the shape of the profile in question. In the first order, in the case of a profile

0·98 A wide at half-maximum, nine approximations were required. For second-order spectra, the instrumental profile correction is much smaller, and two or three approximations were usually sufficient. Fig. 5 shows observed and corrected profiles for one typical prominence in each order.

On account of the labour involved in making the instrumental profile correction, the observed profiles of limb prominences were not individually corrected. Instead, three profiles in each order, which we shall call standard profiles, of half-widths (i.e. widths at half maximum) 0·8, 0·9 and 1·0 A, approximately, were chosen and corrected. Their intensities were reduced to give a central maximum of 1·00, as described in connection with Table II, and their observed profiles were plotted on thin paper. All other profiles, similarly reduced to a maximum of 1·00, were plotted on the same scale as the standard profiles. To correct a given profile, the standard profiles in the same order spectrum were superimposed on it in turn, and the best fit, as regards the shape of the curves near the centre, was picked out. Since the increase in central intensity as a result of instrumental correction was known for the standard profiles, the correction for the profile in question could be estimated satisfactorily. Correction to the half-width could not be estimated in this way, but, as the curves in Fig. 5 show, the correction is small, so that the complete instrumental profile correction was carried out only in particular cases.

7. *Results: prominences on the limb.*—Table III gives the results obtained from all quiescent prominences photographed on the limb. Prominences are defined here as being quiescent when they show no Doppler motions in the line of sight when observed in the spectrohelioscope with the line-shifter, and when their Hα line profile is symmetrical. All of these belong to Class V of the Pettit classification (**15**): that is, they are long-lived stable prominences which often form part of the large dark filaments observed on the disk, and their appearance remains unchanged for at least several hours. The table is divided into two parts—observations made from first- and from second-order plates.

Columns 1 and 2 of the table give the date of observation and the position of the prominence (its latitude and the limb on which it was observed) respectively. The prominence heights entered in column 3 represent the height of the slit above the Sun's limb. There are apparent heights only; the true heights measured from the base of the chromosphere may be greater than this if the base of the prominence is situated either behind the limb or in front of it, so that the heights given are minimum values. In some cases two or more measures are entered opposite a particular height. These have been made on the same plate, but each corresponds to a separate uniform part of the same prominence. The observed central intensities are given in column 4. Column 5 gives these figures corrected for ghosts, according to equation (1) in Section 3, and column 6 gives the same figures corrected for both ghosts and instrumental profile. Column 6 therefore gives fully corrected central intensities, all intensities being expressed in percentages of the continuous spectrum of the centre of the Sun's disk, 13 A outside Hα. The half-widths, uncorrected for the reason already described, are entered in column 7.

8. *Discussion of results.*—We see from column 6 of Table III that the final corrected intensities range from 3 to 28 per cent, the average intensity from all the measurements being 10·4 per cent. All quiescent prominences observed under favourable conditions were photographed, so that these results are considered to be representative of quiescent prominences for the years 1948 and 1949. It is well

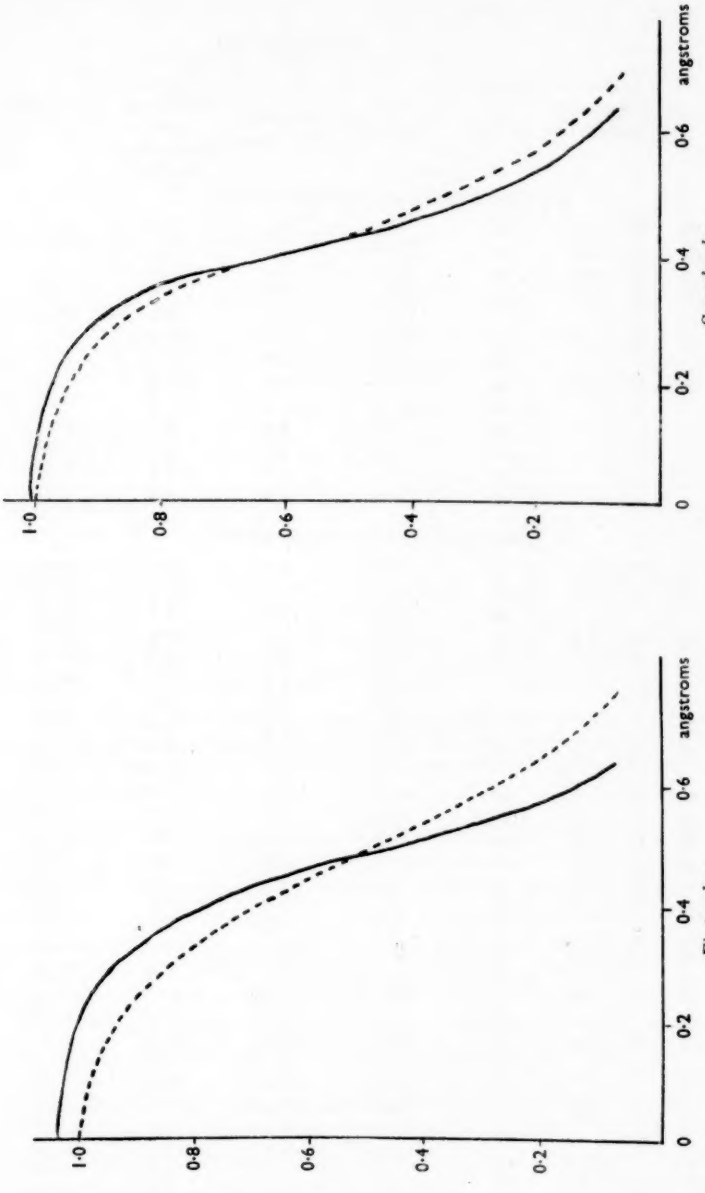

FIG. 5.—*Observed and corrected prominence profiles. The dotted curve is the observed profile; the full curve is the profile corrected for instrumental broadening. Ordinates: Intensity (reduced).*

TABLE III

Central Intensities and Half-widths of Prominences on the Limb

1	2	3	4	5	6	7
			Central Intensity			
Date	Position (Limb and latitude)	Height in 10^3 km	Observed	Corrected for Ghosts	Corrected for Ghosts and Instrumental Profile	Half-width Observed
		(a) Observations from first-order plates				
1948 Sept. 27	W. −30°	15	5·3	5·3	5·6	0·84
1948 Oct. 22	E. +20°	12	8·6	8·7	8·7	1·00
1948 Dec. 4	W. −29°	20	10·9	11·0	11·2	1·04
1949 Feb. 10	W. +28°	30	8·7	8·8	9·2	1·15
			7·6	7·6	8·0	0·92
1949 Feb. 11	W. +26°	30	26·6	26·8	(27·0)	...
		60	9·7	9·8	(9·9)	...
1949 Feb. 12	W. +30°	10	17·1	17·2	(17·4)	...
		20	10·3	10·4	10·6	0·83
		30	8·8	8·9	9·2	1·15
		40	9·1	9·2	9·6	1·26
		50	3·2	3·2	3·2	1·01
		60	4·0	4·0	4·4	0·71
		(b) Observations from second-order plates				
1948 Apr. 23	E. −54°	5	8·8	9·0	9·1	0·88
1948 May 14	E. −11°	10	15·7	16·1	16·2	1·07
		30	15·3	15·7	15·8	0·90
1948 May 15	E. − 8°	30	10·6	10·8	11·0	0·86
1948 July 7	E. − 2°	15	4·4	4·5	4·6	0·90
			4·3	4·4	4·6	0·79
			2·9	3·0	3·0	0·64
			5·3	5·4	5·5	0·82
1948 July 26	E. − 2°	30	14·0	14·3	14·5	0·88
			17·3	17·7	17·9	0·96
1948 Aug. 24	E. +16°	40	10·8	11·1	11·1	1·30
1948 Sept. 22	E. − 4°	30	3·4	3·5	3·5	0·75
1948 Oct. 16	W. −35°	40	7·4	7·5	7·6	1·16
1949 Apr. 26	W. +24°	10	7·6	7·7	8·0	0·76
1949 May 5	W. +30°	5	5·2	5·3	5·4	1·00
1949 May 11	W. + 6°	10	9·6	9·8	10·0	0·93
			7·7	7·9	8·0	0·85
1949 May 19	E. +42°	10	15·6	16·0	16·1	0·96
		20	6·1	6·2	6·4	0·83
1949 May 20	E. +35°	10	2·8	2·9	(2·9)	(0·98)
		20	8·1	8·3	(8·4)	(0·96)
1949 June 2	W. +11°	15	16·8	17·2	(17·4)	...
		20	(19·1)	(19·5)	(19·7)	0·87
		10	19·4	19·9	19·9	1·06
1949 June 20	E. +33°	5	8·1	8·3	8·5	0·90
		20	8·2	8·4	8·5	0·86
			10·4	10·6	10·7	0·92
1949 June 21	E. +41°	20	3·7	3·8	3·9	0·81
1949 July 9	W. − 1°	30	8·9	9·1	9·2	0·89
		30	10·8	11·1	11·2	0·90
		30	10·6	10·8	10·9	0·91
1949 July 25	W. +14°	15	12·2	12·5	12·6	0·88

TABLE III (*cont.*)

1	2	3	4	5	6	7
			Central Intensity			
Date	Position (Limb and latitude)	Height in 10^3 km	Observed	Corrected for Ghosts	Corrected for Ghosts and Instrumental Profile	Half-width Observed
1949 Aug. 10	W. −35°	10	4·9	5·0	5·1	0·76
1949 Aug. 11	W. −41°	15	8·6	8·8	8·9	0·88
		30	11·9	12·2	12·3	0·82
1949 Aug. 16	E. +15°	10	15·7	16·1	16·3	0·89
			14·9	15·2	15·3	0·89
			9·0	9·2	9·5	0·72
		20	12·8	13·1	13·2	0·96
			13·1	13·4	13·4	0·86
			9·4	9·6	9·8	0·73
		40	9·5	9·7	9·8	0·89
			8·5	8·7	8·9	0·79
		60	8·4	8·6	8·8	0·70
			9·0	9·2	9·5	0·73
1949 Aug. 16	W. −11°	10	11·6	11·9	12·1	0·84
		20	12·5	12·8	12·9	0·81
1949 Aug. 19	E. +26°	10	26·8	27·4	27·7	0·96
1949 Sept. 3	E. +49°	10	13·3	13·6	13·6	1·12
		20	3·5	3·6	3·6	1·01
1949 Oct. 8	W. −26°	30	4·2	4·3	4·3	0·89
1949 Nov. 28	W. −16°	10	14·8	15·1	15·2	0·88
1950 Feb. 22	W. +29°	10	7·5	7·7	7·8	1·00
			7·0	7·2	7·3	0·97
		20	5·9	6·0	6·1	0·96
1950 Mar. 7	E. +28°	10	23·0	23·5	23·6	0·93

Note to Table III.—Quantities which were found by extrapolation of the standardization curve are given in brackets. Where half-widths were not measurable, the instrumental profile correction was only approximate; in these cases the intensities in column 6 are also given in brackets.

known that the frequency of low-latitude (less than 40°) prominences follows the sunspot cycle; high-latitude prominences, on the other hand, are rare at times of sunspot maximum, reaching maximum frequency about three years after the sunspot minimum. Although no evidence has yet been brought forward on the subject, it is possible that prominence intensities are also connected with the sunspot cycle. The years 1948 and 1949 were years of very high solar activity, their relative sunspot numbers averaging 135 (**16**), which is higher than the relative numbers for the six sunspot maxima preceding 1947. If such a correlation exists between prominence intensity and sunspot number, the results in Table III must not be taken as a general representation of prominence intensity. They are, however, a true representation for years of high solar activity.

The frequency distribution of quiescent prominences, classified according to their intensity, is given in Table IV. The first column gives the intensity range, intensities being given as usual in percentages of the Sun's continuous spectrum outside Hα at the centre of the disk. The frequency of occurrence of intensities within these ranges is recorded in column 2, and the last column gives similar figures found by Woolley and Newton (**1**).

Woolley and Newton's observations were made in 1935 and 1936, about two years before the sunspot maximum. (Relative sunspot numbers for 1935 and 1936 were 36 and 80 respectively.)

With regard to the half-width of prominence profiles (given in column 7 of Table III), it will be seen that it varies between 0·64 and 1·30 angstroms. In another paper it is proposed to make a theoretical analysis of the observed line profiles with a view to gaining some information on the temperature conditions within a prominence, and on the effect of self-absorption on the Hα emission line. Further data are to be obtained, and observations are to be extended to the D_3 line of helium and the ***H*** and ***K*** lines of calcium. The problem of making corrections for atmospheric scattering is to be pursued.

TABLE IV

Frequency Distribution of Prominences

Intensity Range	Number: Present Observations	Number: Woolley and Newton
1–4	10	10
5–10	31	51
11–15	16	25
16–21	9	10
>21	3	0

9. *Results: prominences on the disk.*—The intensities of prominences photographed as dark markings on the disk are recorded in Table V. Column 1 gives the date of observation and column 2 the heliocentric angle (i.e. the angular distance from the centre of the apparent disk) of the part of the prominence whose spectrum was obtained. The coefficient of limb-darkening, σ, is given in column 3, and was found from the centre-to-limb variation of the continuous spectrum at wave-lengths near Hα as measured by previous workers (**17**). The observed central intensity of the prominences is given in column 4. On each plate the intensity of the centre of Hα on an undisturbed part of the Sun's disk near the prominence was measured; this is called the normal Hα and its observed value is recorded in column 5. In the majority of plates when the prominence was exposed to give a suitable density on the plate for photometry, the continuum was too dense for measurement. For this reason most of the intensities in columns 4 and 5 are absolute intensities, as defined in Section 3, that is, the intensities have been measured with respect to the continuous spectrum of the centre of the Sun's disk, by using the standardization spectrum. In a few cases, however, it was possible to make reliable observations of both the prominence and the continuum on the same exposure, and thus to obtain relative intensities. Such measurements involve no errors due to differences in timing or sky conditions between exposure and standardization, and so are more accurate than the absolute intensity measurements. Observed relative intensities are underlined in the table.

By combining the corrections worked out in Sections 3 and 4 for ghosts and scattered light, we find the combined correction for the relative intensity (see equations (2) and (4)) to be

$$r=\{r'(1+\beta)-(g+\beta)\}/(1-g), \tag{6}$$

and for the absolute intensity (see equations (3) and (5))

$$i=\{i'-\sigma(g+\beta)\}/(1-g). \tag{7}$$

These corrections have been carried out for all observed intensities and are entered in columns 6 and 7 of Table V for the prominences, and in columns 8 and 9 for the normal Hα. Except in cases where relative intensities were observed, the corrected relative intensities were found from the corrected absolute intensities (as given by equation (7)) by using the relation $i/r=\sigma$, which follows from the definition of the limb-darkening coefficient. When relative intensities were observed, they were corrected by equation (6) and then, from the relative intensities so corrected, the corrected absolute intensities were deduced by using the relation $i/r=\sigma$. The instrumental profile correction was not carried out, but was estimated to be equivalent to a reduction in central intensity of about $2\frac{1}{2}$ per cent in the first, and $\frac{1}{2}$ per cent in the second order.

TABLE V

Central Intensities of Prominences on the Disk

1	2	3	4	5	6	7	8	9
Date	Helio-centric angle	σ	Central Intensity		Corrected Intensity			
			Prom.	Normal Hα	Prominence Abs.	Prominence Rel.	Normal Hα Abs.	Normal Hα Rel.
(a) Observations from first-order plates								
1949 Mar. 1	56°	0·78	8·2	16·0	5·6	7·1	13·4	17·2
1949 Mar. 2	42°	0·88	11·5	18·5	8·6	9·7	15·6	17·7
1949 Mar. 2	42°	0·88	13·6	22·9	10·7	12·1	20·0	22·8
1949 Mar. 3	38°	0·90	16·0	25·4	13·0	14·5	22·5	25·0
1949 Mar. 31	44°	0·86	15·6	22·1	12·8	14·8	19·3	22·4
(b) Observations from second-order plates								
1948 Mar. 16	13°	0·99	19·5	27·3	9·8	9·9	17·8	18·0
1948 Mar. 19	34°	0·92	18·9	28·3	9·9	10·8	19·5	21·2
1948 Sept. 20	46°	0·85	19·4	25·4	11·2	13·2	17·3	20·4
1948 Sept. 21	40°	0·89	20·7	26·8	12·1	13·6	18·3	20·5
			23·3	30·2	13·7	15·4	20·5	23·0
1948 Sept. 22	46°	0·85	20·5	29·9	12·3	14·4	21·9	25·8
1948 Sept. 22	53°	0·80	22·5	30·2	14·8	18·5	22·7	28·4
1949 Mar. 2	42°	0·88	12·9	19·2	4·2	4·8	10·6	12·1
1949 Mar. 2	42°	0·88	17·7	27·0	9·1	10·3	18·6	21·1
1949 Mar. 6	51°	0·82	14·6	19·1	6·5	8·0	11·2	13·7
1949 Mar. 6	53°	0·80	13·7	24·0	5·8	7·3	16·4	20·5
1949 Mar. 31	44°	0·86	16·8	22·7	8·4	9·7	14·4	16·7
1949 Apr. 28	48°	0·84	20·7	26·5	12·6	15·0	18·5	22·0
1949 May 12	65°	0·70	27·0	30·5	13·7	19·5	16·3	23·3
1949 May 25	38°	0·90	19·8	24·2	11·0	12·3	15·5	17·2
1949 May 28	39°	0·89	18·6	26·3	9·9	11·1	17·8	20·0
1949 Aug. 17	55°	0·79	14·5	20·9	6·8	8·6	13·3	16·8
1949 Sept. 17	50°	0·83	16·9	22·7	8·8	10·6	14·7	17·7
			17·7	23·6	7·7	9·3	13·1	15·8
1949 Sept. 17	50°	0·83	16·2	21·1	8·2	9·9	13·1	15·8
			19·4	25·1	9·3	11·2	14·4	17·4

Columns 8 and 9 of Table V show a scatter in the central intensity of the normal Hα which is too large and bears no relation to the heliocentric angle, and therefore cannot be accounted for by the centre-to-limb variation. Furthermore,

a comparison of columns 6 and 8 (or columns 7 and 9) shows a correlation between the prominence and normal intensities; for instance, where a particularly low value is recorded for prominence intensity a correspondingly low value is found for the normal Hα intensity on the same plate. This is probably the result of inaccurate timing of the exposures; prominence and standardization spectra were taken separately, and the exposures were rather too short (5 seconds) to allow for accurate timing with a hand-operated camera shutter. Part of the error may also be due in some cases to changed sky conditions between the prominence exposure and the standardization. The intensities recorded are therefore to be taken only as preliminary; the table has been included mainly as an illustration of the order of magnitude of the ghosts and scattered light corrections, which are seen to be considerable.

Acknowledgments.—My sincere thanks are due to Professor W. M. H. Greaves, Astronomer Royal for Scotland, who granted me the facilities of the Observatory, and who always gave his encouragement and advice, and to Dr M. A. Ellison, under whose direction the research was carried out. The term spent at the Royal Observatory, Edinburgh, was made possible by a Travelling Studentship from the National University of Ireland.

Dunsink Observatory,
Co. Dublin, Eire:
1951 *September* 6.

References

(1) R. v. d. R. Woolley and H. W. Newton, *M.N.*, **96,** 5, 1935; **97,** 531, 1937.
(2) A. Unsöld, *Zeits. f. Phys.*, **59,** 372, 1930.
(3) F. A. Jenkins and H. E. White, *Fundamentals of Physical Optics*, p. 159, McGraw-Hill, 1937.
(4) E. A. Baker, *Proc. Roy. Soc. Edinburgh*, **45,** 166, 1925; see also *Pub. R.O. Edinburgh*, **1,** 17, 1949.
(5) M. Minnaert, *Vers. K. Akad. Amsterdam*, **30,** 257, 1922.
(6) M. Minnaert, G. F. W. Mulders and J. Houtgast, *Photometric Atlas of the Solar Spectrum*, Utrecht, 1940.
(7) J. Houtgast, *Variations of Strong Fraunhofer Lines across a Radius of the Solar Disk*, p. 11, Utrecht, 1942.
(8) C. D. Shane, *L.O.B.*, **16,** 76, 1933.
(9) A. D. Thackeray, *M.N.*, **95,** 293, 1935.
(10) M. Fracastoro, *Oss. e Mem. Arcetri*, **64,** 79, 1948.
(11) H. Kienle, *Veroff. Sternwarte Göttingen*, **4,** 89, 1928.
(12) B. Lyot, *M.N.*, **99,** 580, 1939.
(13) C. V. Jackson, *Phil. Trans.*, **236,** 1, 1937.
(14) B. van Albada, *B.A.N.*, **8,** 179, 1937.
(15) E. Pettit, *Ap. J.*, **98,** 6, 1943.
(16) *Quarterly Bulletin on Solar Activity*, I.A.U., Zürich.
(17) C. G. Abbot, *The Sun*, p. 105, Appleton and Co., 1912. W. J. H. Moll, H. C. Burger and J. van der Bilt, *B.A.N.*, **3,** 83, 1925. M. Minnaert, E. van den Hoven van Genderen and J. van Diggelen, *B.A.N.*, **11,** 55, 1949.

SOME EXPERIMENTS ON THE SCINTILLATION OF STARS AND PLANETS

M. A. Ellison and H. Seddon

(Communicated by the Astronomer Royal for Scotland)

(Received 1951 November 6)

Summary

Cathode-ray oscillograms of stellar and planetary scintillation have been recorded over a period of a year. For this investigation selected multiplier photocells (type RCA 931–A) of special sensitivity and high signal/noise ratio have been used at the Cassegrain focus of the 36-inch reflector of the Royal Observatory. The output voltages, after amplification, are applied to the beam of an oscillograph, the "Y-deflections" of the spot being recorded on moving film. The sensitivity and dark current of the cells and the time constant of the circuit are discussed.

Scintillation in integrated light is exhibited as a function of altitude and of seeing conditions. Scintillation amplitudes of 5 to 10 per cent are always present in the zenith, when recording with the full aperture of 36 inches.

The amplitude of scintillation is found to vary with telescope aperture A approximately in the ratio $1/A$, but appears to reach a maximum at an aperture near 3 inches. Under normal conditions at this aperture, high-altitude stars show sudden flashes of light, lasting about one-hundredth of a second, which cause momentary increases in brightness of 1 to 2 magnitudes.

The average size (3 inches) and distance (5 km) of the atmospheric irregularities causing scintillation have been deduced from a comparison of the scintillation patterns of stars, planets and satellites.

Some experiments on colour scintillation, using "monochromatic" light, are described. An attempt has also been made to imitate the main features of scintillation by generating refractional irregularities in a model atmosphere of water.

---

1. *Introduction.*—It is convenient to classify the effects of atmospheric turbulence upon star images under three headings:

(*a*) Changes of apparent brightness (brightness scintillation);

(*b*) Changes of colour (colour scintillation);

(*c*) Changes of position, including "dancing" and "pulsation".

Aristotle, in *De Caelo* (1), refers to "the apparent twinkling of the fixed stars and the absence of twinkling in the planets".* As we shall see (Section 2 *c*), this statement is true of the major planets, not merely of observations made with the unaided eye but also for instruments of much larger aperture: it also applies over the whole recorded range of scintillation frequencies.

The use of a 1P21 multiplier photocell, whose output is amplified and applied to a cathode-ray oscillograph, has made possible an exact study of the intensity variations and their frequency in scintillating starlight. By reason of the exceedingly small time constant (~10 microseconds) which is attainable in such a circuit,

* We are indebted to Professor W. B. Stanford, F.T.C.D., for finding this reference. Aristotle's notion of the cause of scintillation, though attractive, is scarcely consistent with modern ideas in optics. He says "The planets are near, so that the visual ray reaches them in its full vigour, but when it comes to the fixed stars it is quivering because of the distance and its excessive extension".

the equipment is admirably suited to cover frequencies of scintillation ranging from those which are so low as to be easily perceptible to the eye, say, 1 cycle per second, to the highest values recorded, which are in the region of 1 000 c/s. The first recordings of this type, using an electromagnetic oscillograph, were made by Whitford and Stebbins (**2**) in 1936, but the long time constant of their equipment would not permit investigation of frequencies higher than 20 c/s.

Changes in colour are easily discernible * in bright stars seen at low altitude with the unaided eye. From this we may infer that the fluctuations of brightness are not synchronous at all wave-lengths throughout the visible spectrum, and that at any instant some colours fail to reach the eye, either through interference or by refractional de-focusing effects. Colour scintillation can be more readily observed by a simple method due to Montigny (**3**), who mounted behind the eyepiece of a small telescope a thick plane-parallel plate whose normal was set at a small angle to the optical axis of the telescope. When this plate is caused to spin about the telescope axis at five to ten revolutions per second the star image is spread out along the circumference of a circle, and its light is thereby separated into its *time elements*. Colours of many hues are observed at different points on the time base. The same phenomenon may be demonstrated with even simpler apparatus, by observing the star with a pair of field glasses held in the hands, while giving to the objective end a rapid rotatory motion (**4**).

More precise information about colour scintillation may be obtained by means of the objective prism experiment described in Section 4, by Zwicky's photographic method (**5**), or by means of the multiplier photocell equipment used with suitable narrow-band filters.

Lateral movements of star images have been measured photographically by Schlesinger (**6**). These movements have a period which is roughly of the order of one minute of time and an amplitude of about one second of arc. They have been recorded even near the zenith and under good conditions of seeing: they are also familiar to all astronomers who are accustomed to accurate guiding upon a star when the image is bisected by a micrometer wire. Such movements are not to be confused with the much more rapid dancing and pulsation which are observed under conditions of bad seeing. It seems probable that the former arise from the interposition in the beam of large wedge-shaped air masses of abnormal refractive index, having dimensions of the order of 100 metres. Dancing and pulsation, on the other hand, having frequencies comparable with those of scintillation and colour change, most probably have a common origin in the small-scale turbulence (dimensions $\sim$ 10 cm) which we believe to be the cause of scintillation.

2. *Brightness scintillation in integrated light*

(*a*) *Instrumental arrangements.*—A multiplier photocell (type RCA 931–A) was built into a light-tight tube 15 inches long (Fig. 1) which can be inserted in the converging beam of the 36-inch Cassegrain reflector of the Royal Observatory. This instrument has an equivalent focal length of 54 feet. The rays are deflected by means of a 90° prism and brought to a focus in the plane of an iris diaphragm, which serves both for centring the image and for guiding. The iris aperture is kept large enough (0·16 inch, equivalent to 50″) to ensure that its edge will not

* In the well-known nursery rhyme, the twinkling star is described as " like a diamond in the sky ". This is an apposite comparison; for a well-cut diamond held in a beam of sunlight in a darkened room exhibits just such flashes of sparkling colour.

occult any part of the star's light through dancing and turbulence of the image. Guiding is effected by light reflected from the unsilvered face of a second 90° prism; the main beam traverses this prism and passes through a holder for a neutral screen or filter. It is finally focused as a spot 5 mm in diameter upon the sensitive surface of the photocathode. Precise focus upon the cathode is impossible because of the inferior glass in the cell walls; and it is in any case undesirable, in view of the possibility of local variations in the electron emission sensitivity of the cathode surface.

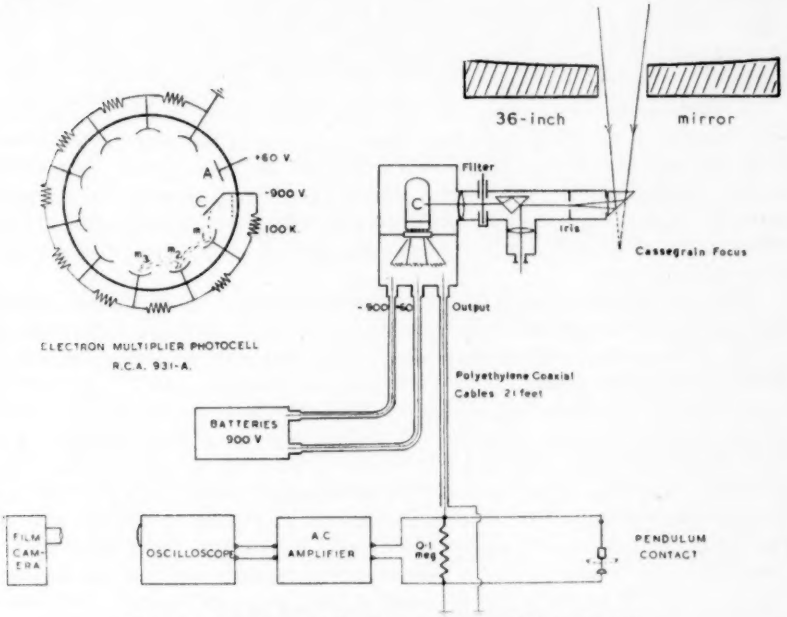

FIG. 1.—*Arrangement of the photomultiplier and its circuits at the Cassegrain focus of the 36-inch reflector.*

The cell output is passed through a high resistance (10^5 ohms) to earth. The voltages across the ends of this resistance are amplified and registered as "Y-deflections" of the light spot on a cathode-ray screen. A mechanical contact is arranged to short-circuit the ends of the resistance at intervals of $0^s{\cdot}8$.* This device continuously imprints on the record both the time-scale and the level of zero light intensity (*cf.* Figs. 3, 6, 9).

The Y-deflections are recorded photographically by means of a camera which operates a continuously moving film: the film runs through horizontally at a speed which is normally about 6 inches per second. In later work a Cossor oscilloscope (Type 1049) with d.c. amplification has been used. This instrument has the advantage over the a.c. amplifier of maintaining the zero level at a fixed point on the screen, despite changes in the amplifier gain. The Y-scale may be varied by

* In the earlier work a pendulum contact was used, giving time intervals of $0^s{\cdot}5$. In the present arrangement a wheel carrying a spring contact is driven by a reduction gear from the synchronous mains motor of the camera, and this contact makes the short-circuit (of duration 5 milliseconds) at $0^s{\cdot}8$ intervals.

control of the accelerating voltages applied to the phototube, by means of the amplifier gain, or by inserting neutral glass screens in front of the phototube.

Power for the photomultiplier was, for the earlier experiments, provided by dry batteries, but owing to the high initial cost of these, their tendency to develop a variable internal resistance, and the danger of having a power supply of such lethal capabilities in the darkened dome, a mains-driven regulated high-voltage supply, based on the design of DeWitt and Seyfert (**7**) was constructed. This supply delivers any voltage required between 400 and 1600 volts with current up to about 1 milliamp. When adjusted to 800 volts, variations in output are less than 1 volt. Switching and overload precautions are effected entirely by relays. The high voltage is conveyed to the photomultiplier by coaxial cable with polythene dielectric.

(*b*) *Observational procedure.*—Over two hundred records of scintillation have been made with the above apparatus during a period of one year, under a wide variety of weather conditions and at many different zenith distances. Notes have been kept of the degree of scintillation observed visually at the time, of the appearances of the star images in the 7-inch guiding refractor attached to the 36-inch reflector, and of general weather phenomena, such as temperature, surface wind speed and direction.

The photocells used in this work were specially selected for high sensitivity and high signal/noise ratio from a large number purchased from government disposal centres. They are, therefore, equivalent to the 1P21 cells so extensively used in stellar photometric work. Our best cell, for example, gave a current of $2{\cdot}5 \times 10^{-5}$ amp from Deneb (A type, mag. 1·33, altitude 49°) with 900 volts across the ten stages of the cell, using the full 36-inch aperture of the telescope. The dark current was measured as 5×10^{-8} amp. The time constant of the whole apparatus, due to the 21-foot coaxial cable and the input resistor of the oscilloscope, was 0·13 millisecond. The timing short-circuit, of duration 5 milliseconds, was also found to give a perfectly square pulse on the film record. The oscilloscope is stated by the makers to produce no distortion so long as the wave form is less than 10^5 c/s. It seems probable that scintillation frequencies are normally well below this value.

It was thought desirable to check the uniformity of the response from different parts of the photocathode in each cell, so as to eliminate the possibility of sharp irregularities in the response from adjacent small areas of the sensitive surface. This investigation was kindly carried out by Mr M. J. Smyth.* His work makes it clear that, so long as the starlight is not focused sharply upon the cathode surface, minute image shifts alone cannot contribute any appreciable irregularities to the cell output currents.

The proportionality between spot deflection on the cathode-ray screen and light intensity incident upon the photocell has been established for all cells used in this work, (*a*) by the use of neutral screens, or (*b*) by a variable-aperture method. It was established that the response is linear, so long as the output voltage of the cell is not allowed to exceed 60 per cent of the voltage applied between each pair of dynodes. This condition obtains at the light levels experienced in the present work.

Fig. 2 exhibits the spectral sensitivity characteristic curve for the 931–A photocells having an S–4 response. This curve has been plotted from data

* See p. 90.

supplied by the makers, and is given for equal values of radiant flux per angstrom at all wave-lengths. The prisms and lenses of crown glass, necessarily employed to focus the beam, will somewhat reduce the response towards the violet end of this curve. It is clear that the main response is to green, blue and violet light with a much lower response to yellow and red.

The film records have been examined by projection through a photographic enlarging camera, the images being focused on to a white screen. Tracings of each record were made upon sheets of squared paper, altering the magnification, when necessary, so as to exhibit all records with equal intensity ordinates (*cf.* Figs. 3, 6, 9). From each tracing the amplitude of maximum light variation was read off and expressed as a percentage of the mean light level (+ above, and − below the mean level). An estimate was also made of the maximum frequency of the light fluctuations in cycles per second.

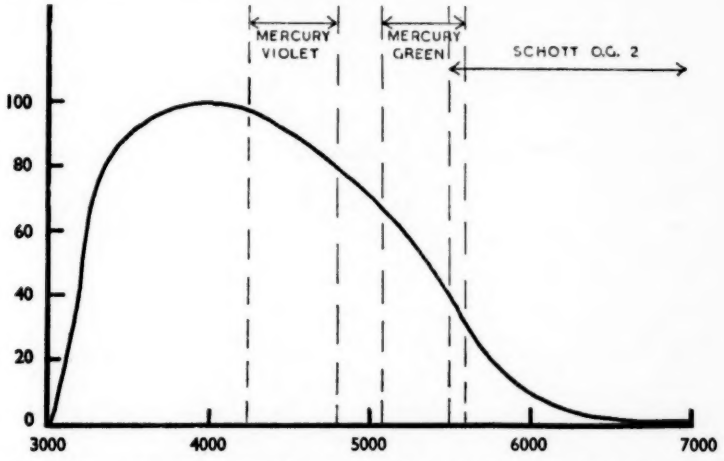

FIG. 2.—*Spectral sensitivity curve for a* 931-A *photomultiplier, as given by the makers, for equal values of radiant flux per angstrom at all wave-lengths. Effective filter transmissions shown by vertical lines.*

Ordinates: *Relative sensitivity.*
Abscissae: *Angstroms.*

(*c*) *Summary of results.*—Using the full spectral response of the cell and the full aperture of the 36-inch reflector:

(1) On all nights the amplitude of scintillation decreases with increasing altitude of the star (*cf.* Fig. 3, Nos. 1–6). In Fig. 4 the connected points show the trend of the amplitude–altitude relation for different nights and for different conditions of seeing. These curves show that even on nights of steady seeing the amplitude of scintillation in the zenith is of the order of ± 5 per cent with the full 36-inch aperture, and, as we shall see later, it is much greater than this for smaller apertures. At an altitude of 10° it lies within the range ± 20 to ± 50 per cent. In Fig. 5 the amplitudes are plotted against sec Z (Z = zenith distance in degrees). These curves illustrate more clearly the convergence to a scintillation value of ± 5 to ± 10 per cent in the zenith on an average night, recording with the 36-inch aperture. It may be emphasized that this is not an instrumental effect, since the

cell dark current is quite negligible at these high light-levels (see, for example, Fig. 9, No. 1).

(2) In low-altitude records ($<10°$) low-frequency scintillation (~ 5 c/s) predominates, though higher frequencies (~ 100 c/s) are usually present: with increasing altitude the low-frequency fluctuations die out while the high-frequency component remains, even up to the zenith.

(3) The amplitude of scintillation appears to be closely correlated with the quality of the star images, as observed visually with the 7-inch auxiliary refractor. When the diffraction disk and rings are visible in this telescope, the scintillation amplitude does not exceed 10 per cent in the larger instrument: amplitude variations of 30 per cent or more are associated with the most violent movements and boiling of the visual image.

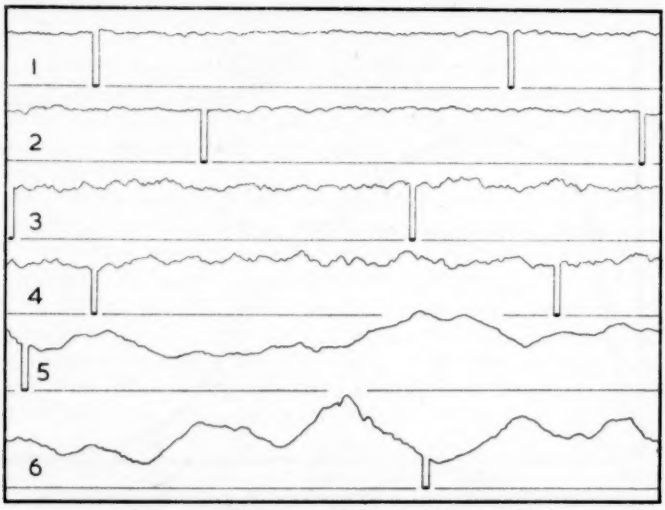

FIG. 3.—*Cathode-ray oscillograms of scintillation in integrated light using the full 36-inch aperture of the telescope.*

Time horizontally: ordinates proportional to light intensity.

1. *Deneb at 68° altitude: zero marks 0ˢ·8 apart.* (*Film No. 138.*)
2. *Vega at 49° altitude: zero marks 0ˢ·8 apart.* (*Film No. 137.*)
3. *Altair at 32° altitude: zero marks 0ˢ·8 apart.* (*Film No. 139.*)
4. *Altair at 25° altitude: zero marks 0ˢ·8 apart.* (*Film No. 149.*)
5. *Betelgeuse at 13° altitude: total time 0ˢ·8.* (*Film No. 152.*)
6. *Betelgeuse at 7° altitude: total time 1ˢ·0.* (*Film No. 150.*)

These records were obtained on the same night during a period of 1½ hours.
(In Figs. 3, 6 and 9 the horizontal straight lines give the zero levels of intensity.)

(4) Under poor conditions of seeing, when light from a star is fluctuating with an amplitude of ± 20 per cent, that from Jupiter or Saturn remains constant to less than 1 per cent (see Fig. 9, No. 1).

The following conclusions are drawn from records obtained with the full spectral response of the cell and using a variable telescope aperture. For these measurements a series of circular stops were used. These were placed across the mouth of the telescope tube, centred upon the circumference of a circle of 9 inches radius so as to avoid as far as possible the shadow of the 10-inch secondary mirror.

(5) Decreasing the aperture of the telescope increases the amplitude of scintillation for all altitudes (Fig. 6, Nos. 1–5). The plotted points of Fig. 7 illustrate the amplitude–aperture relation for a number of stars at various altitudes and for the planet Venus (31″ apparent diameter, crescent 12″ wide).

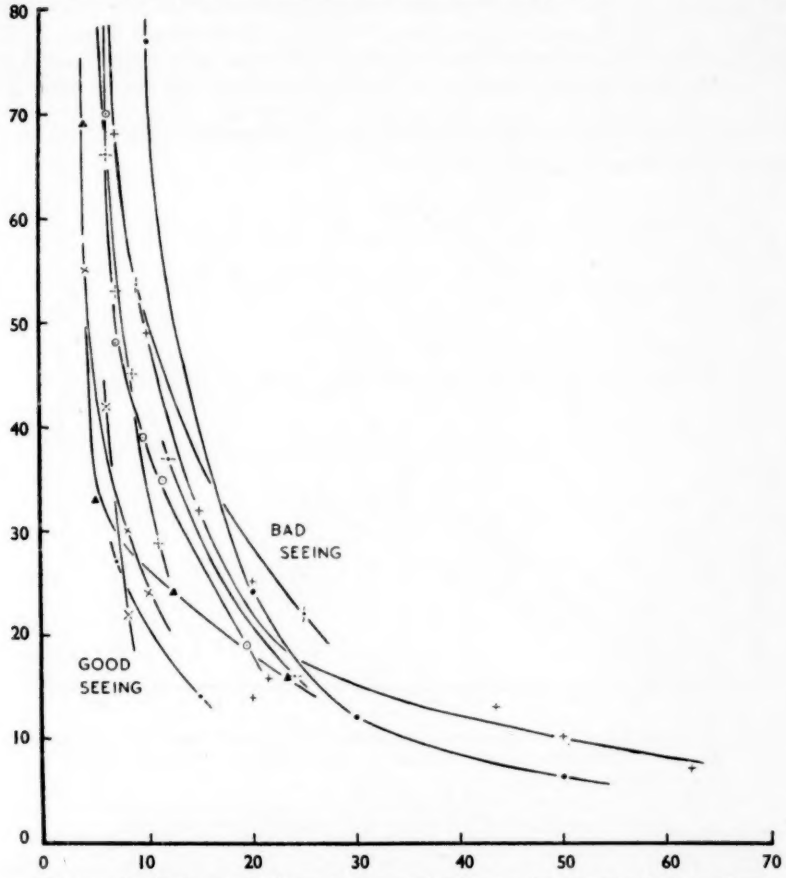

FIG. 4.—*Amplitude of scintillation in integrated light as a function of altitude in degrees. Recordings made with the full 36-inch aperture of the telescope. Records for different nights are shown by characteristic symbols.*

Ordinates: Altitude in degrees.

Abscissae: Amplitude of scintillation as percentage of mean light level.

(6) The most remarkable features in the stellar records from small apertures (of 3 and 6 inches) are the sudden *increases* of light intensity, of 200 to 400 per cent above the mean level and having durations of the order of $0^{s}.01$ (Fig. 6, No. 5). This phenomenon has also been reported by H. E. Butler (**11**). These flashes are usually most pronounced at an aperture of about 3 inches, and there is a suggestion in the shapes of the low-altitude records of Sirius and Rigel that at this aperture we are approaching the maximum amplitude of scintillation. Unfortunately, we cannot work at still smaller apertures to make certain of this conclusion, for we

have here reached such a low light-level that the cell noise, as distinct from the "seeing" noise, is beginning to predominate. We are also at the limit of satisfactory amplification with the existing apparatus.

However, it seems clear from these results that we have to deal with a pattern of light variations crossing the telescope mirror, the effective size of the disturbances being of the order of 3 inches rather than 36 inches. Shadowgrams of such waves crossing the mirror of the Cordoba 60-inch reflector have been photographed by E. Gaviola (**8**), and more recently also by Mikesell, Hoag and Hall*, using the 40-inch reflector of the Naval Observatory, Washington. Observations of the *dark* shadow-bands seen at total eclipses of the Sun also give widths of 2 to 6 inches, separated by distances up to 1 or 2 feet.†

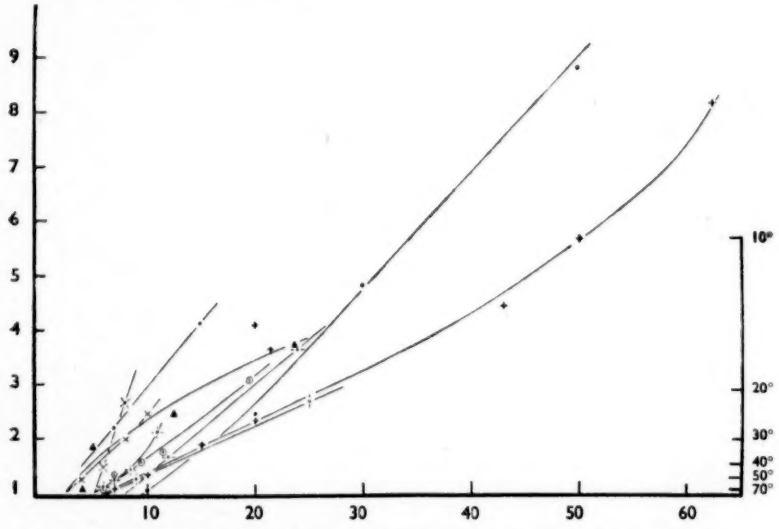

FIG. 5.—*Amplitude of scintillation as a function of sec Z. From the same data as used in Fig. 4. Note the convergence to a value of 5 to 10 per cent in the zenith (sec Z = 1).*
Ordinates: (on left) sec Z.
(on right) Altitude in degrees.
Abscissae: Amplitude of scintillation as percentage of mean light level.

The general effect of using a large aperture in our experiments is to smooth out the light variations, as shown in Fig. 7. We may call this the "integration effect", and we can predict that with apertures of the order of 100 inches brightness scintillation should be negligible.

3. *The size and location of the atmospheric irregularities.*—The evidence summarized in the previous section leads to an estimate of 3 inches as the order of the average *true* size of the atmospheric irregularities responsible for the scintillation phenomena we have been discussing. So far, we have visualized scintillation as brought about by the shadows of these irregularities cast upon the telescope mirror or objective by stellar point sources of light. When the apparent diameter of the source of light becomes appreciable, as for the planets, the moving shadows cast

* Privately communicated.

† See, for example, Pernter and Exner, *Meteorologische Optik*, p. 166, 1910.

upon the telescope aperture will lose their sharpness and the phenomena of scintillation will become less marked. Light from each point in the extended source will still be subject to scintillation, as from a star, but rays emanating from widely separated points upon a planet's disk will traverse *different* atmospheric irregularities whose variations will be out of phase with one another. Therefore, we should expect brightness scintillation to begin to die away at some stage as the apparent diameter of the source increases, just as, when using a point source (star), the scintillation decreases with increasing telescope aperture (integration effect).

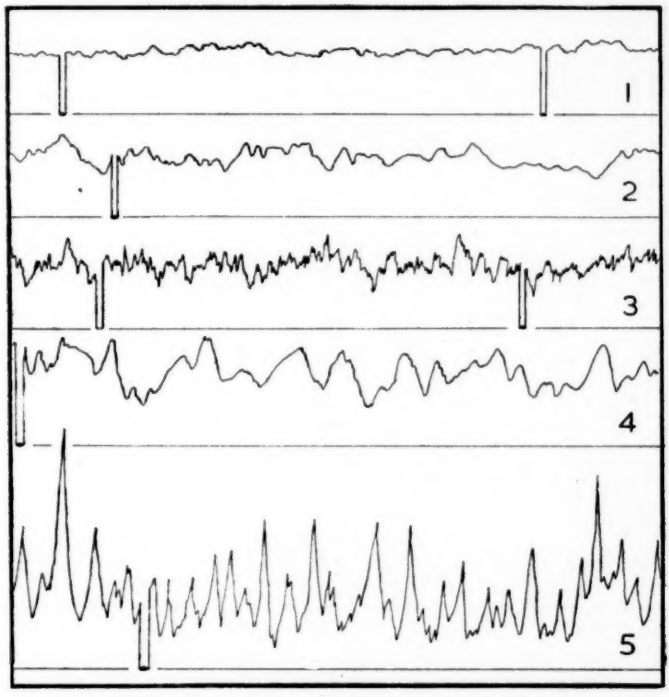

FIG. 6.—*Scintillation patterns in integrated light, recorded with telescope apertures from 36 inches down to 3 inches. All refer to Altair (mean altitude 28°) within a period of 45 minutes. Time horizontally: ordinates proportional to light intensity.*

1. *36-inch aperture.* (*Film No. 139.*) *Time marks* $0^s{\cdot}8$ *apart.*
2. *18-inch aperture.* (*Film No. 140.*) *Total time* $0^s{\cdot}7$.
3. *12-inch aperture.* (*Film No. 141.*) *Time marks* $0^s{\cdot}8$ *apart.*
4. *6-inch aperture.* (*Film No. 145.*) *Total time* $0^s{\cdot}33$.
5. *3-inch aperture.* (*Film No. 144.*) *Note the greatest peak four times the mean level. Total time* $0^s{\cdot}33$.

See also Fig. 7.

It seems clear that this stage must begin to be reached once the apparent diameter of the source becomes equal to that subtended at the receiver by the irregularities concerned. To investigate this problem we have performed numerous experiments using planets as sources. In each case the amplitude of scintillation has been measured and compared with that of a nearby star, both being taken at an altitude of about 30°. Jupiter, apparent diameter 49″, and Saturn, apparent

diameter 20″, showed no measurable scintillation with 36 inches aperture, while the two comparison stars gave scintillation amplitudes of ±20 per cent and ±10 per cent respectively. On another night, scintillation records were obtained of Jupiter, Jupiter III and 20 Tauri, all at the same altitude of 33°. These traces (Fig. 9, Nos. 1, 2, 3) indicate that while the planet's light again is steady, the satellite scintillates precisely like a star of the same magnitude. The apparent diameter of Jupiter III was 1″·5 at the time.

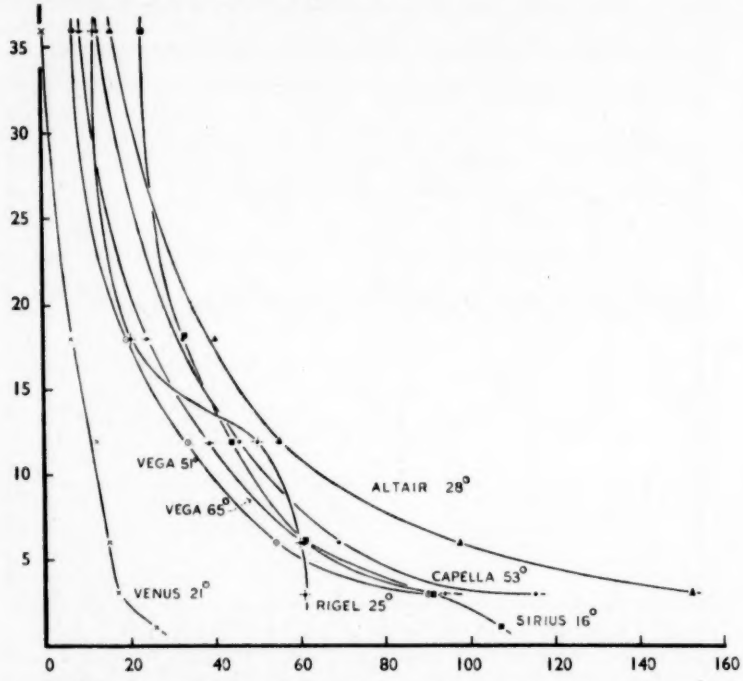

FIG. 7.—*Amplitude of scintillation plotted against telescope aperture for various nights and altitudes.*
Ordinates : Aperture of telescope in inches.
Abscissae : Amplitude of scintillation as a percentage of mean light level.

We infer from this that scintillation begins to die out somewhere within the range of apparent diameter 1″·5 to 20″. But we have been able to narrow the range still further by observations of the planet Mars. At this point we must emphasize the fact that the apparent diameter at which scintillation of a planet begins to disappear is also dependent upon the telescope aperture in use. For example, in Fig. 7 we have plotted the amplitude of scintillation of Venus (altitude 21°) for telescope apertures varying from 36 inches down to 1 inch. The apparent diameter of the planet on this occasion was 31″, but the width of the illuminated crescent was only 12″, so that we might regard the planet for scintillation purposes as equivalent to a circular disk of about 20″. With the full aperture there was no trace of variation in brightness, but scintillation was recorded at 18 inches aperture and increased steadily to a value of ±23 per cent at an aperture of 1 inch. (Because of the great brilliance of the planet it was possible to work at these small

apertures.) It is, consequently, important that all such comparisons between stars and planets should be made with the same telescope aperture. A simultaneous record of Mars, which was only 4° away from Venus and had at the time a disk 4″·4 in diameter, gave scintillation of ± 14 per cent with the full 36-inch aperture, as compared with ± 23 per cent for Sirius at a comparable altitude on the same night. We are thus led to conclude that when the apparent diameter of a planet is in the region of 3″ its scintillation will begin to decrease relative to that of a star at the same altitude, both recorded with the same telescope aperture.

We can now make a tentative estimate of the distance from the telescope of the atmospheric irregularities concerned. We assume that their average diameter is 3 inches (7·6 cm) and that they subtend an angle of 3″: from this we arrive at a mean distance of 5·2 km. This figure may well be in error by a factor of 2, but it is of interest to note that it is of the same order as the value of 4 km derived by Rayleigh (**9**) from his discussion of the refraction theory of scintillation which was based upon the early visual observations of Montigny and Respighi. This theory is referred to more fully in Section 5.

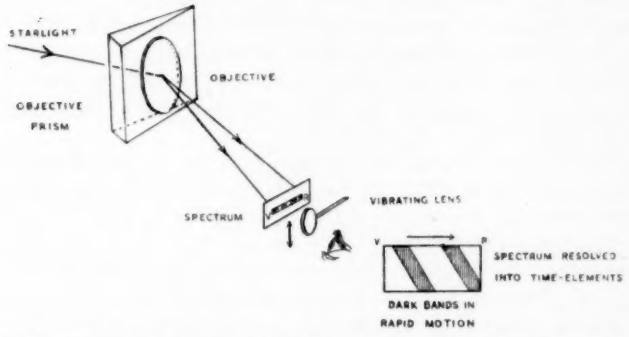

FIG. 8.—*Schematic arrangement for the investigation of the Respighi spectral band phenomenon (destruction of colours by scintillation).*

4. *Colour scintillation.*—The fact that we can observe colour changes in low-altitude stars with the unaided eye or with a small telescope indicates that, at any rate for small apertures, little or no phase coherency exists between the scintillations in different wave-lengths. That is to say, the various colours must fluctuate in brightness independently of one another in time; for if all wave-lengths were to scintillate with equal amplitude and in phase we should expect to observe changes of apparent brightness in the integrated image but no changes of colour.

To investigate the matter further, a 6-inch objective prism was placed in front of a 5-inch aperture objective of 25 inches focal length (Fig. 8). The spectrum of Sirius was focused upon a fine-ground glass screen and observed through a magnifying lens. The lens could be set in vibration in a plane at right angles to the dispersion with a frequency of about 20 oscillations per second. In this way the *time sequence* of the colour changes could be rendered visible to the eye (**4**). At any instant these *elementary* spectra are seen to have one or more broad bands of colour missing: some exhibit only red and violet, others yellow and green, and so on. These dark bands, where the colours are destroyed, or partly so, are of the order of 1 000 A wide and chase one another along the length of the spectrum in an

apparently haphazard fashion. The frequency of fluctuations at any one wave-length is variable, but is in the neighbourhood of 50 c/s.* It seems, therefore, that with this aperture also no phase coherency exists between the scintillations in different wave-lengths. This is not to say that small fluctuations may not also occur in the apparent brightness of the spectrum as a whole, affecting all colours at the same time and to the same extent.

Since this experiment was first described (**4**), F. Zwicky has published (**5**) some very beautiful spectrograms demonstrating the details of the same phenomenon His photographs were taken by means of an objective prism (and, in one case, a large replica grating) mounted in front of the corrector plate of an 18-inch Schmidt camera. The time base was provided, either by the diurnal drift of a bright star across the field, or by swinging the camera by hand in a direction at right angles to the plane of dispersion. These photographs also record the presence of dark bands moving rapidly along the spectrum, showing that individual colours are successively obliterated or greatly reduced in brightness.

Let us consider a simplified model in which the amplitude of scintillation at each separate wave-length is the same fraction x of the mean level at that wave-length. Then if the oscillations in intensity at the various wave-lengths are in phase, the amplitude of scintillation in integrated light will be the same fraction x of the mean integrated level. But if the oscillations in intensity at various wave-lengths are not in phase, then, for integrated light, the amplitude of scintillation will be less than x times the intensity of the mean level.

It was decided to put this matter to the test, using the photomultiplier apparatus attached to the 36-inch reflector, in conjunction with various "monochromatic" filters. The procedure was to make first a scintillation record in "white" light, using the full range of colour response of the cell (see Fig. 2), but with a *neutral screen* interposed in the beam. A "monochromatic" filter† was then substituted for the neutral screen and the monochromatic record was made immediately afterwards. No change of gain of the C.R.O. amplifier was allowed between the records. In this way, by choosing a neutral screen having the same effective transmission as the filter, one could eliminate the possibility of any instrumental alteration between the two records. The results of these tests are entered in Table I, where the amplitudes of scintillation are compared for "white" and "monochromatic" light at various altitudes. Amplitudes are given as a percentage of the mean level, taken as 100 per cent.

There is thus little difference between the amplitude of scintillation in "white" light and in either of the two "monochromatic" bands which were used, from which we infer that the fluctuations in intensity are probably coherent in adjacent wave-lengths. This conclusion is also in agreement with direct measures obtained recently by Mikesell, Hoag and Hall‡, using a split-beam photometer attached to the 40-inch reflector at the Naval Observatory, Washington, and recording simultaneously in two wave-lengths 800 A apart. For the reasons given above it seems that this conclusion can scarcely be true for smaller apertures,

* An earlier investigation of this "band" phenomenon was carried out by Respighi (*Assoc. Française pour l'Avancement des Sciences*, **1**, 148, 1872). A summary of his results is to be found in *Physics of the Air* (W. J. Humphreys, 1920), and in *Meteorologische Optik* (Pernter and Exner, 1910).

† The following filters were used: a "mercury violet", transmitting a band approximately 500 A wide, centred at 4 500 A; a "mercury green", passing 500 A, centred at 5 300 A, and a Schott O.G.2 transmitting from 5500 A to 7000 A (see Fig. 2).

‡ Privately communicated.

in the range 3 to 6 inches, and it is just here that cathode-ray oscillograms taken simultaneously in two colours would be of the greatest interest. Unfortunately, there is insufficient light available with these small apertures to enable us to record *monochromatically* with the existing apparatus.

TABLE I

Amplitude of scintillation in "white" light	Amplitude of scintillation in "monochromatic" light	Filter	Star	Altitude
				°
± 15	± 14	Mercury green	Sirius	14
15	16	Orange green 2	Sirius	14
7	10	Orange green 2	Betelgeuse	27
15	23	Orange green 2	Sirius	13
30	30	Mercury green	Sirius	14
20	20	Mercury green	Spica	23
20	23	Mercury green	Spica	23
6	6	Orange green 2	Arcturus	42
Means ± 16·0 per cent	± 17·8 per cent			

5. *Theories of scintillation.*—The refraction theory of scintillation was first proposed by Montigny. His "Principle" has been summarized as follows: "The individual colours, which go to make up the uniformly coloured or 'white' image seen by the eye, travel through the atmosphere along paths which become more separated the higher one follows them upwards. These path separations are large enough at a certain height to enable small atmospheric irregularities to cross the ray paths of the separate colours in succession and to deviate these colours from their original direction independently of one another, so that first one colour, then another, is removed (or partly so) from vision. Thus the integrated star image shows to the eye not only colour changes but also brightness changes." *

This theory received the general approval of Rayleigh, who developed it in mathematical form (**9**), so as to provide a satisfactory explanation of the spectral band phenomenon, first described by Respighi. Rayleigh calculated that at the top of the atmosphere the separation of the red and violet rays contributing to the light reaching the point O (see Fig. 10) would be of the order of 1 to 2 metres if the apparent altitude of the star were 20°. But he also gives reasons for supposing that, in fact, the irregularities producing these deviations are much lower down in the atmosphere—at a distance from the observer of about 4 km and in dimensions about 4 cm across. Clearly, on this model, colour scintillation would be less marked at smaller zenith distances, which is in good accord with observations, since the whole spectrum rather than single colours would then be affected simultaneously by the passing irregularities. Moreover, the degree of scintillation should be greatest at small apertures (~4 cm), the effect of a larger aperture being to include the pencils of rays refracted by a large number of irregularities simultaneously and thereby to smooth out in the combined effect the larger variations of colour and brightness.

One of the principal difficulties confronting this theory, as Rayleigh himself pointed out †, is to show how *sufficiently refracting* irregularities can occur in the atmosphere, without having to assume improbably large temperature differences

* Translated from *Meteorologische Optik*, p. 175.

† Rayleigh, *loc. cit.*, p. 139.

between adjacent air masses. C. G. Little has recently reviewed this difficulty (**10**), which he considers to be insuperable, and he abandons the refraction theory in favour of a diffraction theory of scintillation. This may be described as a revival, in an improved form, of Arago's interference theory (**12**) which Rayleigh believed he had killed.* Little's theory is based upon a consideration of the distortion of the Fresnel half-period zone pattern of a plane wave viewed through a

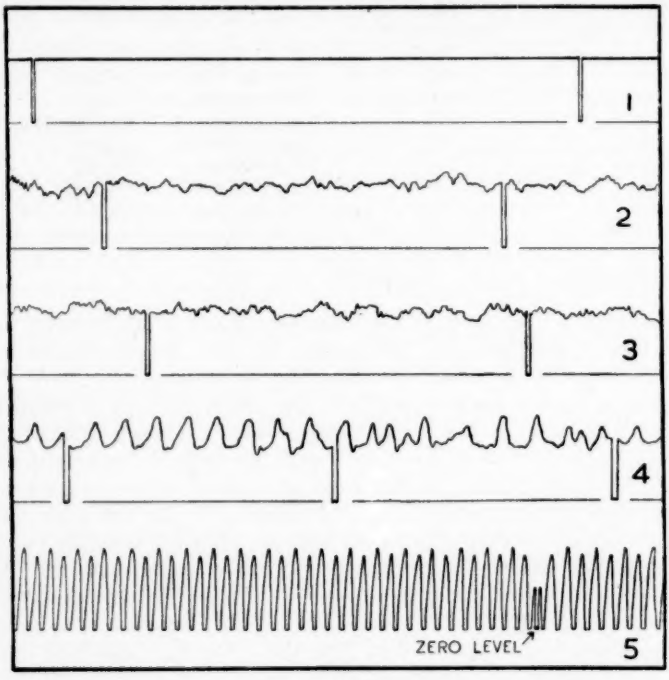

FIG. 9.

1. *Scintillation pattern of Jupiter (apparent diameter 46″) at 34° altitude with 36-inch aperture. (Film No. 157.)*

2. *Jupiter III (mag. 5·3, apparent diameter 1″·5). Altitude 33°. (Film No. 156.)*

3. *20 Tauri. Altitude 33°. (Film No. 158.)*

These three records were taken within a few minutes of one another. The intervals between the time marks in 1, 2 and 3 are 0ˢ·8.

4. *Scintillation of an artificial star shining through water 10 cm deep in a tank. Waves were induced upon the surface of the water by means of a tuning fork. (Film No. 105.) Time intervals here are 0ˢ·5.*

5. *The flashes of a neon lamp recorded with the scintillation apparatus. The successive peaks are 0ˢ·01 apart. (Film No. 174.) Note that the intensity of each flash depends upon the polarity of the alternating current.*

medium of slightly non-homogeneous refractive index. It has the merit of explaining the observed degrees of brightness and colour scintillation, assuming temperature gradients only one-thousandth of those required on the basis of refraction. On the other hand, it is not obvious that it can account for the complex spectral band phenomena of Respighi so well as the earlier ideas.

We have investigated experimentally the question whether it is possible to imitate stellar scintillation effects by the generation of refractional irregularities in a

* Rayleigh, *loc. cit.*, p. 129.

model atmosphere of water. For this purpose a tank was used containing water to a depth of 10 cm. Small waves were generated in the water surface by the action of an electrically operated tuning fork (17 c/s) and paddle. An artificial star, consisting of a d.c. "Pointolite" arc was placed 6 feet above the tank and the light from this "star" was focused upon the cathode of the photomultiplier through a glass window in the flat bottom of the tank.

Waves of small amplitude travelling outwards from the paddle were found to produce brightness scintillation patterns of the type shown in Fig. 9, No. 4, which give a very fair imitation of the scintillation recorded from a real star at low altitude (*cf.* Fig. 3, Nos. 4–6). It is interesting also to note that in Fig. 9, No. 4, the effect of interference between two wave trains can be clearly seen, one series of waves moving outwards from the paddle and the other, of lesser amplitude, returning after reflection from the walls of the vessel.

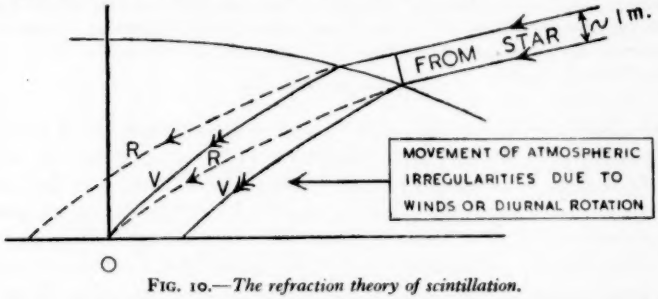

FIG. 10.—*The refraction theory of scintillation.*

We do not wish to maintain that these simple experiments necessarily prove that brightness scintillation is caused by refractional focusing effects in the atmosphere, but they do suggest that such refractional irregularities may contribute largely to the scintillation effects we have recorded, especially at low altitudes.

6. *Acknowledgments.*—We should like to express our thanks to Professor W. M. H. Greaves for his interest in this work; to Professor A. C. B. Lovell and Mr C. G. Little, of the Jodrell Bank Experimental Station of the University of Manchester, for having raised and discussed many of the problems; and to Dr C. B. Childs, of the Department of Natural Philosophy, Edinburgh University and Mr M. J. Smyth, of the Department of Astronomy, Edinburgh University, for their help with instrumental matters.

Royal Observatory,
Edinburgh:
1951 *November* 5.

References

(1) Aristotle, *De Caelo*, Book **2**, chap. 8, par. 290a, 18.
(2) A. E. Whitford and J. Stebbins, ***P.A.A.S.***, **8**, 228, 1936.
(3) C. Montigny, *Bulletins de l'Academie Royale de Belgique*, **37**, 165, 1874.
(4) M. A. Ellison, *Nature*, **165**, 664, 1950.
(5) F. Zwicky, *P.A.S.P.*, **62**, 150, 1950.
(6) F. Schlesinger, *M.N.*, **87**, 506, 1927.
(7) J. H. DeWitt and C. K. Seyfert, *P.A.S.P.*, **62**, 241, 1950.
(8) E. Gaviola, *Astr. J.*, **54**, 155, 1949.
(9) Lord Rayleigh, *Phil. Mag.*, **36**, 129, 1893.
(10) C. G. Little, *M.N.*, **111**, 289, 1951.
(11) H. E. Butler, *The Observatory*, **71**, 28, 1951.
(12) M. Arago, *Annuaire du Bureau des Longitudes pour l'An 1852*, p. 407.

NOTES ON THE 931-A PHOTOMULTIPLIER

M. J. Smyth

(Communicated by the Astronomer Royal for Scotland)

(Received 1951 December 5)

Summary

A number of ex-services RCA 931-A photomultipliers have been examined, and their characteristics are compared with those of the 1P21. The reduction of dark-current is discussed. A method of examining local cathode sensitivity reveals that some tubes have markedly uneven sensitivity and may be unsuitable for astronomical applications. Types of stabilized power supply are discussed, and the effect of geomagnetism on photomultiplier sensitivity is verified.

1. *Introduction.*—In the past eight years multiplier phototubes have found many applications in astronomical photometry (**1, 2, 3, 4, 5, 6**); the specially selected RCA 1P21 in particular has been widely used. Owing to the high cost and difficulty of obtaining this tube, the similar RCA 931-A may be used, if a good specimen is selected. This tube is available at a low price from ex-services equipment suppliers. A number of 931-A photomultipliers have been examined, and performance figures of the best tubes are comparable with those of the 1P21. The method of selection is first considered. Necessary precautions are discussed in later sections.

2. *Selection of tube.*—The 931-A and 1P21 are small blue-sensitive phototubes with nine stages of multiplication (dynodes), and are mounted on moulded bakelite 11-pin bases. The 931-A is not specifically intended for applications involving low light levels, and specimens show widely different characteristics in this respect. A criterion of usefulness is the signal-to-noise ratio at low light levels. Instead of measuring the root-mean-square noise current directly, it was simpler to obtain an indication of its variation from one tube to another by measuring the anode dark-current, which is due to a combination of factors (see Section 3).

Sixteen specimens were tested, using approximately 72 volts per dynode stage, and relative signal intensities and signal-current/dark-current ratios were measured. Dark-currents at about 90 volts per stage were also measured, at an ambient temperature about 18 deg. C. The results are shown in Table I, which illustrates the large variations found. It is remarkable that the first five tubes, which were purchased in light-tight metal holders, show lower dark-current than the remainder, which were purchased in cardboard boxes, although all tubes had subsequently been handled and exposed to daylight before testing.

The dark-currents of the best tubes (e.g. No. 4) are comparable with the figure of 10^{-8} amp given by DeWitt and Seyfert (**6**) for the 1P21, and below the maximum dark-current of 10^{-7} amp quoted by the manufacturers.

As a 1P21 was not available for testing, no direct comparison of luminous sensitivity could be made. Indirect comparisons can be made, but will be only approximate, since the sensitivity is critically dependent upon applied voltage,

and conditions of testing may vary. DeWitt and Seyfert (**6**) find that, using a 1P21, a current of 10^{-7} amp is produced by the light of a 4·5 mag. A-type star with a 12-inch reflector; while Ellison and Seddon (**8**), using the 36-inch reflector of the Royal Observatory, Edinburgh, obtain with the best 931–A tube (No. 4) a current of $2{\cdot}5 \times 10^{-5}$ amp on a 1·33 mag. A-type star. This indicates slightly higher sensitivity for the particular 931–A.

It thus appears that a selected 931–A tube should be equivalent in sensitivity and signal-to-noise ratio to a 1P21.

TABLE I

Tube Number	Relative Sensitivity (72 V/stage)	Signal/Dark-current (72 V/stage)	Dark-current at 90 V/stage (in 10^{-9} amp)
1	6	4	10
2	32	53	14
3	27	22	22
4	530	440	16
5	43	43	21
6	5	2	26
7	150	7	140
8	190	8	170
9	25	0·7	270
10	190	7	170
11	260	14	220
12	180	3	310
13	280	6	310
14	350	20	330
18	300	16	130
19	450	38	100

3. *Reduction of dark-current.*—If the dark-current is large enough to introduce errors, steps must be taken to reduce it. The sources of dark-current have been discussed by Engstrom (**7**) and by DeWitt and Seyfert (**6**). At low voltages ohmic leakage, particularly in the base of the tube, may predominate; amplified thermionic emission from the cathode becomes important at higher voltages; and regenerative ionization effects may occur above 110 volts/stage. The latter effects need not be considered if the tube is operated below 100 volts/stage, as is desirable. Yates (**5**), DeWitt and Seyfert (**6**) and others have found that the thermionic dark-current may be reduced by a factor between 20 and 200 by cooling with solid CO_2. But in most of the 931–A tubes tested, ohmic leakage was much greater than the other effects. This was probably due to the proximity of the anode pin to the cathode pin, which may be at 1 000 volts lower potential. A considerable improvement, for some of the tubes, was produced by the technique of removing the anode pin from the base and insulating the anode lead, as recommended by Kron (**3**). The results of this operation for some tubes are given in Table II.

TABLE II

Tube Number	Dark-current at 100 V/stage	
	Before removal of anode pin (10^{-9} amp)	After removal of anode pin (10^{-9} amp)
2	19	1
4	30	8
9	390	160
18	140	28

Signal-to-noise ratio may be expected to decrease with increasing applied voltage (**7**). However, one of the 931–A tubes measured showed a maximum of this ratio at 90 volts/stage; this was presumably due to the fact that leakage current was predominant at low voltages and increased less rapidly than the signal current with increasing voltage. Using a 931–A in a pulse-counting circuit similar to that described by Yates (**5**), an optimum voltage of 55 volts/stage was found for that particular combination. The pulse-counting technique, with a discriminator stage which removes smaller pulses due to amplifier noise and emission from the dynode stages of the tube, enables an improvement of signal-to-noise ratio to be obtained; also the sensitivity to small changes in overall voltage is diminished.

In measuring the dark currents, the tubes must be "dark-aged" for some time before testing, as exposure to bright light renders them temporarily very "noisy" (**3**). Exposure to bright light when voltage is applied may, of course, permanently damage a tube. Over long periods of use with exposure to low light levels only, a steady improvement is found.

931–A photomultipliers are also subject to fatigue after exposure to light; Engstrom (**7**) has found an average temporary loss of sensitivity of 50 per cent after 40 minutes' exposure with an output current of 100 microamps. The effect varies from one tube to another; the author, using output currents about 5 microamps, has found changes of about 1 per cent in the relative sensitivity of two tubes within a few minutes' exposure. Thus it is desirable in most cases to keep the output current as low as 1 microamp or less.

4. *Uniformity of cathode sensitivity.*—In connection with the work of Ellison and Seddon (**8**) on the photoelectric recording of stellar scintillation, using a 931–A photomultiplier, it was desirable to investigate the uniformity of the light sensitivity of photomultiplier cathodes. Large local variations in sensitivity would cause irregularities in the output current, due to minute image shifts, if the image focused on the cathode were too small.

For this investigation an oscilloscope with short-afterglow tube was set up with its time-base adjusted to about 50 cycles per second, and with no deflection on the Y-plates. The oscillating spot of light was focused on to the rectangular cathode area of the photomultiplier, so as to scan a narrow strip of the cathode, parallel to its long dimension, 50 times per second. The resulting current from the photomultiplier, at 75 volts/stage, was passed to the Y-plate amplifier of a second oscilloscope, whose X-plates were coupled to the time-base of the first. Thus the sensitivity along a narrow strip of the photomultiplier cathode was displayed on the second oscilloscope, the second beam of which was used to provide a zero line.

Direct tracings, made with an enlarger from photographs of these patterns, are shown in Fig. 1. In this figure, (*a*) indicates the usual position of the scanned strip on the projected area of the cathode; for each tube the scanned strip was shifted to and fro parallel to itself, and for some tubes considerable lateral variations were thus found. Since the actual cathode surface is set at 45° to the direction of incident light, shifts along the shorter dimension of the cathode involve a change of focus. Fig. 1 (*b*) shows the trace obtained by focusing the scanning spot on a rhodium step-wedge and thence, using a field lens for uniform cathode illumination, on the photomultiplier; the response is sufficiently rapid and linear. Fig. 1 (*c*) is the trace for the tube with most uniform cathode sensitivity; the

maxima and minima arise from focusing the scanning spot on the wire grill in front of the cathode. Fig. 1 (*d*) is the trace for our most sensitive tube (No. 4), and shows sensitivity uniformly increasing towards the lower end; the spot was again focused on the wire grill. Fig. 1 (*e*) shows a central spot of nearly double sensitivity on an otherwise fairly uniform cathode; a small star image focused near this spot would give rise to large apparent intensity fluctuations. Fig. 1 (*f*) shows a central region of low sensitivity; the apparent sensitivity of this tube would be lowered if this region were used for measurements. Fig. 1 (*g*), (*h*) and (*i*) are traces for the tube used in the stellar scintillation experiments, and show the response of parallel strips of the cathode about 3 mm apart.

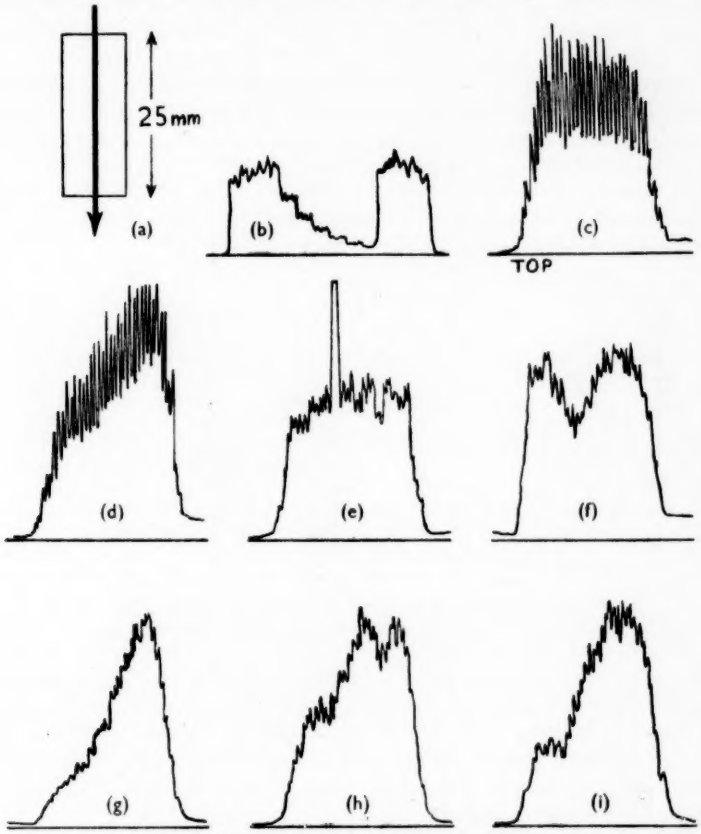

FIG. 1.—*Tracings of oscillograms showing distribution of sensitivity along strips of the cathodes of* 931-A *photomultipliers. For explanation see text.*

Photographs of the cathode patterns of all our photomultipliers have been made and will provide a useful guide in their application to specific problems. No visible indication of high or low-sensitivity areas, as revealed in (*e*) and (*f*), can be seen on inspection of the cathodes.

5. *Power supplies.*—The accelerating potentials for the dynodes may most simply be obtained from ten dry batteries. If variable potentials are required,

to control the gain, the dynodes may be fed from tappings on a potentiometer chain, in the usual manner.

It should be noted that if a potentiometer chain is used, the currents drawn by the dynodes will modify the voltages; consequently, to preserve the intrinsic linearity of the photomultiplier (**7**), the potentiometer current should be at least 1000 times greater than the maximum (mean) anode current. This may impair the constancy of the voltage supplied by dry batteries; for this reason, and because of the bulk and lethal capabilities of batteries, a mains-driven stabilized power supply is often preferable.

A unit is required which will supply about 1 milliamp at 1000 volts; since the sensitivity of the photomultiplier varies approximately as the ninth power of the overall voltage, a voltage stability of 1 part in 10^4 is desirable. Numerous circuits have been published (**6, 9, 10, 11**). Two basic types of circuit which have been found useful by the author are illustrated in Fig. 2; no originality is claimed for these. The rectifying and smoothing arrangements are conventional and have not been included; similarly, component values are omitted, since they may be chosen to suit individual circumstances.

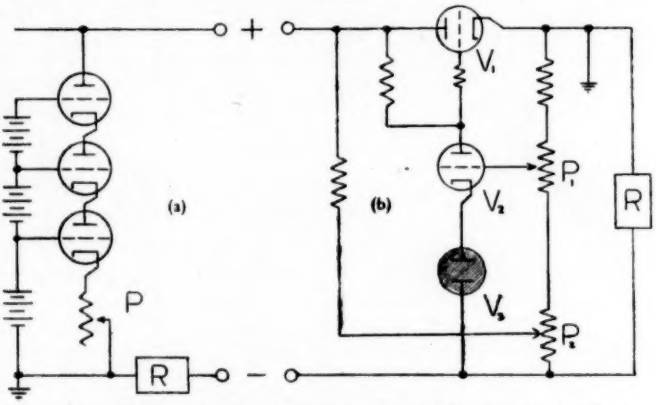

FIG. 2.—*Basic stabilizing circuits. Rectifying and smoothing circuits are omitted. R represents the potentiometer chain supplying the photomultiplier.*

Circuit (*a*) uses dry batteries, from which no current is drawn, to stabilize the current through, and hence the voltage across, the photomultiplier potentiometer chain represented by R. The current can be varied by adjusting potentiometer P; e.g. if the batteries give 90 volts, and P is set at 90000 ohms, the current is approximately 1 milliamp. The circuit reduces input voltage variations, due to mains fluctuations, by a large factor.

Circuit (*b*) is more flexible (*cf.* **6**). The 85A2, a miniature rare-gas voltage reference tube, is used at V_3. This tube appears to be the most stable available (**12, 13**); random voltage changes should not exceed 0·1 per cent over periods of 100 hours (**14**), and the voltage-current characteristic is very smooth above 1 milliamp. Other types of voltage-reference tube show irregular glow-shifts at low currents, and much greater voltage drifts. In this circuit, potentiometer P_1 adjusts the voltage across the photomultiplier potentiometer chain R, and P_2 can be adjusted, at each setting of P_1, to provide complete stabilization against mains input

fluctuations; the settings of P_2 at each voltage may be recorded for reference. An EF–50 (VR–91) strapped as a triode has been used at V_2.

6. *Positional effect.*—The manufacturers of photomultipliers recommend magnetic screening in the presence of strong magnetic fields; but it was found by Eggen (**15**) that changes in orientation with respect to the Earth's magnetic field, due for example to changing positions of a photomultiplier mounted on a telescope, can cause appreciable variations of sensitivity. This "positional effect" is presumably due to defocusing of the electron streams, and was eliminated by Eggen by shielding with demagnetized iron.

The author has verified this effect, using a 931–A mounted in a box with a standard lamp. Little effect was produced by changing the azimuth of the tube, but maximum variation was obtained between the cap-up and cap-down positions. The excess sensitivity in the cap-up position, at constant output current, varied in this case between 11·5 per cent at 50 volts/stage and 9·5 per cent at 90 volts/stage. The constancy of the standard lamp was checked by a barrier-layer cell.

7. *Acknowledgments.*—I am indebted to Dr M. A. Ellison and Mr H. Seddon for valuable discussion and measurements with the 36-inch telescope, and to Professor W. M. H. Greaves for his continued interest and helpful suggestions; also to the Moray Endowment of the University of Edinburgh for an equipment grant.

Royal Observatory,
Edinburgh :
1951 *December* 3.

References

(1) Y. Öhman, *Arkiv för Matematik, Astronomi och Fysik*, Bd. **29B,** 12, 1942.
(2) H. W. Babcock, *Ap. J.*, **96,** 242, 1942.
(3) G. E. Kron, *Ap. J.*, **103,** 326, 1946.
(4) G. E. Kron, *Harvard College Observatory Circular*, No. 451, 1946.
(5) G. G. Yates, *M.N.*, **108,** 476, 1948.
(6) J. H. DeWitt, Jr. and C. K. Seyfert, *P.A.S.P.*, **62,** 241, 1950.
(7) R. W. Engstrom, *J.O.S.A.*, **37,** 420, 1947.
(8) M. A. Ellison and H. Seddon, *M.N.*, **112,** 73, 1952.
(9) F. V. Hunt and R. W. Hickman, *Rev. Sci. Instr.*, **10,** 6, 1939.
(10) J. J. Gilvarry and D. F. Rutland, *Rev. Sci. Instr.*, **22,** 464, 1951.
(11) A. J. Maddock, *J. Sci. Instr.*, **28,** 325, 1951.
(12) F. A. Benson, W. E. Cain and B. D. Clucas, *J. Sci. Instr.*, **26,** 399, 1949.
(13) F. A. Benson, *J. Sci. Instr.*, **28,** 339, 1951.
(14) *Mullard News Letter*, October, 1951.
(15) O. J. Eggen, *Ap. J.*, **114,** 141, 1951.

STELLAR PARALLAXES DETERMINED PHOTOGRAPHICALLY AT THE CAPE OBSERVATORY (EIGHTEENTH LIST)

J. Jackson and J. B. G. Turner

(Communicated by H.M. Astronomer)

(Received 1951 October 22)

The principal list is in the same form as the previous lists beginning in *M.N.*, **89**, 497, 1929.

Approximately half of the stars in the present list are faint stars with a proper motion exceeding 0″·5 annually, given by Luyten in Vol. III, No. 1 of the *Publications of the Astronomical Observatory of the University of Minnesota*. About one-sixth are stars selected from the Cape Astrographic Zone as having an annual proper motion in excess of 0″·2, while most of the remainder were selected from the *General Catalogue* for a similar reason. Three stars, Nos. 1635, 1670 and 1671 appear on account of their relative proximity to Nos. 1634, 1669 and 1672 respectively, and of the consequent uncertainty of the identity of the proper motion star in each case.

Where possible, the magnitudes given are taken from the *Henry Draper Catalogue*; otherwise these are generally as given by the authority quoted for the proper motion.

Eleven of the stars have parallaxes exceeding 0″·1. Of these, nine are stars given by Luyten, and the other two are BD −21° 1051 (No. 1632) and BD +5° 1668 (No. 1650) a star with very large proper motion.

The supplementary list contains twelve stars for which, for various reasons, second determinations of parallax were made. In each case a completely new series of plates was taken; but the reference stars and the ruled reference plates were the same as those used for the first determination made here. The original determination is given under (1) and the second under (2). The means are based upon the relative probable errors.

NOTES

1607. Dr Hoffleit (Harvard special classification for *Cape Zone Photographic Catalogues*, unpublished) classifies this star as Go. Its colour index, as determined at the Cape, is +0·25.

1608. LPM 76 is a white dwarf.

1668. This is CPD −43° 7032, which is possibly CoD −43° 9842.

No.	Name and D.M. No.	Mag. Vis. Phot.	Type	R.A., Dec. (1900.0)	Proper Motion R.A.	Proper Motion Dec.	P.E. Unit Weight	Parallax	P.E.
				h m s					
1601	LPM 32	...	m	0 35 09	+ 437	−263	±29	+ 46	± 8
	−44° 170	13·0		−44° 47′·8	+ 469				± 3
1602	LPM 49	...	K5	0 52 59	+1050	+170	±30	+ 48	± 8
	−62° 75	11·8		−62° 47′·0	+1034				± 4
1603	LPM 50	...	m	0 53 28	+1270	−290	±37	+ 66	±12
	−28° 302	12·7		−28° 23′·6	+1299				± 6
1604	LPM 56	...	g	0 59 19	+ 620	−250	±28	+ 9	± 8
	−35° 360	10·8		−35° 12′·2	+ 585				± 4

No.	Name and D.M. No.	Mag. Vis. Phot.	Type	R.A., Dec. (1900.0)	Proper Motion R.A.	Proper Motion Dec.	P.E. Unit Weight	Parallax	P.E.
				h m s					
1605	LPM 67	...	m	1 13 19	+ 170	−690	±37	+ 45	±10
		12·2		−13° 24′·4	+ 166				± 6
1606	LPM 73	...	m	27 43	− 560	−900	±39	+ 34	±12
	−22° 526	12·3		−22° 23′·7	− 577				± 7
1607	LPM 75	...	F1	1 32 37	− 70	−630	±25	0	± 8
	−61° 122	10·6		−61° 34′·4	− 79				± 2
1608	LPM 76	12·2	A3	1 32 53	+ 580	−335	±26	+ 62	± 9
		12·6		− 5° 29′·8	+ 570				± 3
1609	Ci 20 126	...	...	1 40 26	− 80	−410	±20	− 4	± 6
	Ross 552	10·		−13° 59′·6	− 83				± 2
1610	GC 2286	7·43	Go	1 48 02	− 177	−356	±41	+ 32	±12
	− 2° 311	7·99		− 1° 48′·6	− 210				± 5
1611	GC 2303	4·41	Mb	1 49 38	− 103	− 89	±30	+ 14	± 9
	ZC 890	6·4		−46° 47′·5	− 115				± 6
1612	LPM 97	...	G4	2 00 50	+ 320	+440	±28	+ 49	± 9
	−28° 657	12·6		−28° 33′·6	+ 308				± 6
1613	LPM 100	...	k–m	2 04 21	+ 530	+ 80	±27	+ 32	± 9
	−17° 400	11·5		−16° 48′·9	+ 480				± 7
1614	LPM 104	...	m	2 08 04	+ 470	+210	±24	+ 27	± 8
		11·2		−18° 09′·7	+ 486				± 5
1615	LPM 107	...	m	2 09 26	+ 750	−570	±38	+105	± 9
	−32° 828	11·5		−32° 29′·6	+ 771				± 5
1616	LPM 115	...	m	2 14 00	+ 470	+380	±26	+ 70	± 8
	CoD −54° 487	12·6		−54° 27′·6	+ 457				± 6
1617	LPM 121	8·9	K2	2 24 19	+ 620	+180	±32	+ 64	± 9
	−20° 465	10·0		−20° 26′·0	+ 602				± 5
1618	GC 3141	8·7	Ko	2 31 37	+ 332	+ 51	±29	+ 22	± 8
	− 3° 410	...		− 3° 35′·6	+ 306				± 4
1619	LPM 135	...	m	2 50 01	+ 970	+600	±30	+ 78	±10
		12·4		−64° 06′·4	+ 974				± 8
1620	GC 3734	7·16	Go	3 02 35	+ 13	−261	±32	+ 40	±10
	−14° 604	7·72		−14° 08′·4	− 23				± 9
1621	LPM 144	...	m	3 08 30	+1220	+730	±24	+125	± 7
	−38° 1058	12·0		−38° 29′·0	+1258				± 4
1622	−26° 1207	8·7	K2	3 10 26	+ 252	+ 86	±22	+ 63	± 6
		...		−26° 49′·2	+ 179				± 6
1623	LPM 159	...	f	3 30 36	− 50	−500	±34	+ 23	± 9
	−31° 1454	11·3		−31° 24′·8	− 71				± 6
1624	GC 4313	4·40	G5	3 31 46	− 234	−479	±37	+ 85	±10
	10 Tauri	5·18		+ 0° 05′·1	− 258				± 6

No.	Name and D.M. No.	Mag. Vis. Phot.	Type	R.A., Dec. (1900.0)	Proper Motion R.A.	Proper Motion Dec.	P.E. Unit Weight	Parallax	P.E.
				h m s					
1625	GC 4488	6·96	G5	3 40 28	+ 204	+294	±37	+ 61	± 9
	−38° 1264	7·7		−38° 26′·2	+ 225				± 5
1626	LPM 173	...	k	3 49 35	− 370	−1080	±24	+ 45	± 7
	−37° 1501	12·8		−37° 21′·8	− 409				± 4
1627	FS 1228	...	K7	4 09 08	+ 112	−128	±38	+ 31	±10
	−50° 1302	11·5		−50° 38′·2	+ 135				± 7
1628	GC 5407	7·96	Go	4 24 15	− 35	+324	±28	+ 41	± 6
	−64° 334	9·2		−64° 18′·8	− 66				± 4
1629	LPM 198	...	m	4 49 21	+ 450	−640	±31	+ 89	± 8
		12·5		−17° 55′·2	+ 391				± 4
1630	ZC 2534	7·1	Ma	4 49 27	+ 30	+ 51	±29	+ 20	± 7
	−43° 1590	9·5		−43° 13′·6	+ 41				± 5
1631	LPM 201	...	g5	4 57 55	+ 520	−410	±19	+ 3	± 6
		12·5		−19° 40′·0	+ 525				± 4
1632	−21° 1051	8·3	dM2	4 58 13	− 157	−264	±23	+127	± 6
		9·7		−21° 23′·5	− 152				± 4
1633	GC 6487	5·66	G9	5 13 05	− 13	− 45	±30	+ 30	± 9
	PGC 1263	6·66		−13° 37′·6	− 31				± 6
1634	LPM 211	...	k	5 15 45	+ 230	−470	±18	+ 42	± 6
		13·0		−53° 46′·3	+ 258				± 3
1635	S.f. No. 1634	...	...	5 16 02	...	...	±29	+ 17	± 6
		12·4		−53° 46′·6	0				± 3
1636	GC 6824	7·01	Go	5 26 15	+ 173	−319	±29	+ 13	± 7
	−10° 1204	7·57		−10° 08′·9	+ 142				± 3
1637	LPM 218	...	m	5 44 05	+ 680	− 80	±25	+ 96	± 6
	−36° 2458	11·6		−36° 21′·5	+ 767				± 3
1638	GC 7387	6·87	G5	5 48 04	+ 205	+ 49	±33	− 10	± 8
	−25° 2734	8·3		−25° 58′·1	+ 221				± 4
1639	− 6° 1339	9·5	Mo	5 48 07	+ 4	−181	±28	+ 80	± 7
		...		−06° 00′·8	+ 6				± 4
1640	− 9° 1261	...	k	5 49 48	+ 110	+310	±21	+ 48	± 6
		11·0		−09° 25′·2	+ 124				± 4
1641	GC 7479	5·30	A5	5 52 38	− 16	+244	±25	+ 60	± 6
	−52° 805	6·1		−52° 39′·4	− 25				± 3
1642	GC 7738	8·31	F2	6 01 57	− 13	+208	±22	+ 28	± 5
	−35° 2685	...		−35° 31′·7	− 2				± 3
1643p	GC 7976	7·08	F5	6 11 57	+ 9	+148	±21	− 5	± 6
	−65° 565	7·4		−65° 30′·4	+ 25				± 3
1643f	GC 7979	8·51	G	6 12 00	+ 26	+140	±27	+ 19	± 8
	−65° 566	9·1		−65° 30′·6	+ 24				± 4

No.	Name and D.M. No.	Mag. Vis. Phot.	Type	R.A., Dec. (1900.0) h m s	Proper Motion R.A.	Proper Motion Dec.	P.E. Unit Weight	Parallax	P.E.
	Mean							+ 4	± 5
					+ 25				± 2
1644	LPM 234	...	k	6 17 45	− 640	+230	±23	+ 46	± 6
	−22° 3005	12·2		−22° 40′·3	− 632				± 4
1645	L597–31	...	m	6 28 06	+ 390	−240	±21	+ 65	± 5
		12·7		−26° 57′·1	+ 412				± 3
1646	−26° 3112	...	...	6 29 00	− 10	−350	±26	+ 22	± 7
	L 276	11·2		−26° 41′·6	− 19				± 4
1647	GC 8712	5·78	Ko	6 35 53	− 9	−184	±30	+ 16	± 8
	PGC 1708	7·5		−30° 22′·4	+ 9				± 4
1648	GC 9256	6·75	Ko	6 57 08	+ 204	+ 37	±32	+ 65	± 8
	−25° 3913	7·7		−25° 48′·4	+ 246				± 4
1649	LPM 259	...	F4	7 16 38	+ 330	−450	±21	+ 34	± 6
		11·2		−15° 09′·4	+ 325				± 4
1650	+ 5° 1668	10·3	M5	7 22 00	+ 583	−3694	±20	+311	± 5
		...		+ 5° 32′·3	+ 656				± 3
1651	ZC 4651	7·5	Ma	7 31 32	− 3	+ 70	±18	+ 27	± 4
	−50° 2841	9·1		−50° 37′·4	+ 20				± 3
1652	GC 10425	5·11	Ko	7 40 18	+ 128	−189	±21	+ 52	± 5
	PGC 2039	7·1		−40° 41′·4	+ 132				± 3
1653	GC 10524	7·35	G5	7 44 55	− 80	+271	±19	+ 10	± 6
	−61° 888	8·4		−61° 11′·4	− 71				± 4
1654	LPM 282	...	m	8 08 18	+ 60	−730	±20	+168	± 6
		13·0		−21° 14′·0	+ 22				± 3
1655	LPM 296	...	m	8 36 39	− 430	+800	±23	+113	± 7
		13·0		−23° 07′·7	− 454				± 4
1656	GC 13048	5·44	Go	9 22 49	− 225	− 78	±23	+ 22	± 7
	PGC 2535	6·00		−05° 38′·0	− 223				± 4
1657	LPM 321	...	k	9 31 24	+ 150	−1090	±27	+119	± 7
		12·8		−21° 11′·1	+ 145				± 3
1658	LPM 334	...	m	9 56 52	−1090	+650	±31	+ 68	± 7
	−29° 8019	12·8		−29° 56′·0	−1090				± 4
1659	GC 17025	8·7	G5	12 24 37	− 336	−583	±28	+ 47	± 8
	LPM 432	...		−02° 45′·9	− 332				± 3
1660	FS 10116	...	K7	12 29 30	− 400	− 67	±37	+ 26	± 9
	−46° 8007	11·1		−46° 44′·1	− 354				± 4
1661	GC 17435	8·73	Mo	12 45 36	− 42	−397	±33	+ 54	± 8
	+ 0° 2989	10·08		−00° 12′·7	− 14				± 3
1662	GC 18144	1·21	B2	13 19 55	− 41	− 35	±32	+ 17	± 8
	α Virginis	1·02		−10° 38′·4	− 33				± 3

No.	Name and D.M. No.	Mag. Vis. Phot.	Type	R.A., Dec. (1900.0)	Proper Motion R.A.	Proper Motion Dec.	P.E. Unit Weight	Parallax	P.E.
				h m s					
1663	− 3° 3527	10·8	M2	13 39 55	− 161	− 64	±31	+ 42	± 8
		...		−04° 06′·9	− 149				± 4
1664	ZC 12041	9·2	G5	14 02 29	− 331	−163	±31	− 8	± 6
	−51° 7987	9·4		−51° 27′·5	− 322				± 3
1665	LPM 532	11·4	M4	14 28 54	− 290	+630	±33	+150	± 7
	Ci 20 870	...		−12° 05′·8	− 315				± 3
1666p	LPM 544	...	m	14 43 52	−1200	−190	±37	+ 38	±10
		13·3		−25° 40′·7	−1210				± 5
1666f	LPM 543	...	m	14 43 53	−1200	−190	±34	+ 46	± 9
	−25° 10553	12·8		−25° 39′·6	−1188				± 5
	Mean							+ 42	± 7
					−1199				± 4
1667	GC 20160	6·68	F5	14 53 11	− 194	−134	±25	+ 29	± 6
	ZC 12838	7·5		−43° 24′·5	− 172				± 3
1668	FS 13043	...	G5	15 15 46	− 200	−134	±27	+ 12	± 6
		11·8		−43° 30′·3	− 181				± 2
1669	LPM 575	...	m	15 32 13	− 60	−580	±29	+ 22	± 7
		12·0		−20° 58′·5	− 85				± 4
1670	N.f. No. 1669	...	...	15 32 14	...	...	±27	+ 7	± 6
		12·		−20° 56′·7	− 8				± 4
1671	S.p. No. 1672	...	...	15 41 34	...	...	±34	− 1	± 8
		12·		−13° 17′·1	+ 19				± 5
1672	LPM 585	...	g	15 41 35	− 350	−390	±27	− 3	± 6
	−13° 4246	12·2		−13° 16′·9	− 332				± 4
1673	LPM 590	7·33	Ko	15 59 48	+ 310	−390	±22	+ 54	± 5
	−20° 4399	8·1		−20° 10′·1	+ 303				± 3
1674	LPM 597	...	g:	16 13 30	− 700	+1000	±27	+136	± 8
	−37° 10765	12·0		−37° 18′·9	− 715				± 4
1675	LPM 598	...	k	16 14 57	− 330	−340	±27	− 3	± 6
	Ci 20 980	12·2		−17° 23′·8	− 318				± 2
1676	LPM 617	...	m	16 36 24	− 510	−460	±37	+ 49	± 9
		13·0		−72° 48′	− 472				± 5
1677	LPM 619	...	G:	16 42 19	− 520	−110	±35	+ 49	± 8
		12·4		−64° 15′·5	− 514				± 5
1678	LPM 630	...	g	17 07 31	+ 180	−670	±19	+ 48	± 5
		12·7		− 4° 59′·1	+ 193				± 3
1679	FS 16429	...	Go	17 15 18	− 142	−105	±34	+ 8	± 8
		10·9		−43° 03′·3	− 157				± 3
1680	GC 23597	4·28	Fo	17 20 16	0	−123	±39	+ 34	± 8
	PGC 4420	4·56		−24° 05′·0	+ 29				± 4

No.	Name and D.M. No.	Mag. Vis. Phot.	Type	R.A., Dec. (1900.0) h m s	Proper Motion R.A.	Proper Motion Dec.	P.E. Unit Weight	Parallax	P.E.
1681	LPM 661	...	G	17 50 12	0	−600	±27	+ 23	± 7
		11·0		−16° 22′·6	+ 7				± 4
1682	LPM 663	...	f–g	17 52 27	+ 150	−650	±31	+ 41	± 7
	−30° 15026	10·2		−30° 08′·6	+ 183				± 4
1683	LPM 671	...	m	18 13 58	+ 360	−400	±33	+ 50	± 9
		13·6		−05° 48′·2	+ 378				± 4
1684	LPM 689	...	k–m	18 44 24	− 250	−760	±36	+ 31	±10
		13·4		−57° 13′·7	− 248				± 5
1685	GC 25941	2·14	B3	18 49 04	+ 12	− 58	±18	+ 6	± 4
	σ Sagittarii	1·97		−26° 25′·3	+ 12				± 2
1686	FS 18390	...	...	18 51 15	− 380	−225	±36	+ 32	± 9
	CAZ −47° 176	13·7		−46° 23′·9	− 391				± 4
1687	GC 26161	2·71	A2	18 56 15	− 19	− 5	±28	+ 20	± 7
	ζ Sagittarii	2·77		−30° 01′·4	− 28				± 4
1688	UOC 53	...	...	18 59 03	+ 110	−380	±36	+ 17	± 8
	Ci 20 1126	12·8		−65° 24′·4	+ 71				± 4
1689	Wolf 1062	...	...	19 07 02	+1770	−630	±36	+ 77	±10
	Ci 20 1136	12·7		+ 2° 44′·1	+1802				± 5
1690	LPM 701	...	m	19 13 25	+ 610	−2880	±25	+180	± 7
		13·4		−45° 39′·5	+ 619				± 3
1691	FS 18826	...	Ko	19 38 04	+ 205	+ 58	±30	+ 22	± 6
		10·5		−40° 28′·6	+ 181				± 4
1692	LPM 709	...	g	19 42 21	− 110	−540	±32	+ 33	± 7
	−59° 7535	10·0		−59° 25′·2	− 96				± 5
1693	LPM 727	9·0	K5	20 04 33	− 420	−370	±35	+ 47	± 9
	−20° 5833	10·3		−20° 46′·6	− 453				± 5
1694	LPM 741	...	m	20 21 39	− 220	−870	±42	+ 68	±11
	−28° 16676	12·8		−28° 03′·0	− 180				± 7
1695	LPM 746	9·1	Ko	20 35 47	+ 620	−540	±29	+ 38	± 7
	−22° 5504	11·0		−22° 39′·7	+ 660				± 5
1696	LPM 748	...	m	20 37 18	+ 670	−1000	± 24	+ 65	± 7
		13·2		−79° 40′	+ 676				± 5
1697	GC 29787	8·5	K2	21 12 52	+ 450	−180	±40	+ 57	±10
	− 0° 4195	9·6		−00° 15′·1	+ 476				± 8
1698	LPM 814	...	M5	22 04 21	+1030	− 20	±22	+121	± 6
	Ci 20 1340	11·8		−05° 07′·9	+1139				± 3
1699	GC 31165	8·6	Ko	22 11 22	+ 190	−122	±32	+ 29	± 8
	ZC 19833	9·3		−49° 08′·8	+ 217				± 4
1700	GC 31437	6·86	Go	22 24 53	− 159	−204	±34	+ 33	± 9
	ZC 19958	7·9		−49° 56′·4	− 152				± 4

Second Determinations

No.	Name and D.M. No.	Mag. Vis. Phot.	Type	R.A., Dec. (1900.0)	P.M. in R.A.	P.E.	Relative Parallax	P.E.	
				h m s					
1207	GC 1920	7·19	G5	1 30 23	+140	±5	+111	± 8	(1)
	−30° 529	8·0		−30° 25′·5	+132	±1	+ 57	± 8	(2)
					+132	±1	+ 84	± 6	Mean
1108	FS 1254	...	Mo	4 13 36	+170	±8	+ 7	±10	(1)
	CAZ −41° 66	13·7		−41° 02′·8	+219	±2	+ 59	± 9	(2)
					+216	±2	+ 36	± 7	Mean
1038	GC 9824	9·0	Ko	7 17 09	−358	±5	− 1	± 8	(1)
	− 1° 1677	10·0		−01° 40′·8	−368	±2	+ 19	± 7	(2)
					−367	±2	+ 10	± 5	Mean
774	Ci 18 918	7·25	K2	7 34 59	+123	±8	+114	± 8	(1)
	− 3° 2001	8·32		−03° 21′·6	+ 77	±1	+ 96	± 6	(2)
					+ 78	±1	+102	± 5	Mean
1362	FS 10138	...	Mo	12 31 21	− 88	±4	+ 31	± 7	(1)
	−41° 7290	11·9		−41° 09′·8	− 86	±2	+ 9	± 6	(2)
					− 86	±2	+ 18	± 5	Mean
1372	FS 13662	...	M	15 34 44	−124	±5	+ 19	± 7	(1)
	−50° 9730	12·4		−50° 34′·8	−136	±2	+ 3	± 7	(2)
					−134	±2	+ 11	± 5	Mean
1379	FS 17279	...	Mo	17 39 14	+ 5	±3	+ 8	± 4	(1)
	CAZ −49° 362	12·3		−48° 03′·0	+ 6	±1	+ 2	± 2	(2)
					+ 6	±1	+ 3	± 2	Mean
1476	FS 18216	Var.	M5e	18 35 53	+ 15	±4	+ 6	± 6	(1)
	−45° 12699	...		−45° 52′·5	+ 19	±2	− 5	± 6	(2)
					+ 18	±2	0	± 4	Mean
1178	FS 18799	...	M1	19 35 44	− 98	±6	+ 34	± 8	(1)
	−45° 13383	11·4		−45° 18′·5	− 77	±3	+ 27	±11	(2)
					− 81	±3	+ 32	± 6	Mean
1179	FS 18800	...	Go	19 35 50	−106	±4	+ 8	± 5	(1)
	−45° 13385	10·8		−45° 16′·7	−114	±1	+ 15	± 6	(2)
					−114	±1	+ 11	± 4	Mean
995	FS 19718	...	Mo	21 51 07	− 67	±8	+ 65	± 7	(1)
	CAZ −51° 83	12·1		−51° 28′·3	− 45	±2	+ 66	± 9	(2)
					− 46	±2	+ 65	± 5	Mean

Royal Observatory,
Cape of Good Hope :
1951 *October* 15.

THE PHOTO-CHEMISTRY OF SOME MINOR CONSTITUENTS OF THE EARTH'S ATMOSPHERE (CO_2, CO, CH_4, N_2O)

D. R. Bates and Agnes E. Witherspoon

(Received 1951 October 3)

Summary

Carbon dioxide and carbon monoxide: The rate of photo-dissociation of CO_2 is appreciable only in the region above about 100 km. If local equilibrium prevails the carbon would occur mainly as the monoxide in this region, and as the dioxide below. However, oxidation may proceed so slowly that the life of a CO molecule is long compared with the characteristic time associated with atmospheric mixing effects. In this case the CO resulting from photo-dissociation would not be confined to above the 100 km level, but would extend much lower; its total abundance could scarcely be great enough to produce the observed absorption lines. It is estimated that the various forms of combustion taking place on the Earth would provide the CO content of the atmosphere within perhaps four years or even less.

Methane: Dissociation of CH_4 in the upper atmosphere is brought about mainly by collision processes. These prevent the existence of appreciable CH_4 above the 100 km level and probably keep the concentration low even down to 70 km. The yield to date from oil wells and coal mines appears to be less than the amount of the gas now in the atmosphere. Seepage from fuel beds, and the anaerobic decay of vegetable matter, are the only obvious naturally occurring sources of significance. As far as can be judged at least ten years (and probably much longer) is required for the production of the atmospheric abundance.

Nitrous oxide: Information on the necessary rate of formation of N_2O is obtained by calculating the photo-dissociation rate. One hypothesis is that soil micro-organisms produce the gas, but it appears that the yield would only be sufficient if N_2O were a major end-product of denitrification. Many of the homogeneous gas reactions suggested by earlier workers must be rejected, since there is an inadequate supply of the requisite parent particles. The only acceptable parent particles seem to be those arising directly or indirectly from the photo-dissociation of O_3 in the Herzberg continuum. Various reactions involving O, O_3 and N_2 are discussed. Though they are very slow they might nevertheless give rise to sufficient N_2O.

---

1. *Introduction.*—The photo-chemistry of atmospheric oxygen has been studied by many scientists (**1**), and though much detailed work remains to be done, the researches of Chapman and others have led to a general understanding of the factors involved in the formation of the ozone layer and of the atomic region. While the desirability of a similar study of nitrogen has long been realized, comparatively little has yet been achieved because of some special difficulties that arise and because of lack of certain basic data; and as nitrogen is obviously the next most important gas to investigate there has been a neglect of the other constituents—though Meinel's discovery (**2**) of the hydroxyl bands in the spectrum of the airglow recently stimulated Bates and Nicolet (**3**) to carry out an exploratory survey of the photo-chemistry of water vapour. The object

of the present paper is to remedy this omission partially by investigating the position regarding carbon dioxide, carbon monoxide, methane and nitrous oxide. Originally the research was directed at obtaining information on the altitude distribution of the polyatomic molecules (which is of importance in connection with studies of the thermo-balance in the upper atmosphere). During the course of it the existence of several interesting cycles was realized, and these are also discussed.

2. *Model atmosphere.*—Table I gives the current estimates of the particle concentrations, $n(M)$, and temperatures, T, at various altitudes, z, up to 130 km (**3**). They are significantly different from those accepted at the time of the main work on the O–O_2–O_3 equilibrium. Since this equilibrium is of importance in the study of the minor constituents it had therefore to be re-investigated. The processes involved have been discussed fully by earlier writers (**1**), so that we need only indicate them briefly, and record the assumptions made in calculating the rates at which they occur.

TABLE I

Structure of Atmosphere

Altitude z (km)	Particle Concentration $n(M)$ (cm^{-3})	Temperature T (deg. K)
130	$1{\cdot}2\times10^{12}$	450
120	$2{\cdot}7\times10^{12}$	360
110	$7{\cdot}4\times10^{12}$	305
100	$2{\cdot}3\times10^{13}$	270
90	$8{\cdot}7\times10^{13}$	245
80	$3{\cdot}9\times10^{14}$	215
70	$2{\cdot}5\times10^{15}$	190
60	$8{\cdot}2\times10^{15}$	275
50	$2{\cdot}3\times10^{16}$	290
40	$6{\cdot}8\times10^{16}$	250
30	$3{\cdot}9\times10^{17}$	225
20	$2{\cdot}0\times10^{18}$	220
10	$8{\cdot}8\times10^{18}$	220
0	$2{\cdot}6\times10^{19}$	285

Photo-dissociation of molecular oxygen is produced by the absorption of solar radiation in the strong Schumann–Runge continuum beginning at λ 1759:

$$O_2 + h\nu \rightarrow O(^3P) + O(^1D), \tag{1}$$

and in the weak Herzberg continuum beginning at λ 2421:

$$O_2 + h\nu \rightarrow 2O(^3P). \tag{2}$$

In the presence of a third body the atoms thus liberated may recombine

$$O + O + M \rightarrow O_2 + M, \tag{3}$$

or they may unite with oxygen molecules

$$O + O_2 + M \rightarrow O_3 + M, \tag{4}$$

forming ozone. This substance may be destroyed by the collision process

$$O + O_3 \rightarrow 2O_2, \tag{5}$$

and by photo-dissociation in the strong Hartley continuum beginning about λ 3500:

$$O_3 + h\nu \rightarrow O_2 + O(^1D), \tag{6}$$

and in the weak Chappuis continuum beginning about $\lambda 8000$:

$$O_3 + h\nu \rightarrow O_2 + O(^3P). \tag{7}$$

Following the usage of other authors the reciprocals of the life-times of oxygen and ozone molecules towards photo-dissociation by (1) and (2), and by (5) and (6), will be denoted by J_2 and J_3, and the rate coefficients associated with (3), (4) and (5) by k_1, k_2 and k_3 respectively.

The intensity of the incident radiation down to $\lambda 2200$ has been determined by means of rocket-borne instruments {*cf.* Durant (**4**)}, and in the spectral region of interest beyond it probably approximates to that which would ensue if the Sun were a 5000 deg. K black body {*cf.* Nicolet (**5**), Greenstein (**6**)}. Since the relevant absorption cross-sections are also known * the values of J_2 and J_3 at various optical depths can hence be computed. The position regarding the rate coefficients is much less satisfactory. For reasons discussed elsewhere (**3**) it was tentatively assumed that in ordinary air

$$k_1 = 5 \times 10^{-34} T^{1/2} \text{ cm}^6/\text{sec}, \tag{8}$$

$$k_2 = 5 \times 10^{-36} T^{1/2} \text{ cm}^6/\text{sec}, \tag{9}$$

where T, as usual, is the temperature; and that the relative efficiencies of O_2, N_2 and O as third bodies are as 1·0 : 0·6 : 0·1 approximately {Penndorf (**8**)}. Since Eucken and Patat (**9**) have measured the ratio of k_2 to k_3 this latter is then also determined.

At altitudes down to about 70 km it is usually supposed that the concentrations $n(O_2)$ and $n(O)$ are controlled by processes (1), (2) and (3), so that

$$J_2 n(O_2) = k_1 n(O)^2 n(X), \tag{10}$$

where $n(X)$ is the *effective* number of third bodies found by weighting O_2, N_2 and O in the manner indicated above. In addition, if $n(M)$ is the total particle concentration (given in Table I) then

$$n(O_2) + n(N_2) + n(O) = n(M), \tag{11}$$

and since the relative abundance of oxygen and nitrogen is presumably the same as at ground level,

$$n(O) + 2n(O_2) = 0{\cdot}53 n(N_2). \tag{12}$$

These equations are somewhat troublesome. They were solved by commencing at the 130 km level (which is at essentially zero optical depth) and proceeding downwards to the 80 km level in altitude intervals so narrow that the attenuation in each is small {*cf.* Penndorf (**8**)}. The labour involved was however scarcely justified, since eqn. (10) over-simplifies the situation. Atomic hydrogen and certain radicals, which are present in the upper atmosphere, catalyse the formation of molecular oxygen. Bates and Nicolet (**3**) have investigated the extent to which this is likely to influence the equilibrium. They found that the effect may be significant below 85 km, and gave crude estimates of $n(O)$ and $n(O_3)$ down to the 65 km level. These were adopted, as there are insufficient basic data to improve upon them. At low altitudes catalysis becomes unimportant and (2), (4), (5), (6) and (7) are the dominant reactions. In principle the equilibrium

* Reference (**3**) lists the principal original papers on the subject and discusses the extrapolation of some of the experimental results. Its recommendations were followed, except that in the case of the Herzberg continuum the absorption cross-section curve obtained by Buisson, Jausseran and Rouard (**7**) was adopted.

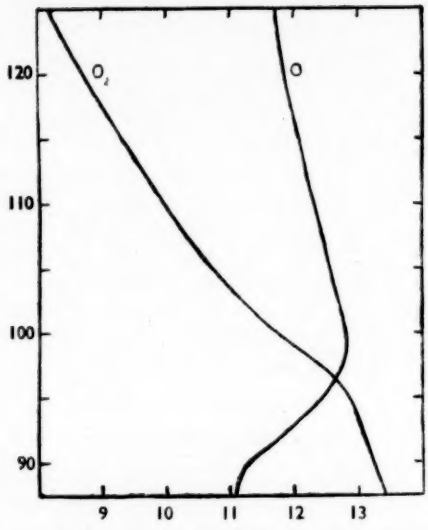

FIG. 1.—*Distribution of* $n(O)$ *and* $n(O_2)$. (*Day equilibrium.**)
Ordinates: *Altitude in kilometres.*
Abscissae: Log_{10} (*particle concentration*).

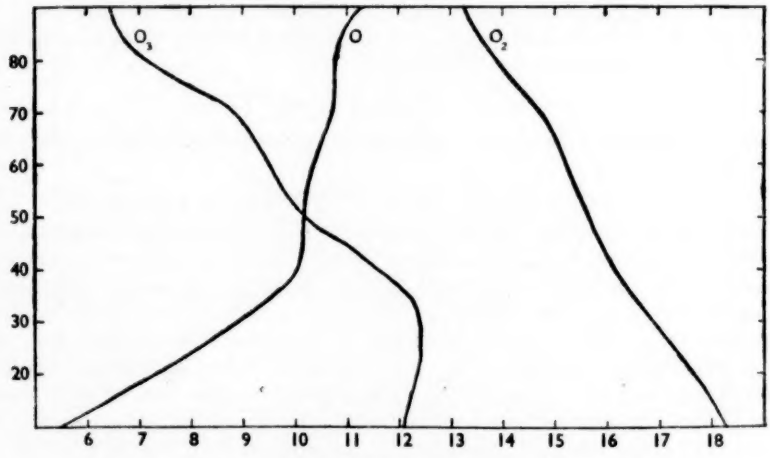

FIG. 2.—*Distribution of* $n(O)$ *and* $n(O_2)$ *and* $n(O_3)$. (*Day equilibrium.*)
Ordinates: *Altitude in kilometres.*
Abscissae: Log_{10} (*particle concentration*).

* In the region covered by Fig. 1, $n(O_3)$ is too small to be of interest. (It should be noted that the moderate rate of fall-off shown in Fig. 2 does not continue to greater altitudes, it becomes much more rapid at the O_3–O transition layer.)

can be determined using theory alone, but various difficulties enter and the full calculations were carried out only near the 50 km level. For altitudes up to 40 km it was judged best to accept the measurements on $n(O_3)$ {Fabry (**7**)} and to deduce $n(O)$ from them by means of the relation

$$n(O) = n(O_3)\{J_3/k_2 n(O_2) n(M)\} \tag{13}$$

with

$$n(O_2) = 0{\cdot}21 n(M) \tag{14}$$

{*cf.* (**3**)}. As has already been mentioned k_2 is not known reliably. It is possible that steric hindrance is not as severe as assumed {*cf.* Bamford (**10**)}, so that the use of (13) may cause $n(O)$ to be overestimated.

The distributions in the different regions were finally combined together as shown in Figs. 1 and 2. It may perhaps be mentioned that the main changes in the slopes of the $n(O)$ and $n(O_3)$ curves are due to the fact that the coefficient k_3 is extremely sensitive to the temperature. While such qualitative features are likely to be real the general accuracy of the results is unfortunately very poor.

Some of the reactions of interest involve atomic hydrogen, hydroxyl and perhydroxyl. Estimates of $n(H)$, $n(OH)$ and $n(HO_2)$ are available from the work of Bates and Nicolet (**3**).

3. *Carbon dioxide and carbon monoxide.*—The fractional volume concentration of carbon dioxide is not the same all over the Earth's surface, even apart from purely local effects {*cf.* Rankama and Sahama (**11**)}. However, for present purposes it may with sufficient accuracy be taken as constant and equal to 3×10^{-4} {Paneth (**12**)}. In the altitude range concerned diffusive separation is unimportant.

In 1949 Migeotte (**13**), then working at Columbus, Ohio, announced that certain lines in the 4·7 μ region of the solar spectrum are due to atmospheric carbon monoxide. Later in Switzerland he and Neven (**14**) succeeded in confirming this. Adel (**15**), in Flagstaff, Arizona, failed to detect the lines, but as they appear in a spectrum recently obtained by Shaw, Chapman, Howard and Oxholm (**16**) (also working at Columbus, Ohio), their reality is not in doubt. The lines observed are members of the fundamental vibrational band. Matheson, and Penner and Weber (**17**) have carried out laboratory measurements on them. The former found the Lorentz half-breadth in air at atmospheric pressure to be 0·10 cm^{-1}, and the latter found the associated Einstein spontaneous transition coefficient to be 33/sec. Combining these data with equivalent widths obtained from the published spectrograms (in particular from those of Shaw and his collaborators, as they include some weak lines attributed to the isotopic molecule $C^{13}O$ which probably lie on the linear part of the curve of growth), it is estimated that there is about 0·2 atm-cm of carbon monoxide in the atmosphere. The figure is of necessity rather crude—an error by a factor of perhaps 3 either way is possible. Much more reliable determinations have recently been made by Migeotte and Neven*, who on two different days obtained about 0·4 atm-cm and 0·1 atm-cm at the Jungfraujoch (showing that the abundance is variable). The lower value (which is presumably the least affected by any local contamination) will be tentatively adopted; it corresponds approximately to a fractional volume concentration of 1×10^{-7} or to 3×10^{18} CO molecules/cm^2 column.

* We wish to thank Dr Migeotte for informing us of the results prior to their publication.

The photo-chemistry of the two gases is clearly closely related. Radiation to the short wave-length side of λ1690 dissociates carbon dioxide into carbon monoxide and excited (^{1}D) atomic oxygen

$$CO_2 + h\nu \rightarrow CO + O(^1D). \tag{15}$$

The cross-section for the process has been measured by Wilkinson and Johnston (**18**). Using their results, taking the Sun as usual to be a 5000 deg. K black body (*cf.* Section 2) and averaging over day and night, it may be shown that in the region just above the 100 km level $\tau(CO_2)$ the life-time of a CO_2 molecule towards photo-dissociation through (15) is about 5×10^6 sec. Owing to absorption in the Schumann–Runge continuum of molecular oxygen the intensity of the active radiation falls off rapidly below this level. Consequently $\tau(CO_2)$ becomes extremely long, being very many years even at 95 km, and essentially infinite at 90 km.

Carbon dioxide may be re-formed through

$$CO + O + M \rightarrow CO_2 + M. \tag{16}$$

This process has been studied by Groth (**19**) and by Jackson (**20**), who find that the probability that it occurs in a normal three-body collision is some 100 times less than the probability of (4), which itself is small. If the estimate given in (9) is correct, then the rate coefficient for (16) would only be $5 \times 10^{-38} T^{1/2}$ cm^6/sec. As is well known (*cf.* **21**), the oxidation of carbon monoxide is accelerated by the presence of moisture. This is generally attributed to the reactions

$$CO + OH \rightarrow CO_2 + H, \tag{17}$$

$$CO + HO_2 \rightarrow CO_2 + OH. \tag{18}$$

These must also be taken into account in the upper atmosphere. The rate coefficients may be expressed in the form

$$k = \eta P \exp(-E/RT), \tag{19}$$

where R is the gas constant (1·987 cal/deg-mole), η is the collision frequency for unit concentrations, P is the steric hindrance factor and E is the activation energy. Unless there is evidence to the contrary it is usual in order-of-magnitude calculations to take the product ηP to be about $1{\cdot}5 \times 10^{-11} T^{1/2}$ cm^6/sec or rather less (*cf.* **22**). At the temperatures prevailing in the upper atmospheric region of interest the rate coefficients depend critically on the activation energy. Unfortunately the values appropriate to (17) and (18) do not appear to have been determined. To explore the situation two alternative arbitrary assumptions were made: (*a*) that for both reactions E is zero, (*b*) that for both it is 5 kcal. Calculations were then carried out on τ(CO), the mean life-time of a CO molecule towards oxidation by (16), (17) and (18) in the model atmosphere already described. In spite of the uncertainties some general conclusions can be reached.

Even with the highest possible rate coefficients it is found that τ(CO) is of the order of centuries near the 110 km level and is longer at greater altitudes. Life-times so extended have of course little real meaning. Below 100 km however τ(CO) may be moderate: at the 90, 80 and 70 km levels assumption (*a*) gives it

to be about 10^5, 10^3 and 10 sec and assumption (*b*) gives it to be about 10^9, 10^8 and 10^7 sec respectively. Thus

$$\tau(CO_2) \ll \tau(CO) \text{ for } z > 110 \text{ km} \tag{20}$$

and

$$\tau(CO_2) \gg \tau(CO) \text{ for } z < 90 \text{ km}. \tag{21}$$

In equilibrium

$$n(CO)/n(CO_2) = \tau(CO)/\tau(CO_2), \tag{22}$$

and therefore the carbon would be almost entirely in the dioxide form below the 90 km level and in the monoxide* form above the 110 km level. The altitude of the transition level is difficult to estimate precisely but it is certainly very close to 100 km. For reasons which will be apparent later the significance to be attached to the derived relative abundances does not justify giving them in full. To demonstrate their trend it is sufficient to mention that at 130 km (where (16) is the only oxidation process of importance) the calculated value of $n(CO)/n(CO_2)$ is 10^6 approximately.

It is natural to enquire at this stage whether the photo-dissociation would give rise to enough carbon monoxide to account for the observed infra-red absorption lines. At first it might be thought obvious that this is utterly impossible; for the fractional volume concentration of carbon dioxide in the lower atmosphere is 3×10^{-4}, and the total particle concentration and local scale-height at 100 km are $2{\cdot}3 \times 10^{13}/\text{cm}^3$ and 10 km respectively. Hence there would only be about 7×10^{15} CO molecules/cm^2 column above the transition level, which is much too small a number. However, such an argument is faulty, in that it assumes that equilibrium conditions prevail. This assumption is only justified if $\tau(CO_2)$ and $\tau(CO)$ are short compared with a characteristic atmospheric parameter, $\tau(M)$, which is a measure of the time required for winds and diffusion to produce mixing. The value of $\tau(M)$ is unfortunately unknown, but it must be considerable in view of the stabilizing effect of the positive temperature gradient of the atmosphere in the region of the transition layer. As has already been noted, $\tau(CO_2)$ is about 5×10^6 sec at altitudes above 100 km. This is not unduly long, so that, in general, the degree of dissociation may well be high (though perhaps not as high as simple equilibrium calculations would indicate). At altitudes below 100 km, $\tau(CO)$ is the life-time of importance. Its value is here mainly controlled by processes (17) and (18). Or, referring to the figures already given, it can be that if the activation energy E is zero then $\tau(CO)$ would be quite short. In this case the mean concentration of carbon monoxide would be kept low by oxidation. However, if, as is more probable, E is 5 kcal or above, the position would be quite different, since $\tau(CO)$ would be several months or more even at 70 km. Consequently the equilibrium calculations would be unlikely to be correct. Instead of carbon monoxide being mainly confined to the region above the transition level it would also be prevalent in the region below, for any reaching there would remain for a very long time before becoming oxidized. In extreme circumstances the altitude at which photo-dissociation ceases would not be apparent from the carbon monoxide distribution curve, which would closely follow that of the main atmospheric gases down to perhaps 70 km or even lower. The total abundance resulting from photo-dissociation cannot be calculated until $\tau(CO)$ and $\tau(M)$ are known. Though the departure from chemical equilibrium may well be very pronounced, the associated

* Further breakdown of the carbon oxides is unlikely to occur to any marked extent, since CO (like the isoelectronic N_2) is difficult to photo-dissociate {*cf.* Gaydon (23)}.

increase in the abundance is unlikely to be sufficient to explain the spectroscopic observations; for this would only be possible if the monoxide were as prevalent as the dioxide down to the 30 or 40 km level. A measurement of the altitude of the region in which the CO lines are formed would be of considerable interest.

It must not be forgotten that carbon monoxide is a major by-product of modern civilization. Vast quantities are vented into the atmosphere both by internal combustion engines and by solid-fuel furnaces.

The first source is the easier to assess quantitatively. Petrol consists of about 85 parts of carbon to 15 parts of other elements (**24**). The annual consumption of it is about $1{\cdot}5 \times 10^{14}$ g. From an analysis of the exhaust gases of motor vehicles given by Dunstan (**25**) it appears that as much as 40 per cent of the carbon is emitted as the monoxide. Hence the amount of carbon monoxide released into the atmosphere is approximately $1{\cdot}2 \times 10^{14}$ g/year. Since the surface area of the Earth is $5{\cdot}1 \times 10^{18}$ cm^2, and the mass of a CO molecule is $4{\cdot}7 \times 10^{-23}$ g, this is equivalent to a mean of 5×10^{17} CO molecules/cm^2/year. Diesel engines give but a minor contribution, as they are highly efficient and as the quantity of heavy oil used is relatively small.

Coal is by far the most important solid fuel. Its composition varies widely. The carbon content may be as low as 60 per cent in lignites and as high as 95 per cent in anthracites (**26**). On an average it may be taken to be perhaps 80 per cent. The amount of coal used in a year is about $1{\cdot}7 \times 10^{15}$ g. Unfortunately it is difficult to obtain representative data on the proportion of carbon monoxide in the combustion products, as this is critically affected by the conditions under which burning takes place. Thus Hurley and Sparks (**27**) have analysed the flue gases from boiler furnaces and find that the CO/CO_2 ratio ranges from 0·005 to 0·20, depending on such factors as the air draft. Fuel engineers of course try to keep the ratio as low as possible in the interests of thermal efficiency. When it equals 0·02 the heat loss is only 1 per cent (**26**), which suggests that little effort would be made to ensure a more complete combustion (especially as the use of too much excess air also causes losses). Forest and prairie fires are estimated by Kalle (*cf.* **11**) to add as much carbon dioxide to the atmosphere as does the burning of coal, but no information is available on the carbon monoxide. From the figures given above it would seem not unreasonable to suppose that the mean value of the CO/CO_2 ratio for all forms of non-explosive combustion is at least 0·01 and is probably rather more. On this assumption the contribution to the production rate (averaged over the Earth) is 3×10^{17} CO molecules/cm^2/year or greater.

Volcanic emanations contain some carbon monoxide, but from data given by Rankama and Sahama (**11**) it is at once apparent that the quantity released in this way is small.

Summation of the sources mentioned gives that the total production rate is at least some 8×10^{17} CO molecules/cm^2/year, which is sufficient to provide the estimated carbon monoxide content of the atmosphere within four years or less. Unless some destruction process occurs on the ground itself or at low altitudes, such a production rate must be of importance in determining the equilibrium abundance. For comparison it may be mentioned that the action of solar radiation on the upper atmosphere would yield fewer than 1×10^{16} CO molecules/cm^2/year even if the fractional volume concentration of carbon dioxide in the region concerned were kept as high as one-fifth of what it would be if photodissociation did not occur.

Combustion processes certainly lead to considerable localized contamination: for example, while the presumed global average of the fractional volume concentration of carbon monoxide is 1×10^{-7}, it appears from measurements made by various investigators that the value in busy streets is frequently 1×10^{-4}, that in cities 5×10^{-6} and that in urban areas 2×10^{-7} or less (**28**).* Clearly winds would ensure a widespread dispersal of the contamination even if the mean life of the CO molecules (which has yet to be discussed) should prove to be only a few days. In spite of its remoteness the Bernese Oberland (where Migeotte and Neven conducted their experiments) would be affected. On the other hand, the fact that the combustion occurring in the northern hemisphere is far greater than that occurring in the southern hemisphere might conceivably cause carbon monoxide to be more abundant in the former than in the latter. Thus the meridional circulation of the atmosphere (**30**) is not such as to facilitate the transfer of contamination from one hemisphere to the other; and in any case even a steady breeze having a N.–S. component of 20 km/hour would take about a month to travel 90° of latitude. It would be interesting in this connection to have data on the amount of carbon monoxide above some southern observatory (say in New Zealand).

The carbon monoxide molecules resulting from combustion apparently cannot have a life exceeding four years (*v. supra*). It would appear therefore that oxidation processes occurring in the upper atmosphere can be ignored. Thus the particle concentration at the 50 km level is more than 10^3 times smaller than that at ground level. Hence if a molecule were normally to reach the 50 km level within the time stated it would follow that a molecule at this level would normally take only a day to fall to ground level, which seems unlikely.

It is difficult to reach any final conclusion about the rate of oxidation of carbon monoxide in the dense lower atmosphere. For a process might restrict τ(CO) to less than four years and yet be so slow as to have escaped detection in the laboratory. Some relevant information is however available.

The reaction between carbon monoxide and molecular oxygen is exothermic, but it can probably be dismissed, since Mellor (**31**) reports that Berthelot could find no evidence for its occurrence when he exposed dry and moist mixtures of the two gases to sunlight for seven years. As can readily be verified from the estimated rate coefficient of (16), and the concentrations given in Fig. 2, atomic oxygen cannot cause appreciable loss. Ozone also is a very inefficient oxidizer of carbon monoxide. Zatsiorskii, Kondrateev and Solnishkova (**32**) find that the activation energy of

$$O_3 + CO \rightarrow O_2 + CO_2 \qquad (23)$$

is about 20 kcal. On substituting in (19) it can hence be seen that the process is unimportant. A prohibitively high activation energy appears indeed to be characteristic of the reaction with many oxygen compounds. For example, that associated with

$$NO_2 + CO \rightarrow NO + CO_2 \qquad (24)$$

* Abnormally high concentrations of carbon dioxide of course also occur but the departure from the mean is less pronounced. Thus Haldane (**29**) states the fractional volume concentration in the air of London is about $6{\cdot}5 \times 10^{-4}$ which is little over twice the global average of 3×10^{-4}. Judging from the ratio of the excess CO to excess CO_2 in town air it would seem unlikely that we have overestimated the rate of production of carbon monoxide.

In view of the spectroscopic estimates, the figure for urban areas is surprisingly small.

is thought to be 28 kcal {Brown and Crist (**33**)}. However, the atmosphere may contain minute traces of some highly active substances and it is not easy to exclude the possibility of one of them oxidizing carbon monoxide through a chain such as

$$\left.\begin{aligned} &CO+X+M\rightarrow COX+M,\\ &COX+O_2\rightarrow CO_2+OX,\\ &OX+h\nu\rightarrow O+X,\\ &OX+CO\rightarrow CO_2+X. \end{aligned}\right\} \qquad (25)$$

Quite a moderate collision efficiency would suffice even if the abundance of the catalyst at low levels were only 10^{-12} times that of all other constituents.

Reactions on the surface of the Earth may also occur. (i) Carbon monoxide unites readily with haemoglobin. The process is however reversible and in fact very little of the gas is oxidized in the body tissues. Clark, Stannard and Fenn (**34**) have recently investigated the effect. From their results it may easily be demonstrated that the global average of the rate of oxidation is negligible. (ii) Plants are affected by the presence of carbon monoxide (**35**) which may therefore be undergoing destruction by them (though the chlorophyll reaction may also be reversible). Quantitative data appear to be lacking. But noting that the life-time of a CO_2 molecule towards assimilation is about ten years {*cf.* Rankama and Sahama (**11**)} it would seem rather improbable (though not impossible) that the corresponding life-time of a CO molecule is four years or less. (iii) As has long been known, carbon monoxide in contact with soil is rapidly oxidized by various micro-organisms, in particular B. oligocarbophilus (**36**). The effect has been investigated by a number of workers but it is difficult to make quantitative deductions from their results. Most of the experiments consisted of introducing an air–carbon monoxide mixture into a flask containing some form of organic matter and studying how its composition changed with time. Usually there was little change during an initial period, but after one or two weeks (during which the micro-organisms presumably multiplied) oxidation began, and after another one or two weeks was complete. The interpretation of all such laboratory studies is of course complicated by the fact that both the carbon monoxide content of the air used and the surface to volume ratio of the apparatus had values far in excess of those typical of the lower atmosphere. Nevertheless it is clear from them that B. oligocarbophilus is a very powerful agency for the destruction of carbon monoxide. Some suggestive field observations have also been reported. Thus after an extensive fire in an anthracite mine Jones and Scott (**37**) carried out periodic analysis of the gases in some sealed galleries of volume 2×10^{11} cm^3. They found that the carbon monoxide disappeared within 20 days and attributed this to the oxidizing action of micro-organisms.

From the foregoing discussion it is apparent that the mechanism responsible for the removal of carbon monoxide from the air near ground level cannot yet be identified with certainty; and that only a lower limit can be given to the rate of the process concerned. In the circumstances no final decision can be reached as to the extent to which combustion influences the equilibrium. But so much of the gas is produced in this way that considerable quantities must get carried into the stratosphere in spite of the possible rapid destruction near ground level. Bearing in mind that the yield from the photo-dissociation of carbon dioxide is relatively very small, it would seem likely that combustion is the main source of the carbon monoxide observed spectroscopically.

4. *Methane.*—The only hydrocarbon so far detected in the Earth's atmosphere is methane.* Migeotte (**40**) identified some of its characteristic lines in the $3{\cdot}4\mu$ region of a solar spectrogram taken in Columbus, Ohio, and later (**41**) identified further lines in the $7{\cdot}7\mu$ region of a spectrogram obtained by Adel in Flagstaff, Arizona. The discovery was confirmed by McMath, Mohler and Goldberg (**42**) working in Pontiac, Michigan, on the $2{\cdot}0\mu$ region. Later measurements at the same observatory (**43**) give the abundance as 1·2 atm-cm or $3{\cdot}2 \times 10^{19}$ CH_4 molecules/cm^2 column.

Photo-dissociation of methane,

$$CH_4 + h\nu \rightarrow CH_3 + H, \tag{26}$$

begins about λ1450, and reaches its peak between λ1300 and λ1200. The absorption cross-sections in the region up to λ1365 have been determined by Wilkinson and Johnston (**18**). Those in the region beyond are relatively unimportant because of the fall-off in the intensity of the solar emission. They were estimated with sufficient accuracy by extrapolation using as a guide crude data provided by the work of Duncan and Howe (**44**). On carrying out the usual computations the rate of (26) at zero optical depth was found to be only about 4×10^{-7}/sec per CH_4 molecule. It will be seen later that photo-dissociation is not the major disruptive process.

Recombination of methyl radicals and hydrogen atoms requires the presence of a third body

$$CH_3 + H + X \rightarrow CH_4 + X \tag{27}$$

{Steacie (**45**)} and consequently is very slow at the low gas densities prevailing in the upper atmosphere. Indeed a collision between a methyl radical and a hydrogen atom is more likely to lead to further break-down through

$$CH_3 + H \rightarrow CH_2 + H_2. \tag{28}$$

For this is a two-body process and its activation energy is probably less than 5 kcal {Gorin, Kauzmann, Walter and Eyring (**46**)}. Moreover the methyl radicals are destroyed by numerous other collision reactions {*cf.* (**45**)} which convert them finally to carbon monoxide or carbon dioxide. Amongst the primary processes likely to be important is

$$CH_3 + O_2 \rightarrow CH_2O + OH. \tag{29}$$

Van Tiggelen (**47**) has given evidence for supposing that this proceeds very rapidly (the estimated activation energy being only some 1·5 kcal). It is apparent therefore that the removal of a single hydrogen atom from a methane molecule leads to the essentially permanent destruction of that molecule. The concentration of methane at any particular altitude is thus not determined by the local equilibrium between dissociation and recombination, but rather by that between dissociation and atmospheric mixing effects. As a result the distribution of the gas cannot be calculated at present. But some general information on it may be obtained from the consideration of $\tau(CH_4)$, the mean life-time of methane molecules at various levels.

In addition to the direct photo action (already discussed) $\tau(CH_4)$ is influenced by several collision processes. Methane reacts rather slowly with atomic oxygen,

* The suggestion that ethylene is present {Sutherland and Callendar (**38**)} is not supported by the recent observations of Shaw and Claassen (**39**) in Columbus, Ohio, which were sufficiently sensitive to have revealed much less than 0·01 atm-cm of the gas.

atomic hydrogen and hydroxyl. Thus the activation energy of the more probable of

$$CH_4 + O \rightarrow CH_2 + H_2O \tag{30}$$

and

$$CH_4 + O \rightarrow CH_2O + H_2 \tag{31}$$

is about 8 kcal {Steacie and Parlee (**48**)}; that of

$$CH_4 + H \rightarrow CH_3 + H_2 \tag{32}$$

is about 11 kcal {Geib and Steacie (**49**)}; and that of

$$CH_4 + OH \rightarrow CH_3 + H_2O \tag{33}$$

is also about 8 kcal {van Tiggelen (**47**)}. However, Geib and Harteck (**50**) find that when perhydroxyl radicals are present methane is rapidly oxidized even at temperatures below 100 deg. K, so that with these there must be a reaction with a very low activation energy (probably not exceeding 2 kcal).

The activation energies indicated were substituted in (19) to obtain crude estimates of the rate coefficients. These estimates were used in the compilation of Table II, which gives the approximate values of $\tau(CH_4)$ at various altitudes, and records which of the reactants is the most important.

TABLE II

*Oxidation of Methane by Collision Processes**

Altitude (km)	Principal Reactant	$\tau(CH_4)$ (sec)
120	O	10^2
100	O	10^3
90	O, HO_2	10^5
80	HO_2	10^5
70	HO_2	10^4

* In the region below 70 km the calculated values of $\tau(CH_4)$ are too unreliable to be worth giving. One major source of error is the uncertainty in the perhydroxyl concentration (**3**). This concentration probably decreases at altitudes much less than 70 km so that $\tau(CH_4)$ increases. However, because of the rise in temperature the atomic oxygen reaction again becomes important and between 60 km and 50 km it limits $\tau(CH_4)$ to perhaps 10^5–10^6 sec.

Clearly methane must be almost completely absent from the region above the 100 km level, since $\tau(CH_4)$ is there very short. Remembering that a thermo-incline hinders mixing, it seems probable indeed that oxidation keeps its abundance low, down to at least near the temperature minimum at 70 km. Little can be said about the equilibrium in the thermo-decline immediately below, but it should be noted that there is likely to be a significant loss of methane between the 60 km and 50 km levels where the temperature is a maximum. Owing to the nature of the reaction products the destruction of CH_4 molecules at such moderate altitudes may be a very significant factor in the chemistry of the upper atmosphere.

In view of the immense amount of fuel won from the Earth's crust during the past century it is natural to enquire if the methane now in the atmosphere could have escaped from oil wells and coal mines and thus be of comparatively recent origin.* The following figures are of relevance.

* We wish to thank Mr P. Kerr of the Institute of Petroleum, London, and Mr F. S. Hartwell of the Safety in Mines Research and Testing Establishment, Sheffield, for helpful correspondence on this topic.

Volume of atmospheric methane (*v. supra*)	$=6\times10^{18}$ cm^3	(34)
Amount of crude oil raised to date	$=6\times10^{10}$ barrels	(35)
Average volume of methane associated with one barrel of crude oil	$=7\times10^{7}$ cm^3	(36)
Volume of methane associated with total crude oil raised	$=4\times10^{18}$ cm^3	(37)
Amount of coal raised to date	$=1\times10^{11}$ tons	(38)
Average volume of methane associated with one ton of coal	$=5\times10^{6}$ cm^3	(39)
Volume of methane associated with total coal raised	$=5\times10^{17}$ cm^3	(40)

The main uncertainty clearly lies in the assumed quantitative relations between the methane and the crude oil and coal. Those quoted are based on information given in the standard treatise of Bone and Himus (**26**). Confirmation of relationship (36) was obtained from published statistical data on the production of natural gas (which is of course mainly methane) and crude oil {*cf.* Thorp (**28**)}. High accuracy is not required, since the methane released by oil-field operations is normally not deliberately vented into the atmosphere because of the risk of an explosion. Some is pumped back underground (to increase the oil output); some is used for local power generation; the remainder is either piped away from the field for general industrial or household purposes, or (in undeveloped countries where this is not practicable) is simply burnt in flares. Consequently the volume of methane which has actually escaped must be much less than 4×10^{18} cm^3. As almost all the methane released in mining operations passes into the atmosphere relationship (39) is rather critical. Fortunately most authorities seem to make much the same estimate as do Bone and Himus. Thus by averaging the methane content of the upcast air of 500 pits Hinsley (**51**) deduces that the annual discharge of the gas from British collieries is some 2×10^{15} cm^3, which corresponds to 1×10^{7} cm^3/ton *; and this is consistent with the generally accepted ventilation requirement {*cf.* Statham (**52**)}. To be sure, many of the mines described in the literature are much richer in methane; for example, in the Lancashire coalfield some have yields of about 1×10^{8} cm^3/ton {Fraser (**53**)} and in the N. Staffordshire coalfield some have yields of almost 2×10^{8} cm^3/ton {Jones (**54**)}. But such cases are reported because of the exceptional fire-damp hazard and should not be taken as representative.

The conclusion would hence appear to be that though the quantity of methane which has escaped from oil wells and coal mines is vast it is nevertheless probably smaller than the amount now in the atmosphere.

There are only two obvious naturally occurring sources of methane: seepage from fuel beds and vegetable matter decaying under anaerobic conditions. No direct quantitative information on the yield could be found but a limit to it can at least be set.

* Since this was written we have received an almost identical (but slightly smaller) estimate from Mr G. H. Watson of the National Coal Board, London, who also informs us that the figure for continental Europe is about the same, and that for America is probably less.

Assimilation deprives the atmosphere of about 4×10^{20} C-atoms/cm^2/year {*cf.* Rankama and Sahama (**11**)}. The gain of CH_4 molecules must certainly be far less: that it should be more than 0·01 times as much is indeed scarcely credible. Consequently the time required to produce the observed $3{\cdot}2 \times 10^{19}$ CH_4 molecules/cm^2 column must be quite long—probably well in excess of ten years. Far too little is known about the loss processes in the lower atmosphere to make a discussion of them profitable at present, but it may be remarked that methane (like carbon monoxide) is oxidized by certain chemically active substances and by various micro-organisms (**36**).

Slobad and Krogh (**55**) have carried out some mass spectrographic analyses of the air near ground level. They found the fractional volume of hydrocarbons to be 5×10^{-8} to 1×10^{-7}, which is some 40 to 20 times smaller than the fractional volume concentration methane would have if it were uniformly distributed through the atmosphere.* The natural inference is that the gas is largely confined to a layer at moderate or high altitudes. Migeotte (**56**), too, claims that the absorption lines are formed in a region where the temperature is 236 deg. K. This temperature is encountered at only four levels (*cf.* Table I). Only the two lower, one at about 8 km and another at about 35 km, need be considered, since any methane formed near the two upper would not have a sufficiently prolonged existence (*v. supra*), and since in any case if it were confined to a layer near these upper levels its fractional volume concentration would have to be improbably high in order to provide the observed total content in a vertical column.

Opposing evidence on the altitude distribution has recently been presented by Goldberg (**57**), who considers that it is essentially the same as that of the main atmospheric constituents. He reached this conclusion from a study of curves of growth of the absorption lines obtained at Mt. Wilson, California, and Lake Angelus, Michigan, and from a comparison of the total abundance of methane over these two stations (which are at altitudes of 1·7 km and 0·3 km respectively). In addition he pointed out that the true temperature of the methane is appreciably higher than the effective temperature obtained from the spectroscopic measurements, and on applying the necessary correction deduced a value only slightly lower than that at ground level. This disposes of one of the original arguments for a methane layer at moderate or high altitude. But the positive evidence on the methane distribution is hardly final, since the curve of growth test is not yet very sensitive and since (as Goldberg himself realized) the comparison of abundances test involves the implicit assumption that the methane content of the air depends only on the altitude and not on the geographical position.† There is clearly a grievous conflict with the measurements of Slobad and Krogh. A check on these is urgently required. As data up to 25 km would be useful, the facilities offered by balloon flights should be exploited. The altitude of the centre of mass of the methane is of considerable interest, since it determines the fractional volume concentration in the mesosphere, and hence the importance of the gas as a source of hydrogen (**3**).

* In view of possibility of the escape of hydrocarbons from oil fields it is interesting to note that the air analysed included samples from different parts of Texas. It is desirable that the investigations be extended to cover tropical regions (where anaerobic decay is particularly important).

† To emphasize the importance of this assumption it may be noted that there is only a 20 per cent difference in the observed abundances over Lake Angelus and over Mt. Wilson. Methane production by decay would be greater near the former station than near the latter—though whether it is appreciable in either is uncertain.

A layer such as that apparently indicated by the results of Slobad and Krogh would scarcely be anticipated. It is of course conceivable that the main production takes place in the tropics and that the methane is carried rapidly to the stratosphere by the rising air currents there prevalent {*cf.* Rossby (**30**)}; furthermore, the lower atmosphere is probably being depleted of methane (for example, through destruction on the Earth's surface caused by micro-organisms). But if the characteristic time parameter associated with the gas is ten years or more, as estimated, it would be expected that mixing effects would be sufficient to keep the distribution fairly uniform. Goldberg's results are thus favoured.

5. *Nitrous oxide.*—The first evidence for the presence of nitrous oxide in the atmosphere was obtained by Adel (**58**) from observations on the 7·6μ region of the solar spectrum. Confirmatory evidence has since been obtained by other infra-red spectroscopists (**59**), and the abundance has been estimated to be 0·8 atm-cm or 2×10^{19} molecules/cm^2 column. The location has not yet been properly determined. However, if the nitrous oxide were mainly confined to a 10 km thick layer* the mean concentration would be as much as 2×10^{13}/cm^3; and since the total particle concentration at an altitude of 70 km is only $2{\cdot}5 \times 10^{15}$/cm^3 it would seem most unlikely that any such layer could lie so high. More definite evidence will be reported later.

The long wave-length limits of the nitrous oxide continua are rather ill-defined, but it appears that a very weak absorption begins at about λ 3070 and that the main absorption begins at about λ 2400 or slightly above. The products of dissociation have not yet been identified with certainty but there is little doubt that in the low-energy region the process taking place is

$$N_2O + h\nu \rightarrow N_2 + O(^3P \text{ or } ^1D), \qquad (41)$$

and there is considerable support for the view that that in the high-energy region is

$$N_2O + h\nu \rightarrow NO + N(^4S) \qquad (42)$$

{*cf.* Bamford (**10**), Gaydon (**23**)}. Dutta, and Romand and Mayence (**60**), have determined the absorption cross-sections to the short wave-length side of λ 2700. Their results are in harmony. Unfortunately quantitative measurements have not been made in the remaining spectral region of interest. A qualitative study has however been carried out by Sponer and Bonner (**61**), who find that the absorption diminishes as the wave-length is increased up to about λ 2820, and that it then rises to a broad maximum near λ 2900. The variation does not appear to be very pronounced between λ 2800 and the limit at λ 3070; and from an estimate given by Sponer and Bonner the cross-section in this region appears to be of order 1×10^{-23} cm^2. Sufficient data are thus available to calculate the approximate photo-dissociation rate at various altitudes. The values obtained are displayed in Table III. Those at very low levels may be considerably in error because of uncertainty regarding the extent of the attenuation of the incoming solar radiation.

The destruction of nitrous oxide by collision processes is relatively unimportant. Thus

$$N_2O + O \rightarrow N_2 + O_2 \qquad (43)$$

and

$$N_2O + O \rightarrow 2NO \qquad (44)$$

* 10 km is of course the approximate scale height in the lower and middle atmosphere.

can be neglected, since the activation energy of both exceeds 13 kcal {Henrique, Duncan and Noyes (**62**)}; and the experiments of Willey and Rideal (**63**) on the chemical action of active nitrogen on various substances indicate that

$$N_2O + N \rightarrow N_2 + NO \qquad (45)$$

is also slow.

As it is by no means obvious that there is any upper atmospheric reaction capable of yielding the replenishment necessary to maintain the observed abundance, it is worth examining whether the nitrous oxide could originate on, or near, the surface of the Earth.

TABLE III

Photo-dissociation Rate of Nitrous Oxide

Altitude (km)	Rate ($/N_2O$ molecule/sec) Process (41)	Process (42)	Total
⩾100	$4{\cdot}5\times10^{-8}$	$2{\cdot}0\times10^{-6}$	$2{\cdot}0\times10^{-6}$
80	$4{\cdot}5\times10^{-8}$	$1{\cdot}5\times10^{-6}$	$1{\cdot}5\times10^{-6}$
60	$4{\cdot}5\times10^{-8}$	$1{\cdot}0\times10^{-6}$	$1{\cdot}0\times10^{-6}$
50	$4{\cdot}0\times10^{-8}$	$8{\cdot}0\times10^{-7}$	$8{\cdot}5\times10^{-7}$
40	$2{\cdot}5\times10^{-8}$	$5{\cdot}5\times10^{-7}$	$6{\cdot}0\times10^{-7}$
30	$1{\cdot}0\times10^{-8}$	$2{\cdot}5\times10^{-7}$	$2{\cdot}5\times10^{-7}$
20	$4{\cdot}5\times10^{-9}$	$1{\cdot}0\times10^{-8}$	$1{\cdot}5\times10^{-8}$
10	$3{\cdot}0\times10^{-9}$	3×10^{-12}	$3{\cdot}0\times10^{-9}$
0	$2{\cdot}5\times10^{-9}$	$\sim10^{-21}$	$2{\cdot}5\times10^{-9}$

The gas is known to be produced by a variety of widely distributed micro-organisms (**36**), and Adel (**64**) advocates the view that these are responsible for its presence in the atmosphere. Proper quantitative data to test the hypothesis are lacking. Bearing in mind other loss processes {such as the leaking of nitrates into the subsoil or into the drainage water (**65**)}, it is reasonable to assume however that the rate of formation of nitrous oxide by soil micro-organisms is less than the rate of fixation of nitrogen over the land which, according to Hutchinson (**66**), averages only some 2×10^{17} to 1×10^{18} N_2 molecules/cm^2/year.* The reliability of this figure is difficult to assess.† As would be expected, it is much less than the rate of assimilation of carbon (*cf.* Section 4): but the difference is not so great as to suggest that it is a gross underestimate. A yield of perhaps 5×10^{17} N_2O molecules/cm^2/year would thus seem the maximum possible; and a much smaller yield would seem more probable. If this is correct, then 40 years or more would be required to produce the amount of nitrous oxide indicated by the spectroscopic observations. It will be noted that 5×10^{17} N_2O molecules/cm^2/year is equivalent to a production rate of 3×10^4 N_2O molecules/cm^3/sec distributed over an altitude range of 6 km, which is of the same order as the calculated destruction rate in the troposphere (*cf.* Table III). Thus if the upper limit to the estimated possible yield from them is approached, micro-organisms might well be the source of the nitrous oxide. Research is required to determine if indeed the gas is not merely an important intermediary, but is a major end-product of denitrification (as is necessary). It would be surprising if this should prove to be the case.

* It may be remarked that lightning discharges give only a minor contribution to the fixation rate and moreover lead mainly to compounds other than nitrous oxide. As may easily be verified, they are therefore unimportant in the present connection.

† In a discussion of the nitrogen cycle in agriculture Russell (**65**) quotes rates which are more than an order of magnitude higher; but how representative these are he does not indicate.

Nitrous oxide seems to occur in the air near ground level. The mass spectroscopic measurements of Slobad and Krogh (**55**) indicate that its fractional volume concentration there is about 5×10^{-7}, which is not significantly different from the mean (1×10^{-6}) deduced from the total amount in a vertical column. Confirmatory evidence for its presence was obtained by Gebbie *et al.* (**67**) during the course of some work on the atmospheric transmission in the infra-red. It has been argued (**64**) that this strongly favours the suggestion that the nitrous oxide originates in the soil. But as will be seen, homogeneous gas reactions may also provide a source at low levels.

The various possibilities can easily be listed In examining them it must be remembered that in general the parent particles concerned must themselves be appearing at a rate at least equal to the rate at which they are reacting; and this in turn must be at least equal to the rate of photo-dissociation of the nitrous oxide. Many of the mechanisms which have been discussed by earlier workers fail to satisfy the requirement.

Bamford (**10**) has suggested that N_2O may be formed from O^+ ions in some unspecified way, Nicolet (**68**) that it may be formed from O^- ions through associative detachment

$$O^- + N_2 \rightarrow N_2O + e \tag{46}$$

(though this is endothermic). Both suggestions are unacceptable, since the rate of production of neither ion {*cf.* Bates and Massey (**69**)} even approaches the necessary value.

Amongst Bamford's other proposals is that metastable nitrogen molecules $N_2(A\,^3\Sigma_u^+)$ may be involved. The reactions envisaged are presumably

$$N_2(A\,^3\Sigma_u^+) + O + M \rightarrow N_2O + M, \tag{47}$$

$$N_2(A\,^3\Sigma_u^+) + O_3 \rightarrow N_2O + O_2, \tag{48}$$

$$N_2(A\,^3\Sigma_u^+) + O_2 \rightarrow N_2O + O. \tag{49}$$

These are not at all attractive. Under upper atmospheric conditions the formation of $N_2(A\,^3\Sigma_u^+)$ is difficult. The rate of direct excitation by solar radiation is utterly negligible. In connection with the theory of the airglow much abortive effort has been directed to finding a plausible collision process. The only ones which provide sufficient energy appear to be the three-body association of nitrogen atoms through

$$N + N + M \rightarrow N_2(A\,^3\Sigma_u^+) + M \tag{50}$$

or

$$N + N + N_2 \rightarrow N_2 + N_2(A\,^3\Sigma_u^+). \tag{51}$$

Even if the rate coefficients of these are high (which is unlikely in view of the electronic transition incurred), there remains the necessity of providing an adequate source of nitrogen atoms. Photo-dissociation of molecular nitrogen seems to be the sole possibility. Laboratory experiments prove that this does not occur readily {*cf.* (**70**)}; and reference to the figures given above shows that it should actually be taking place in the upper atmosphere at a rate which is comparable with the rate of photo-dissociation of molecular oxygen. There can therefore be little doubt * that the supply of atomic nitrogen (and so of metastable nitrogen molecules) is quite insufficient. Moreover the attenuation of the incoming

* The fact that some of the nitrogen atoms may be regenerated through (42) does not appreciably weaken the argument, since only a small fraction of them would follow the reaction path leading to nitrous oxide.

radiation is such that any supply there is would be well above the probable location of the nitrous oxide layer. It may also be urged that (48) is unimportant in this region. Again, the concentration, $n(N_2A\,^3\Sigma_u^+)$, is unlikely to exceed $1\times10^5/cm^3$ (*cf.* Appendix). On taking * $n(O)$ to be $1\times10^{13}/cm^3$ and $n(M)$ to be $3\times10^{13}/cm^3$ at the 100 km level, it can be seen that in order that (47) should yield the required 4×10^7 N_2O molecules/cm³/sec its rate coefficient would have to be some 10^{-24} cm⁶/sec, which is of course impossible. In the case of (49) this alternative approach is also useful. For since $n(O_2)$ does not exceed $5\times10^{12}/cm^3$ a rate coefficient of at least 10^{-10} cm³/sec would be needed. Similarly

$$N+N+O_2\rightarrow N_2O+O \tag{52}$$

is most unpromising, as the rate coefficient would have to be more than 10^{-31} cm⁶/sec even if $n(N)$ were $1\times10^{12}/cm^3$. Though these last two rate coefficients do not imply collision cross-sections exceeding gas kinetic values, they are improbably large. It is to be noted in this connection that the formation of nitrous oxide from active nitrogen and molecular oxygen does not appear to have been reported {*cf.* (**71**)}.

No process involving metastable oxygen molecules, $O_2(a\,^1\Delta_g$ or $b\,^1\Sigma_g^+)$, is at all plausible. For example,

$$O_2(a\,^1\Delta_g \text{ or } b\,^1\Sigma_g^+)+N_2\rightarrow N_2O+O \tag{53}$$

is strongly endothermic, so that it can be dismissed without detailed consideration.

The low heat of formation of N_2O also prevents most oxides from interacting with molecular nitrogen. To be sure

$$HO_2+N_2\rightarrow N_2O+OH \tag{54}$$

may be almost thermochemically neutral {*cf.* Bodenstein, Schenk and Kornfeld (**72**) and Gaydon (**23**)}. However, its rate is probably slow, since the influence of molecular nitrogen on the hydrogen–oxygen reaction seems to be merely that of an inert gas {Gibson and Hinshelwood (**73**)}. Furthermore it may be shown from the work of Bates and Nicolet (**3**) that the perhydroxyl radicals in the upper atmosphere are not replenished sufficiently rapidly.

The main processes thus far discussed (that is, processes involving positive or negative ions, metastable molecules or oxides) all fail, in that the supply of the parent particles is inadequate to balance the loss that would be incurred in producing the nitrous oxide at as great a rate as it is being destroyed. This rate is indeed so great that it was clear from the onset that the only mechanism likely to give sufficient parent particles is the photo-dissociation of molecular oxygen. The reactions following such photo-dissociation would have been considered earlier, but that it was judged important to demonstrate the need for invoking them as conclusively as possible by first disposing of the alternatives that had been proposed.

The altitude distribution of the rate of photo-dissociation of molecular oxygen was obtained in the course of the calculations outlined earlier. It is characterized by two maxima, one due to the Schumann–Runge continuum and another due to the Herzberg continuum, located at altitudes of approximately 100 km and 30 km respectively. The yield of oxygen atoms in the first is some $1\times10^7/cm^3/sec$; that in the second is some $5\times10^7/cm^3/sec$. When the particular reactions which might lead to the formation of nitrous oxide are described it

* Rather high values of the concentrations are deliberately chosen.

will be apparent that they could not occur to a sufficient extent at the altitude of the Schumann–Runge maximum. For this and other reasons attention will be confined to the Herzberg maximum.

In the region near 30 km the atomic oxygen initially formed reacts rapidly to give ozone, from which it is rapidly re-liberated by further photo-dissociation (*cf.* Section 2). As a result the supply of either substance is sufficient to meet the nitrous oxide requirement. With even normal oxygen atoms and ozone molecules there is the possibility of

$$O + N_2 + M \rightarrow N_2O + M \tag{55}$$

and

$$O_3 + N_2 \rightarrow N_2O + O_2. \tag{56}$$

These processes certainly do not occur readily {*cf.* Bamford (**10**)}, but as the concentrations of the reactants are considerable it does not follow that they are unimportant. In addition both types of particle will make collisions while still retaining some of their energy of formation. The $O(^1D)$ atoms* provided by (6), and the activated O_3* molecules provided by (4), may yield N_2O by reactions which take the same course as (55) and (56) and will be referred to as (55′) and (56′) respectively.

Just above ground level the temperature is approximately 285 deg. K, $n(N_2)$ is $2 \times 10^{19}/cm^3$; $n(O_2)$ is $5 \times 10^{18}/cm^3$; $n(O_3)$ is perhaps some $5 \times 10^{11}/cm^3$ and $n(O)$ is perhaps of order $1 \times 10^4/cm^3$: further O_3* molecules and $O(^1D)$ atoms are being formed at rates of about $2 \times 10^8/cm^3/sec$ and $4 \times 10^7/cm^3/sec$ respectively. Thus there would be a yield of say 5×10^4 N_2O molecules/cm^3/sec† provided either

(i) the rate coefficient of (55) is 1×10^{-38} cm^6/sec;

(ii) the rate coefficient of (56) is 5×10^{-27} cm^6/sec;

(iii) there is a 1 in 1×10^3 chance that an $O(^1D)$ atom interacts through (55′) before deactivation (as would be the case if, for example, the rate coefficient of (55′) were 1×10^{-36} cm^6/sec and that associated with deactivation were 2×10^{-14} cm^3/sec); or

(iv) there is a 1 in 4×10^3 chance that an O_3* molecule interacts through (56′) before deactivation (as would be the case if, for example, the rate coefficient of (56′) were 6×10^{-14} cm^3/sec and that associated with deactivation were 1×10^{-10} cm^3/sec).

It is difficult to determine whether any one of these requirements is actually met. The following comments are however offered.

If (55) leads to normal $X\,^1\Sigma$ N_2O molecules the rate coefficient would scarcely be expected to be great as 1×10^{-38} cm^6/sec, since a reversal of electron spin would be involved and since the activation energy would probably be appreciable {*cf.* Stearn and Eyring (**75**)}. However, a final decision cannot yet be reached theoretically. Laboratory investigations, too, provide but inconclusive evidence on the matter. The most significant experiments are those carried out by Leighton and Steiner (**76**), who passed mixtures of molecular nitrogen and oxygen through a cell illuminated by radiation in the Schumann–Runge continuum so that oxygen atoms (half of them in the ^1D state) were freed and

* There does not appear to be an adequate source of $O(^1S)$ atoms {*cf.* Bates and Seaton (**74**)}.

† This is greater than the rate of photo-dissociation of molecular oxygen at ground level, but no difficulty arises, since the time scale is such that mixing with the air at higher levels ensures an ample supply of *odd* oxygen atoms and since moreover (41) tends to replace those lost.

reactions involving them could proceed. In one run the $n(N_2)/n(O_2)$ ratio was as high as 10^3; no nitrous oxide could be detected and apparently only ozone was formed. However, on referring to the detailed results it will be seen that it cannot be inferred with complete certainty that condition (i) is not satisfied.

There appears no reason to suppose that the rate coefficient for (56) could not be 5×10^{-27} cm^3/sec: for such a rate coefficient would be possible even with an activation energy of 20 kcal; and, as it would allow an ozone molecule to have a life of several months in nitrogen at room temperature and atmospheric pressure, the process would not have been detected during any of the laboratory investigations.

Conditions (iii) and (iv) also do not appear to be excluded by the published experimental data. Neither is particularly severe. Thus judging from the potential energy curve along which an $O(^1D)$ atom and an $N_2(X\,^1\Sigma_g^+)$ molecule approach each other {*cf.* Stearn and Eyring (**75**)} (55′) should not be abnormally slow; since (56′) involves an O_3^* molecule its activation energy might well be small, as is implied by the suggested rate coefficient; and the assumptions regarding the deactivation of $O(^1D)$ and O_3^* are not unreasonable.

As the high activation energy makes the rate of (56) extremely sensitive to the temperature the yield of nitrous oxide from it must decrease through the troposphere. In view of the increase in the photo-dissociation rate (*cf.* Table III) it would clearly lead to a low-lying bank. Examination of the other processes shows that with them also the greatest equilibrium concentration would occur near ground level. However, the fall-off with altitude would be comparatively slow. Consequently (42) would give rise to a considerable number of *odd* nitrogen atoms. Now in the lower mesosphere their re-association is hindered by the rapid oxidation occurring {Bates (**77**)}. There is therefore the possibility that (55), (55′) or (56′) would lead to an unacceptable accumulation of nitric and higher oxides if they were as effective as required. With (56) no such difficulty arises.

APPENDIX

The concentration of $N_2(A\,^3\Sigma_u^+)$ *molecules in the upper atmosphere*

Illuminated metastable nitrogen molecules readily absorb and re-emit through the First Positive band system

$$\left.\begin{aligned} &N_2(A\,^3\Sigma_u^+) + h\nu \rightarrow N_2(B\,^3\Pi_g), \\ &N_2(B\,^3\Pi_g) \rightarrow N_2(A\,^3\Sigma_u^+) + h\nu. \end{aligned}\right\} \qquad (1)$$

Resonance scattering at twilight should therefore provide a sensitive means of detecting their presence in the upper atmosphere. To investigate the effect it is necessary first to determine the transition probability. This can be done by standard quantal methods.

The oscillator strength is given by the formula

$$f = (1/3Ra_0^2\lambda)D, \qquad (2)$$

where R is Rydberg's constant, a_0 is the radius of the first Bohr orbit, λ is the wave-length of the radiation concerned and D is

$$|\int X(\sigma_g 2p\,|\,\mathbf{r})\mathbf{r}X^*(\pi_u 2p\,|\,\mathbf{r})\,d\tau|^2 \qquad (3)$$

with $X(\sigma_g 2p|\mathbf{r})$ and $X(\pi_u 2p|\mathbf{r})$ the normalized wave functions of the active electron in the $A\,^3\Sigma_u^+$ and $B\,^3\Pi_g$ states respectively and $\mathbf{r}$ its position vector (*cf.* Mulliken (**78**)}. On the crude LCAO approximation

$$X(\sigma_g 2p) = N_0(\psi_0{}^a - \psi_0{}^b), \tag{4}$$

$$X(\pi_u 2p) = N_1(\psi_1{}^a + \psi_1{}^b), \tag{5}$$

where N_0 and N_1 are normalizing factors, a and b denote the atom on which the orbital is based, and

$$\psi_0 = f(r)\cos\theta, \tag{6}$$

$$\psi_1 = f(r)\sin\theta \begin{cases} \cos\phi \\ \sin\phi. \end{cases} \tag{7}$$

Representing $f(r)$ by the function

$$(\gamma^5/\pi)^{1/2} r \exp(-\gamma r) \tag{8}$$

and substituting in (3) it can be shown that when the internuclear distance is Ra_0 then

$$D = T^2/(1 - S_0)(1 + S_1), \tag{9}$$

where

$$T = \frac{\alpha^5 R}{240}\left\{5A_4 - 6A_2 + A_0\right\}, \tag{10}$$

$$S_0 = \frac{\alpha^5}{120}\left\{5A_4 - 18A_2 + 5A_0\right\}, \tag{11}$$

$$S_1 = 2T/R, \tag{12}$$

$$\alpha = \gamma R, \tag{13}$$

and

$$A_n = \int_1^\infty \exp(-\alpha x) x^n \, dx. \tag{14}$$

Spectroscopic measurements show that R is approximately $2{\cdot}4a_0$ {*cf.* Herzberg (**79**)}. As usual α is poorly determined: a value of about 4 is indicated by the self-consistent field wave functions of Brown, Bartlett and Dunn (**80**) and a value of about 5 by Slater's rules (which, though crude, have proved remarkably successful in molecular calculations). On carrying out the necessary computation it was found that D is either 0·068 or 0·026, depending on whether the smaller or larger α is used. Adopting the mean, 0·05, and taking the wave-length to be 6 000 A (*v. infra*), it can be seen from (2) that the oscillator strength is of order 2×10^{-3}. The corresponding Einstein coefficient A is 2×10^5/sec.

If the effect of vibration in producing energy spread is neglected, then the photon emission due to (1) is

$$P = s\Omega A \exp(-hc/\lambda kT)/N_2(A\,^3\Sigma_u^+) \text{ molecule/sec.} \tag{15}$$

where s is the ratio of the statistical weight of upper state to that of the lower (2), Ω is the dilution ($5{\cdot}4 \times 10^{-6}$) and T is the temperature (6 000 deg. K) of the solar radiation, k is Boltzmann's constant, and the other symbols are as already defined (**81**). Numerical substitution yields

$$P = 4 \times 10^{-2}/N_2(A\,^3\Sigma_u^+) \text{ molecule/sec.} \tag{16}$$

Montgomery and Nicholls (**82**) have recently evaluated the nuclear overlap integrals associated with the individual bands. The intensity distribution through the system can thus be deduced (**81**). This need not be given in detail.

It is sufficient to mention that approximate calculations indicate that λλ6705, 6624, 6545 and 6468 of the $v' - v'' = 3$ sequence should be prominent, the photon emission in each being at least 0·05 times the total. Now resonance scattering of the First Positive system at twilight has never been observed.* If the photon emission in any of the bands mentioned were as great as 2×10^2/cm³/sec it could scarcely have escaped detection. From the estimated efficiency of the scattering process it is hence apparent that the concentration of metastable nitrogen molecules does not exceed 10^5/cm³. The assumed upper limit to the twilight intensity of the First Positive bands is considered to be conservative. A precise spectroscopic determination of this limit would be very useful in that it would enable a more severe restriction to be placed on the concentration of metastable molecules.

Dept. of Applied Mathematics,
Queen's University,
Belfast:
1951 *October* 2.

Dept. of Physics,
University College,
London.

References

(1) *cf.* S. K. Mitra, *The Upper Atmosphere*, Royal Asiatic Society of Bengal, Calcutta, 1947.
(2) A. B. Meinel, *Ap. J.*, **111,** 207, 333, 1950.
(3) D. R. Bates and M. Nicolet, *J. Geophys. Res.*, **55,** 301, 1950.
(4) E. Durant, *The Atmospheres of the Earth and Planets* (ed. G. P. Kuiper), University of Chicago Press, Chicago, 1948.
(5) M. Nicolet, *Inst. R. Met. Belgique Misc.*, **18,** 1945.
(6) J. L. Greenstein, *The Atmospheres of the Earth and Planets* (ed. G. P. Kuiper), University of Chicago Press, Chicago, 1948.
(7) *cf.* C. Fabry, *L'ozone atmosphérique*, Centre National de la Recherche Scientifique, Paris, 1950.
(8) R. Penndorf, *J. Geophys. Res.*, **54,** 7, 1949.
(9) A. Eucken and F. Patat, *Z. Physik Chem.* B, **33,** 459, 1936.
(10) C. H. Bamford, *Rep. Prog. Phys.*, **9,** 75, 1943.
(11) K. Rankama and Th. G. Sahama, *Geochemistry*, University of Chicago Press, Chicago, 1949.
(12) F. A. Paneth, *Quart. J. Roy. Met. Soc.*, **63,** 433, 1937.
(13) M. V. Migeotte, *Phys. Rev.*, **75,** 1108, 1949.
(14) M. V. Migeotte and L. Neven, *Physica*, **16,** 423, 1950.
(15) A. Adel, *Phys. Rev.*, **75,** 1766, 1949.
(16) J. H. Shaw, R. M. Chapman, J. N. Howard and M. L. Oxholm, *Ap. J.*, **113,** 268, 1951.
(17) L. Matheson, *Phys. Rev.*, **40,** 813, 1932. S. S. Penner and D. Weber, *J. Chem. Phys.*, **19,** 807, 1951.
(18) P. G. Wilkinson and H. L. Johnston, *J. Chem. Phys.*, **18,** 190, 1950.
(19) W. Groth, *Z. Physik Chem.* B, **37,** 307, 1937.
(20) W. F. Jackson, *J. Am. Chem. Soc.*, **56,** 2631, 1934.
(21) W. Jost, *Explosion and Combustion Processes in Gases*, McGraw-Hill Book Company, London, 1946.
(22) W. A. Noyes and P. A. Leighton, *The Photo-Chemistry of Gases*, Reinhold Publ. Corp., New York, 1941.
(23) A. G. Gaydon, *Dissociation Energies*, Chapman and Hall Ltd., London, 1947.
(24) J. Griswold, *Fuels, Combustion and Furnaces*, McGraw-Hill Book Company, London, 1946.
(25) A. E. Dunstan, *Chemistry and Industry*, **10,** 846, 1932.
(26) W. A. Bone and G. W. Himus, *Coal—its Constitution and Use*, Longmans, Green and Co., London, 1936.
(27) T. F. Hurley and W. J. Sparks, *Proc. Inst. Mech. Engineers*, **162,** 20, 1950.

* It is to be noted that Elvey (83) has withdrawn the claim that λ6560 (which might be a blend of several of the First Positive bands) is enhanced during twilight.

(28) *Thorp's Dictionary of Applied Physics* (fourth edition), Longmans & Co., London, 1941. W. P. Yant, E. Levy, R. R. Sayers, G. E. Brown, C. C. Traubert, H. W. Frevert and K. L. Marshall, *U.S. Bur. Mines, Rept. Investigations* 3585, 1941. D. Vita, *Ann. Chim. Applicata*, **31**, 302, 1941. M. A. Reaugh and A. F. Stribley, *Petroleum Processing*, **4**, 391, 1949.
(29) J. B. S. Haldane, *Nature*, **137**, 575, 1936.
(30) C. G. Rossby, *The Atmospheres of the Earth and Planets* (ed. G. P. Kuiper), University of Chicago Press, Chicago, 1947.
(31) J. W. Mellor, *A Comprehensive Treatise on Inorganic and Theoretical Chemistry*, Longmans & Co., London, 1924.
(32) M. Zatsiorskii, V. Kondrateev and S. Solnishkova, *J. Phys. Chem.* (*U.S.S.R.*), **14**, 1521, 1940.
(33) F. B. Brown and R. H. Crist, *J. Chem. Phys.*, **16**, 361, 1947.
(34) R. T. Clark, J. N. Stannard and W. O. Fenn, *Science*, **109**, 615, 1949.
(35) E. I. Rabinowitch, *Photosynthesis and Related Processes*, Interscience Publishers, New York, 1945.
(36) *cf.* S. A. Waksman, *Principles of Soil Microbiology* (second edition), Bailliere, Tindall and Cox, London, 1931. M. Stephenson, *Bacterial Metabolism* (third edition), Longmans, Green and Co., London, 1949.
(37) G. W. Jones and G. S. Scott, *Ind. Eng. Chem.*, **31**, 775, 1939.
(38) G. B. B. M. Sutherland and G. B. Callendar, *Rep. Prog. Phys.*, **9**, 18, 1943.
(39) J. H. Shaw and H. H. Claassen, *Phys. Rev.*, **81**, 462, 1951.
(40) M. V. Migeotte, *Ap. J.*, **107**, 400, 1948.
(41) M. V. Migeotte, *Phys. Rev.*, **74**, 112, 1948.
(42) R. R. McMath, O. C. Mohler, L. Goldberg, *Phys. Rev.*, **73**, 1204, 1948; **74**, 623, 1948.
(43) R. R. McMath and L. Goldberg, *Proc. Amer. Phil. Soc.*, **93**, 362, 1949.
(44) A. B. F. Duncan and J. P. Howe, *J. Chem. Phys.*, **2**, 851, 1934.
(45) E. W. R. Steacie, *Atomic and Free Radical Reactions*, Reinhold Publ. Corp., New York, 1946.
(46) E. Gorin, W. Kauzmann, J. Walter and H. Eyring, *J. Chem. Phys.*, **7**, 633, 1939.
(47) A. van Tiggelen, *Ann. Mines Belg.*, **43**, 117, 1942.
(48) E. W. R. Steacie and N. A. D. Parlee, *Can. J. Research*, B, **16**, 203, 1938.
(49) K. H. Geib and E. W. R. Steacie, *Z. Physik Chem.* B, **29**, 215, 1935.
(50) K. H. Geib and P. Harteck, *Z. Physik Chem.* A, **170**, 1, 1934.
(51) F. B. Hinsley, *Iron and Coal Trades Review*, **162**, 1029, 1951.
(52) I. C. F. Statham, *Coal Mining*, English Univ. Press, London, 1951.
(53) E. H. Fraser, *Trans. Inst. Mining Engineers*, **104**, 108, 1944.
(54) T. D. Jones, *Proc. Nat. Assoc. Colliery Managers*, **29**, 810, 1932.
(55) R. L. Slobad and M. E. Krogh, *J. Am. Chem. Soc.*, **72**, 1175, 1950.
(56) M. V. Migeotte, *The Atmospheres of the Earth and Planets* (ed. G. Kuiper), University of Chicago Press, Chicago, 1948.
(57) L. Goldberg, *Ap. J.*, **113**, 567, 1951.
(58) A. Adel, *Ap. J.*, **88**, 186, 1938; **90**, 627, 1939; **93**, 509, 1941.
(59) J. H. Shaw, G. B. B. M. Sutherland and T. W. Wormell, *Phys. Rev.*, **74**, 978, 1948. R. McMath, *Ap. J.*, **54**, 214, 1949. O. Mohler and A. K. Pierce, *P.A.S.P.*, **61**, 221, 1949. M. V. Migeotte, *Ap. J.*, **112**, 136, 1950.
(60) A. K. Dutta, *Proc. Roy. Soc.* A, **138**, 84, 1932. J. Romand and J. Mayence, *Comptes Rendus* (*Paris*), **288**, 998, 1949.
(61) H. Sponer and L. G. Bonner, *J. Chem. Phys.*, **8**, 33, 1940.
(62) F. C. Henrique, A. B. F. Duncan and W. A. Noyes, *J. Chem. Phys.*, **6**, 518, 1938.
(63) E. J. B. Willey and E. K. Rideal, *J. Chem. Soc.*, **129**, 669, 1927.
(64) A. Adel, *Science*, **103**, 280, 1946; **113**, 624, 1951.
(65) E. J. Russell, *Soil Conditions and Plant Growth* (eighth edition revised by E. W. Russell), Longmans, Green and Co., London, 1950.
(66) G. E. Hutchinson, *American Scientist*, **32**, 178, 1944.
(67) H. A. Gebbie, W. R. Harding, C. Hilsum, A. W. Pryce and V. Roberts, *Proc. Roy. Soc.* A, **206**, 87, 1951.
(68) M. Nicolet, *Mem. R. Met. Inst. Belgium*, **19**, 1, 1945.
(69) D. R. Bates and H. S. W. Massey, *Proc. Roy. Soc.* A, **187**, 261, 1946; **192**, 1, 1947.

(70) S. Chapman and W. C. Price, *Rep. Prog. Phys.*, **3**, 55, 1936. W. C. Price, *ibid.*, **9**, 10, 1943.
(71) S. K. Mitra, *Active Nitrogen*, Indian Ass. Cult. Sci., Calcutta, 1945.
(72) M. Bodenstein and P. W. Schenk, *Z. Physik Chem.* B, **20**, 420, 1933. G. Kornfeld, *ibid.*, **35**, 236, 1937.
(73) C. H. Gibson and C. N. Hinshelwood, *Proc. Roy. Soc.* A, **118**, 170, 1928; **119**, 591, 1928.
(74) D. R. Bates and M. J. Seaton, *Proc. Phys. Soc.* B, **63**, 129, 1950.
(75) A. E. Stearn and H. Eyring, *J. Chem. Phys.*, **3**, 778, 1935.
(76) *cf.* P. A. Leighton, *Determination of the Mechanism of Photo-Chemical Reactions*, Hermann & Co., Paris, 1938.
(77) D. R. Bates (in course of publication in *Ann. Geophys.*).
(78) R. S. Mulliken, *J. Chem. Phys.*, **7**, 14, 1939.
(79) G. Herzberg, *Diatomic Molecules*, D. van Nostrand Company, New York,1950.
(80) F. R. Brown, J. H. Bartlett and C. G. Dunn, *Phys. Rev.*, **44**, 296, 1933.
(81) D. R. Bates, *Proc. Roy. Soc.* A, **196**, 217, 1949.
(82) C. E. Montgomery and R. W. Nicholls, *Phys. Rev.*, **82**, 565, 1951.
(83) C. T. Elvey, *Ap. J.*, **111**, 432, 1950.

CONTENTS

PAGE

Meeting of 1952 January 11 :

Fellows elected 1

Junior Members elected 2

Presents announced... 2

Award of the Gold Medal to Dr John Jackson 2

T. R. Tannahill, Star-streaming from the proper motions of the Boss *General Catalogue* 3

P. A. Wayman, A two-plate catadioptric system for astronomical photography ... 18

Mary Almond, J. G. Davies and A. C. B. Lovell, The velocity distribution of sporadic meteors. II 21

D. R. Bates, Absorption of radiation by an atmosphere of H, H^+ and H_2^+—semi-classical treatment 40

Ida W. Busbridge, On emission lines in stellar spectra 45

Mary T. Conway, Studies of Hα line profiles in prominences 55

M. A. Ellison and H. Seddon, Some experiments on the scintillation of stars and planets 73

M. J. Smyth, Notes on the 931–A photomultiplier 88

J. Jackson and J. B. G. Turner, Stellar parallaxes determined photographically at the Cape Observatory (Eighteenth List) 94

D. R. Bates and Agnes E. Witherspoon, The photo-chemistry of some minor constituents of the Earth's atmosphere (CO_2, CO, CH_4, N_2O) 101

Printed in London by Taylor & Francis, Ltd., 1952 *June.*